The global biogeochemical cycle of mercury: Insights from modeling atmospheric chemistry and all-time emissions from human activity

The global biogeochemical cycle of mercury: Insights from modeling atmospheric chemistry and all-time emissions from human activity

A dissertation presented
by
Hannah Marie Horowitz
to
The Department of Earth and Planetary Sciences

in partial fulfillment of the requirements
for the degree of
Doctor of Philosophy
in the subject of
Earth and Planetary Sciences

Harvard University
Cambridge, Massachusetts
March 2017

Thesis advisors: Profs. Daniel J. Jacob & Elsie M. Sunderland Hannah Marie Horowitz

The global biogeochemical cycle of mercury: Insights from modeling atmospheric chemistry and all-time emissions from human activity

Abstract

Methylmercury, a neurotoxin formed from inorganic mercury (Hg), bioaccumulates in aquatic food chains and adversely affects human health on a global scale through fish consumption. A global treaty, the Minamata Convention, aims to reduce human and wildlife Hg exposure by tackling anthropogenic emissions sources, but major uncertainties remain in predicting and assessing its impact. First, prior best understanding of anthropogenic atmospheric emissions suggested global emissions increased sharply from 1990 to present, in conflict with observed declining trends in atmospheric Hg concentrations over the same period. Historical atmospheric Hg deposition in lake sediment records since 1850 also appeared to conflict with historical emissions estimates that showed peak emissions occurred in the late 19th century. Second, Hg is transported near-globally through the atmosphere, but the chemistry driving the atmospheric lifetime of Hg and where it is deposited is not well-constrained due to measurement limitations. Therefore, we must turn to theoretical chemistry and modeling tools.

This dissertation aims to improve our understanding of the global Hg biogeochemical cycle and how anthropogenic emissions impact past, present, and future environmental Hg by using multiple global Hg modeling tools (7-box biogeochemical model; 3-D chemical transport model coupled to 3-D ocean general circulation model and 2-D land surface) evaluated against a suite of available observations. The objectives of this work are: (1) quantify emissions and releases of Hg from intentional use in commercial products and its impact on global environmental Hg loading from year 1850 to 2010; (2) develop a state-of-the-science mechanism for atmospheric Hg redox chemistry and evaluate its effects on the global Hg budget and deposition patterns. The first dissertation chapter concludes that releases of Hg from commercial products more than double previous estimates of

total anthropogenic Hg sources to the environment from 1850 to 2010 and that including this source improves our ability to reproduce historical and recent trends in atmospheric Hg, with peak emissions occurring in 1970 followed by sharp declines. Secondly, the state-of-the-science theoretical understanding of atmospheric Hg oxidation and reduction chemistry implies reduction takes place, improves modeled representation of low wet deposition over China, and suggests greatest deposition of Hg^{II} occurs over the tropical oceans.

Contents

To my grandparents, Irving and Tillie Horowitz, and Ann and Ezio Armillei

Acknowledgments

First and foremost, I want to thank my advisors, Daniel Jacob and Elsie Sunderland. I have learned so much from you and it has been an honor and a pleasure working closely with you both. Thank you for sharing your experiences with me, for your flexibility and support during my health problems, and for giving me so many great scientific opportunities. Elsie - thank you also for the extra support over the last few months! I am very lucky to have had two phenomenal advisors and scientists to train me. I am also fortunate to be a part of the larger Jacob-Mickley and Sunderland groups and to benefit from the support and friendship of the many grad students, post-docs, researchers, and support staff within them. It has been wonderful getting to know you all and you have made the day-to-day experience of grad school infinitely better. Special thanks to Loretta, my officemates (Katie T, Dan C, Eloise, Alex, Lei, and neighbors Kevin and Chris), my mentor Helen, my mentee Rachel, the GEOS-Chem support team (Bob, Melissa, Lizzie), and Brenda for everything. Thanks also to my committee, Dave Johnston, Steve Wofsy, and Miaki Ishii, who have I have thoroughly enjoyed interacting with over the years. I really appreciate you making my 8AM defense!

This research was made possible through the help of my co-authors (in alphabetical order): Helen M. Amos, Elizabeth (Bess) S. Corbitt, Theodore S. Dibble, Eloise A. Marais, Johan A. Schmidt, Franz Slemr, David G. Streets, Yanxu Zhang. It has been rewarding to work closely with you, especially those from other institutions. I am grateful to Bess who paved the way for my second PhD project. I also want to thank my supervisor Dr. Rebecca Garland at the CSIR in South Africa and my friends and collaborators there. Although this work is not in my PhD thesis, it was an important research and life experience and I am grateful for your continued friendship from halfway around the world! I want to thank Sheryl Goodridge, Dr. Lisa Starobin and her res-

ident, Dr. Rachel Nardin, and Liz Scholder, and Paul Kelley, Sarah, Jerry, Mitra and Larry for helping me be able to get my work done during ongoing neck/shoulder and concussion-related health issues.

The larger EPS department has been a wonderful community to me throughout undergrad and graduate school. Thanks to Sarah Colgan, Paul Kelley, Maryorie Grande, and Chenoweth Moffat for your help and support over the years. To my friends: all the grad students in the EPS department (especially my cohort, wine time, women in climate), the Harvard University Band and other friends from undergrad, roommates (Maura, Zheina, Amanda, Katie D, Rachel, Grace, Christine), Wethersfield friends, the Romanians, Bar League and Bowling teams (Sarah, Christine, Kheli, and Sara). You kept me sane, lifted me up, inspired me, made me laugh, and I will miss you all dearly. MVPs for the last few weeks of my PhD - Karen, Katie T, Katie D, Rachel - thank you doubly!

Thank you to my family, in Connecticut, Kansas City, Texas, and now New York, Canada, and Romania, for your support and pride in me, and for giving me a relaxing and loving place to be when I needed it. Thank you for your patience and trying to understand the oft-confusing PhD process. To my parents especially - thank you for your unconditional love and pride, and for raising me to care about others and the environment. Finally, I can't thank my husband, Cristi, enough for his support and unfailing confidence in me, throughout our relationship and especially in the last few months. Life is so much better when you're around. (and thanks for LaTeX-ing most of this thesis for me!)

1

Overview

Methylmercury, a neurotoxin formed from inorganic mercury (Hg), bioaccumulates in aquatic food chains and adversely affects human health on a global scale through fish consumption (Mahaffey et al., 2011; Karagas et al., 2012). Human activities like mining and fossil fuel combustion liberate Hg sequestered in the lithosphere into biologically active surface reservoirs (Selin et al., 2008; Streets et al., 2011; Amos et al., 2013). Once in the atmosphere, Hg has a lifetime of $\approx$ 6 months determined by its chemistry and deposition, allowing near-global transport (Corbitt et al., 2011). Hg deposited to the oceans can also be transported through global ocean circulation (Sunderland et al., 2009). The slow burial of Hg in coastal and deep ocean sediment means anthropogenic perturbations leave a lasting legacy, and future trends in Hg concentrations and exposures are affected by the trajectory of past environmental releases (Amos et al., 2013, 2015). The work presented in this dissertation aims to improve our understanding of the global Hg biogeochemical cycle and how anthropogenic emissions impact past, present, and future environmental Hg by addressing two major themes: (1) the impact of historical Hg releases from commercial products on global environmental Hg loading; (2) the effects of atmospheric Hg

redox chemistry on the global Hg budget and deposition patterns.

The intentional use of mercury (Hg) in products and processes ('commercial Hg') has contributed a large and previously unquantified anthropogenic source of Hg to the global environment over the industrial era, with major implications for Hg accumulation in environmental reservoirs. Here I present a global inventory of commercial Hg uses and releases to the atmosphere, water, soil, and landfills from 1850 to 2010. Cumulative anthropogenic atmospheric Hg emissions since 1850 were estimated at 215 Gg (only including commercial Hg releases from chlor-alkali production, waste incineration, and mining). I find that other commercial Hg uses and non-atmospheric releases from chlor-alkali and mining result in an additional 540 Gg Hg released to the global environment since 1850 (air: 20%, water: 30%, soil: 30%, landfills: 20%). Some of this release has been sequestered in landfills and benthic sediments, but 310 Gg actively cycles among geochemical reservoirs and contributes to elevated present-day environmental Hg concentrations. Commercial Hg use peaked in 1970 and has declined sharply since. I use the inventory of historical environmental releases to force a global biogeochemical model that includes new estimates of the global burial in ocean margin sediments. Accounting for commercial Hg releases improves model consistency with observed atmospheric concentrations and associated historical trends.

Second, I implement a new mechanism for atmospheric Hg^0/Hg^{II} redox chemistry in the GEOS-Chem global model and examine the implications for the global atmospheric Hg budget and deposition patterns. Hg is emitted to the atmosphere mainly as volatile elemental Hg^0, but oxidation to water-soluble Hg^{II} controls Hg deposition to ecosystems. I find that atomic bromine (Br) is the main atmospheric Hg^0 oxidant, and that second-stage HgBr oxidation is mainly by the NO_2 and HO_2 radicals. The resulting lifetime of tropospheric Hg^0 against oxidation is 2.7 months, shorter than in previous models. Fast Hg^{II} atmospheric reduction must occur in order to match the 6-month lifetime of Hg against deposition implied by the observed atmospheric variability of total gaseous mercury (TGM$\equiv Hg^0+Hg^{II}(g)$). Reduction is implemented in GEOS-Chem as photolysis of aqueous-phase Hg^{II}-organic complexes in aerosols and clouds. The resulting simulated TGM lifetime of 5.2 months matches mean observed TGM and its variability. The model reproduces observed Hg wet deposition fluxes over North America, Europe, and China, including the maximum over the US Gulf Coast driven by HgBr oxidation by NO_2 and HO_2. Low Hg wet deposition observed over rural China is attributed to

fast Hg^{II} reduction in the presence of high organic aerosol concentrations. I find 80% of global Hg^{II} deposition takes place over the oceans, most of which takes place to the tropical oceans due to the availability of HO_2 and NO_2 for second-stage HgBr oxidation.

2

Historical mercury releases from commercial products: global environmental implications

Abstract

The intentional use of mercury (Hg) in products and processes ('commercial Hg') has contributed a large and previously unquantified anthropogenic source of Hg to the global environment over the industrial era, with major implications for Hg accumulation in environmental reservoirs. We present a global inventory of commercial Hg uses and releases to the atmosphere, water, soil, and landfills from 1850 to 2010. Previous inventories of anthropogenic Hg releases have focused almost exclusively on atmospheric emissions from 'by-product' sectors (e.g., fossil fuel combustion). Cumulative anthropogenic atmospheric Hg emissions since 1850 have recently been estimated at 215 Gg (only including commercial Hg releases from chlor-alkali production, waste incineration, and mining). We find that other commercial Hg uses and non-atmospheric releases from chlor-alkali and mining result in an additional 540 Gg Hg released to the global environment since 1850 (air: 20%, wa-

A version of this chapter was published with Daniel J. Jacob, Helen M. Amos, David G. Streets, and Elsie M. Sunderland, Environmental Science & Technology, vol 48, p. 10242-10250, 2014.

ter: 30%, soil: 30%, landfills: 20%). Some of this release has been sequestered in landfills and benthic sediments, but 310 Gg actively cycles among geochemical reservoirs and contributes to elevated present-day environmental Hg concentrations. Commercial Hg use peaked in 1970 and has declined sharply since. We use our inventory of historical environmental releases to force a global biogeochemical model that includes new estimates of the global burial in ocean margin sediments. Accounting for commercial Hg releases improves model consistency with observed atmospheric concentrations and associated historical trends.

2.1 Introduction

Methylmercury, a neurotoxin formed from inorganic mercury (Hg), bioaccumulates in aquatic food chains and adversely affects human health on a global scale through fish consumption(Mahaffey et al., 2011; Karagas et al., 2012). Hg has been mined since antiquity and extensively used in many commercial products Nriagu (1979), leading to its eventual release to the environment upon disposal. Hg cycles rapidly between air, water, and soil reservoirs so that releases to any of these reservoirs can contribute to oceanic Hg levels (Amos et al., 2013). Background levels of Hg in the environment have increased ~3 fold since pre-industrial times (Fitzgerald et al., 1998) and may be 5-10 times above natural levels (Amos et al., 2013; Serrano et al., 2013). This has been conventionally attributed to atmospheric emissions from mining and combustion(Mason et al., 1994; Selin et al., 2008). Here we show that releases of commercial Hg to air, water, and soil have contributed a large, previously unquantified source of Hg to the global environment over the industrial era, with major implications for historical and present-day conditions.

Hg is transferred from its stable lithospheric reservoir to surface environmental reservoirs by natural geological processes, fossil fuel combustion, and mining (including for commercial products). It then is exchanged between the atmosphere, surface ocean, and terrestrial ecosystems on time scales of years to decades (Amos et al., 2013). The atmospheric lifetime of gaseous elemental Hg is of the order of a year, allowing transport and deposition on a global scale (Slemr et al., 1985). Hg is eventually transferred to long-lived soil and deep-ocean pools over hundreds of years, and returns to the lithosphere to close the cycle on a timescale of thousands of years (Andren & Nriagu, 1979). The lasting environmental legacy of Hg released to surface reservoirs mandates a historical perspective for understanding present-day environmental burdens and for evaluating the effectiveness

of regulatory actions such as the Minamata Convention (UNEP, 2013a).

While an estimated 112 Gg of Hg have been emitted directly to the atmosphere since 1850 from by-product sources (fuel combustion, cement production, metals smelting, large-scale gold mining with non-Hg methods), 720 Gg of Hg were mined during the same period for commercial use (Streets et al., 2011). This 'commercial Hg' includes Hg-containing products (e.g. batteries) and manufacturing processes that involve Hg (e.g. vinyl chloride monomer production). Commercial Hg enters the environment either during use or following product disposal. Previous studies have estimated present-day environmental releases of Hg from commercial products and processes only for a subset of uses and fate pathways, with a predominant focus on atmospheric emissions. (Jasinski, 1995; Engineering, 2001; ACAP, 2005; Cain et al., 2007; Kindbom & Munthe, 2007; Pacyna et al., 2010; Pirrone et al., 2010; Wilson et al., 2010; Sundseth et al., 2011; AMAP/UNEP, 2013; Chakraborty et al., 2013). Streets et al. (2011) estimate that 103 Gg were emitted to the atmosphere from chlor-alkali production, mining of silver and gold using Hg amalgamation, and waste incineration from the 720 Gg of Hg mined for commercial use since 1850, leaving unresolved the fate of the remaining 617 Gg.

Commercial Hg can enter the environment by various pathways. For example, Hg in paint rapidly volatilizes to the atmosphere (Taylor, 1965). The chemical manufacturing industry historically discharged large amounts of Hg directly into waterways, reflected by legacy contamination in many estuaries today (D'Itri & D'Itri, 1977; Rudd et al., 1983; Gill et al., 1999; Kocman et al., 2013). Hg-containing agricultural fungicides and pesticides were applied to soil in large quantities for much of the 20th century (Rissanen & Miettinen, 1972). Discarded Hg-containing batteries have generally been incinerated or landfilled (U.S. Environmental Protection Agency, 1992; Li et al., 2010). More recently, many industries have made progress toward recycling Hg in commercial products or phasing out its use (Brooks & Matos, 2005). Here we quantify the global time-dependent historical releases of commercial Hg to different environmental reservoirs (air, water, soil, landfills), and include these in a global biogeochemical model (Amos et al., 2013) to investigate their impact on historical and present-day global Hg accumulation. Water releases include effluent discharges to both estuaries and inland freshwater systems, and soil releases are deposited to soil or vegetation. A current conundrum that we try to resolve is the apparent inconsistency between anthropogenic atmospheric emission inventories, which indicate rising or flat emissions over the past decades (Wilson et al., 2010; Streets et al., 2011), and environmental archives, which often imply

a peak in atmospheric Hg deposition in the 1970s (Kamman & Engstrom, 2002; Engstrom et al., 2007; Fain et al., 2009; Allan et al., 2013). Atmospheric observations also indicate a 20% to 50% decrease in total gaseous mercury in the Northern Hemisphere since 1995 (Slemr et al., 2011; Soerensen et al., 2012), which Soerensen et al. (2012) attributed to declining ocean evasion driven by changes in seawater concentrations. Commercial use of Hg peaked in the 1970s and has declined dramatically since (Hylander & Meili, 2003; Streets et al., 2011), and we investigate the role of the related decline in commercial Hg releases in driving environmental trends.

2.2 Methods

We present a global, historical analysis tracking Hg from when it is mined, through all intentional uses and fate pathways, to its final time-dependent releases to different environmental reservoirs. Commercial Hg uses are grouped by similar environmental release patterns for a total of 14 use categories (Table 2.1). We estimate global environmental releases of Hg and track recycled and landfilled quantities from each use category on a decadal scale between 1850 and 2010. We first estimate the quantity of Hg consumed in each use category constrained by the total amount of Hg mined globally. We then distribute commercial Hg to environmental reservoirs following a simplified substance flow analysis approach that aims to quantify each transfer of Hg over its life cycle (Engineering, 2001, e.g.). Finally, we investigate the environmental impacts of these global time-dependent releases using a seven-box biogeochemical Hg model.

2.2.1 Global Commercial Hg Consumption Patterns, 1850-2010

We assume that significant Hg release from non-mining commercial Hg uses began in 1850. Anthropogenic releases prior to 1850 were mainly from mining (Streets et al., 2011). Overall decadal estimates of the magnitude of Hg used throughout the industrial era are constrained by global primary production of Hg from mining between 1850 and 1980 (Hylander & Meili, 2003; Streets et al., 2011) combined with changes in the Hg supply available for consumption due to government stockpiling(2012) (Figure 2.1). We assume that primary mined Hg that is not stockpiled is used in products and processes within a decade. Secondary Hg sources (releases from strategic stockpiles, recovery from mining and smelting, and recycling of Hg-containing products) became significant after 1980 (Jasinski, 1995; Maxson, 2004; Brooks & Matos, 2005). Therefore, for 1990-2010, we use total

Category name	Description
Chlor-Alkali Plants	Electrochemical production of caustic soda and chlorine with Hg cathode
Silver and Large-scale Gold Mining	Extraction from ore by Hg amalgamation
Artisanal and Small-Scale Gold Mining (ASGM)	Hg amalgamation by individual miners
Vinyl Chloride Monomer (VCM) and Other Chemical	Production of chemicals with Hg catalysts, felt hat manufacturing, and laboratory uses
Paint	Hg fungicide in marine anti-fouling paint, felt hat manufacturing, and laboratory uses
Lamps	All types of Hg-containing lightbulbs (fluorescent, high intensity discharge, etc.)
Batteries	Button cells and cylinders using Hg as cathode or to prevent corrosion
Wiring Devices and Industrial Measuring Devices	Switches and relays, thermostats, barometers, manometers
Medical Devices	Thermometers and sphygmomanometers (blood pressure meters)
Pharmaceuticals and Personal Care Products	Vaccines and medicines, soaps, cosmetics
Dental amalgam	Cavity fillings with Hg/silver/tin/copper amalgam
Dyes/Vermilion	Pigments containing Hg compounds
Pesticides and Fertilizer	Fungicides used in agriculture and pulp and paper
Explosives/Weapons	Munitions, blasting caps, fireworks
Other	Ritual, cultural, and miscellaneous uses

Table 2.1: Intentional uses of Hg in products and processes.

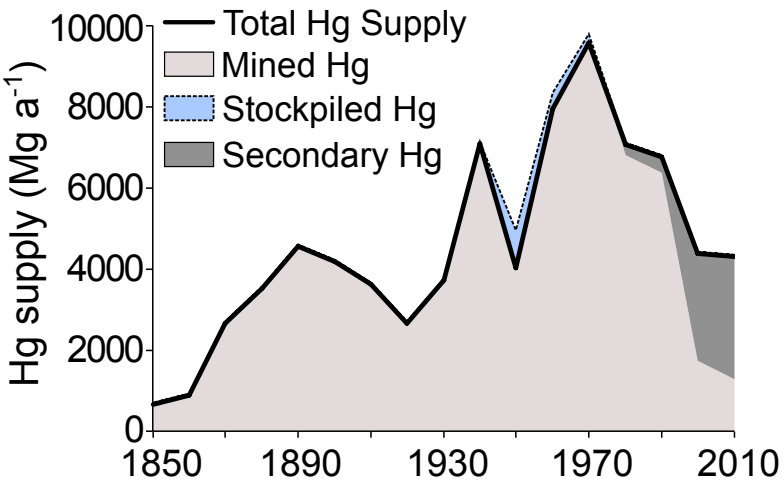

Figure 2.1: Historical global supply of Hg for commercial uses. This supply includes primary mined Hg (1850-2008 data from Streets et al. (2011)), minus the amount stockpiled by the United States between 1945 and 1970, and augmented by secondary Hg including recycled, recovered as a byproduct, and released from stockpiles after 1980.

Hg consumption from Wilson et al. (2010) that includes both primary mining and secondary sources. Wilson et al. (2010) do not fully account for Hg consumption in liquid crystal display (LCD) screens (and potentially other specific uses), so total Hg consumption in recent decades may be underestimated (AMAP/UNEP, 2008).

We then partition the global total Hg supply into individual uses. Methods used to estimate Hg consumption for each category vary depending on data availability. We divide countries into two groups, developed countries (North America, OECD/EU Europe, Oceania) and developing countries including economies in transition (rest of world), based on similarities in environmental regulations and control technologies within each group that lead to differences in Hg use and release patterns. Data from Streets et al. (2011) are used to constrain total Hg consumed globally for the chlor-alkali industry between 1850 and 1930 and silver and gold mining between 1850 and 1990, including artisanal and small-scale gold mining (ASGM). Decadal use patterns available for the United States (USGS/Bureau of Mines, 1929; U.S. Bureau of Mines, 1968) are used to estimate global consumption of Hg by the remaining uses for 1850-1960. During this period, the US consumed $\sim$ 25% of total Hg mined globally and its Hg use data is the most complete. This may underestimate the fraction of Hg used by the chlor-alkali industry, historically more important in Western Europe than in the US (Emerson, 1974). However, using available data from Sweden (Hylander & Meili, 2005) for Hg consumption patterns instead of the US does not affect significantly our estimate of all-time environmental releases and model results

(see SI).

The ca. 1970 onset of environmental regulations targeting Hg releases in developed countries resulted in major changes in Hg consumption patterns (D'Itri & D'Itri, 1977). We therefore estimate Hg consumption separately for developing countries from 1970 to present. For 1970 and 1980, we divide the global total Hg supply between the developed and developing world by the fraction of global GDP held by each group of countries United Nations Statistics Division (2012).Consumption patterns for the developed world are assumed to follow those of the US in 1970 and 1980 (American Metal Mart, 1995) .Consumption patterns for the developing world in 1970 and 1980 are assumed to be similar to those of the US in 1960, when Hg use was unregulated. For 1990-2000, we use regionally resolved Hg consumption data from Wilson et al. (2010). For 2010, we use annual consumption data from AMAP/UNEP (2013) for the uses available, and extrapolate the 2000-2005 trend from Wilson et al. (2010) for the remaining uses.

2.2.2 Environmental Releases of Commercial Hg

Figure 2.2 shows a generic diagram of our simplified substance flow analysis that tracks the fate of commercial Hg for each decade and use category (Table 2.1) to its eventual release in different environmental reservoirs. First, the Hg consumed in each use category is divided among direct releases to air, water, and soil, recycling, and disposal to solid waste or wastewater treatment ('Tier 1' distribution factors). Certain use categories have additional disposal pathways with environmental fates that are distinct from general solid waste or wastewater disposal. Hg entering the three waste disposal pathways is divided further ('Tier 2' distribution factors). Solid waste is split between disposal in landfills, incineration, and direct release to air and to soil (representing open burning and dumping of waste). Wastewater is partially captured in sewage sludge and the rest is released to water. 'Other Disposal' is distributed between air, land, and landfills. A third tier of distribution factors is needed to characterize environmental releases for solid waste incineration (emitted to air, or captured in ash and then deposited to soil or in landfills) and sewage sludge (incinerated and emitted to air, applied to soil, or disposed of in landfills). Historical waste incineration emissions are estimated in Streets et al. (2011) using a population-based method and total waste activity data, but here we generate a different estimate that involves tracking the Hg content in products that are incinerated (see Figure A.1 and discussion in the Appendix A).

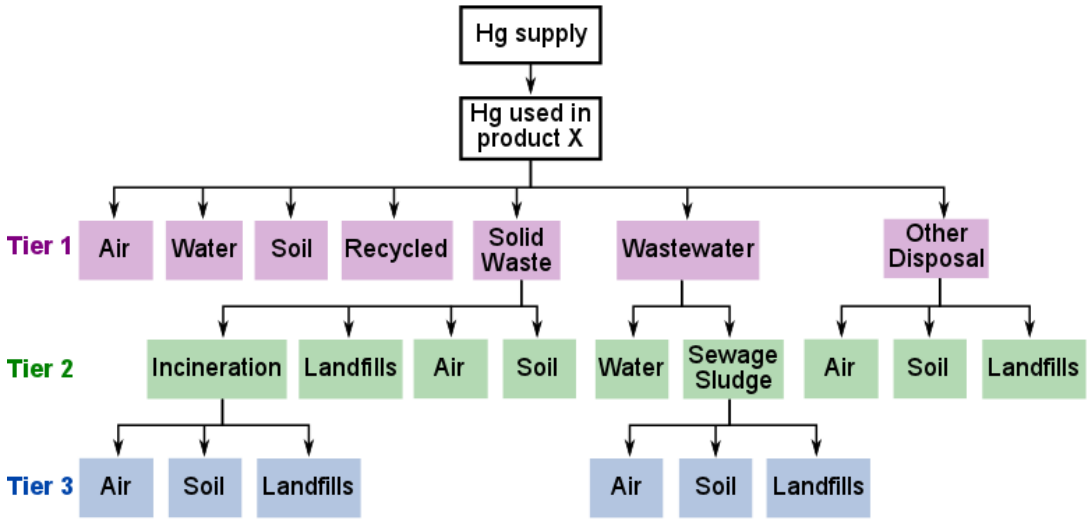

Figure 2.2: Generic substance flow analysis diagram for commercial Hg. Each arrow is a distribution factor quantified in this work (Table A.5). This diagram applies to all intentional use categories with the exception of dental amalgam, which has additional pathways (see Methods, section 2.2, and Figure A.2). ``Other disposal'' refers to medical waste incineration (for Medical Devices and Dental use categories) and iron and steel recycling (for Wiring Devices and Industrial Measuring Devices use category).

Dental amalgam Hg may be released to air, water, and soil upon cremation and has unique fate pathways not represented in Figure 2.2 (see Figure A.2). Hg in teeth is assumed to be permanently sequestered during burial as there is no evidence of release to cemetery soil (Arenholt-Bindslev, 1998).

Distribution factors for each use category were estimated from a variety of sources (Tables A.1-A.4). Distribution factors are applied globally for 1850-1960, and separately for the developed and developing world between 1970 and 2010. We use previous decadal estimates from Streets et al. (2011) for global atmospheric emissions from chlor-alkali plants, silver and large-scale gold mining, and ASGM, except for 2010 ASGM emissions that are based on AMAP/UNEP (2013) estimates.

Temporal variability in distribution factors is governed by the availability of evidence that releases have changed from one decade to another due to regulatory controls and other factors. Global distribution factors are held constant in time through 1950, with variation in 1960 for three use categories (VCM and Other Chemical, Paint, and Pesticides and Fertilizer). This reflects significant changes in consumption patterns (a change from chemicals to laboratory uses, marine anti-fouling paint to home interior/exterior latex paint, and agricultural to pulp and paper fungicides, respectively). Different distribution factors in the developed world are applied for each decade between 1970 and 2010. Developing world distribution factors are assumed con-

stant for 1970-2010. The 'Other' category in Table 2.1 (9% of 1850-2010 global consumption) encompasses a diverse set of uses with an unknown distribution, and we assume for this category the average fate of all other categories.

Releases to different environmental reservoirs are calculated on a global scale by multiplying the Hg consumed in each use category and decade by the corresponding distribution factors. The only exceptions are for Wiring Devices and Industrial Measuring Devices and Dental use categories, for which we estimate delayed releases based on the long lifetime of Hg in these products after the original consumption of Hg. Most products are disposed of and enter the environment within the decade when they were produced, and manufacturing processes generally consume and release Hg within a year (U.S. Environmental Protection Agency, 1992; Jasinski, 1995; U.S. Environmental Protection Agency, 1997; Floyd et al., 2002; Hagreen & Lourie, 2004; ACAP, 2005; Cain et al., 2007; UNEP, 2008). Our inventory has a decadal resolution, thus delays of less than a decade between production and release can be ignored. Products in the Wiring Devices and Industrial Measuring Devices category are often in use for 20-50 years before disposal (U.S. Environmental Protection Agency, 1992; Jasinski, 1995; Engineering, 2001; Hagreen & Lourie, 2004; ACAP, 2005). For these products we follow the methods of Jasinski (1995) and Cain et al. (2007) and assume that 10% are discarded after 10 years, 40% after 30 years, and the remaining 50% after 50 years. Dental amalgams generally remain in living teeth for 10 to 30 years or more. We estimate excretion and exhalation releases from dental amalgam to air and water during this time and track the remaining Hg that will be released through cremation pathways or permanently stored through burial after 30 to 50 years, depending on average life expectancy (United Nations Department of Economic and Social Affairs Population Division, 2011) and ages of individuals receiving fillings (Cain et al., 2007).

Recycled Hg is estimated separately for (1) internal reuse of Hg in chemicals manufacturing and large-scale mining (U.S. Environmental Protection Agency, 1992; NRDC., 2006; UNEP, 2013b), (2) external recycling of products like batteries that returns Hg to the global Hg supply for future use (UNEP, 2013b). External recycling did not become widespread until 1990 (Jasinski, 1995). We do not tie our estimates of recycled Hg to global Hg supply, and instead use estimated total Hg consumption from Wilson et al. (2010). that includes secondary sources for 1990 - present. Following UNEP methods (UNEP, 2013b), we assume that no Hg is released to the environment during the recycling process.

2.2.3 Implications for the Biogeochemical Hg Cycle and Atmospheric Trends

We use the fully-coupled global biogeochemical Hg box model from Amos et al. (2013, 2014) to track the fate of commercial Hg after it has been released to the environment. The model includes seven reservoirs that represent the atmosphere, ocean (surface, subsurface, deep), and terrestrial pools (fast, slow, armored). Fluxes between reservoirs are determined by first-order rate coefficients applied to the inventory of the exporting reservoir (Table A.5). Riverine rate coefficients have been updated by Amos et al. (2014) to include the permanent removal of Hg to benthic sediment at ocean margins. Primary anthropogenic and geogenic emissions are treated as external forcings.

We added a landfill reservoir to this model. Landfills can emit Hg into the atmosphere through vent pipes, diffusion from cover soil, and from the "working face" where waste is exposed and actively dumped (Li et al., 2010). They can also release Hg into groundwater and soils through the base of the landfill but this appears to be negligible (Li et al., 2010). Data available on Hg emissions for managed landfills in China (Li et al., 2010; Zhu et al., 2013), the United States (Lindberg et al., 2005), and Korea (Kim et al., 2010) indicate very low values. We estimate a mean lifetime of 20,000 years for Hg in landfills by combining emissions values for each site with estimated Hg reservoirs inferred from the waste content and disposal magnitudes. Landfills can therefore effectively be viewed as a permanent sink on centurial time scales. Commercial Hg enters the biogeochemical cycle as an external forcing to the atmosphere, water, soil, and landfills. Hg releases to soil are distributed among the three terrestrial reservoirs of the model in the same manner as atmospherically deposited Hg (Amos et al., 2013). Hg releases to water are distributed to inland freshwater systems (90%) and to estuaries (10%) based on the locations of present-day point sources (Amos et al., 2014; Kocman et al., prep). We assume that 75% of the Hg input to inland freshwater systems is sequestered permanently in sediments and 25% evades to the atmosphere, based on models for a variety of lakes and rivers (Knightes et al., 2009). Based on previous work, we assume that 50% of the Hg directly released to estuaries is transported to the surface ocean, 10% evades to the atmosphere, and 40% is sequestered permanently in coastal sediments (Mason et al., 1999; Sunderland et al., 2010). In this manner, we estimate that 70% of Hg released to water is permanently sequestered, 23% enters the atmosphere, and 7% enters the surface ocean.

We apply the box model to time-dependent simulations from 2000 BC to 2010 following the methods

described in Amos et al. (2013) We simulate 1850-2010 with anthropogenic atmospheric emissions from Streets et al. (2011) plus the releases from commercial Hg quantified in this study. We evaluate the model with three global observational constraints, following Amos et al. (2013): (1) the present-day atmospheric inventory (best estimate of 5000 Mg, range 4600-5600 Mg), (2) the present-day mean concentration in the upper (0-1500 m) ocean (best estimate of 1.0 pM, range 0.5-1.5 pM), and (3) the relative anthropogenic enrichment factor (AEF) in atmospheric deposition between pre-industrial and present-day (best estimate of 3, range 2 to 5). We define AEF as the ratio of 1985-2000 deposition to 1760-1880 deposition (Sonke, 2014; Amos et al., prep).

2.3 Results and Discussion

2.3.1 Global Commercial Hg Consumption Patterns, 1850-2010

Figure 2.3 shows the global commercial use of Hg since 1850 for all categories in Table 2.1, and partitioned between the developed and developing world after 1970. Prior to 1900, almost all mined Hg was used in silver and gold mining. Hg uses diversified greatly in the 20th century. Consumption in large-scale mining declined following the end of the gold rush and as extraction methods that did not require Hg became widespread. The 1940s peak in Figure 2.3 is driven by chemicals production for munitions during WWII. The 1970s peak represents the height of Hg use in consumer products like paint and batteries and in chlor-alkali plants. Total consumption declined after the 1970s when many developed countries implemented regulations on Hg uses and environmental releases. Since 1990, the developing world has dominated global Hg consumption. ASGM in developing countries is presently the largest use of Hg globally, and is increasing (Telmer & Veiga, 2009; AMAP/UNEP, 2013).

2.3.2 Environmental Releases of Commercial Hg

Figure 2.4 compares the historical atmospheric emissions inventory of Streets et al. (2011) (including sources from fuel combustion, cement production, metals smelting, mining, chlor-alkali plants, and some waste incineration) with our best estimate of additional releases to air, water, soil, and landfills from commercial Hg. Streets et al. (2011) estimate total emissions to air of 215 Gg since 1850. We estimate additional environmental releases over the same period of 540 Gg. Of these, 230 Gg are permanently sequestered in landfills or in benthic

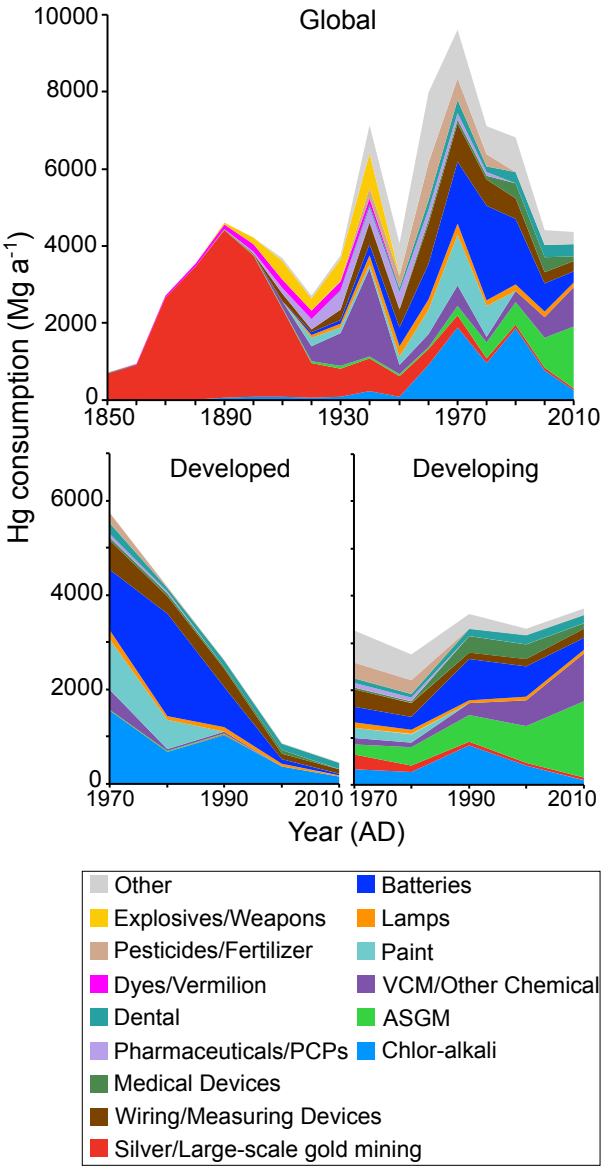

Figure 2.3: Global historical Hg consumption in commercial products. Consumption is partitioned for each decade between the different use categories of Table 2.1, and further partitioned between developed countries and developing countries after 1970.

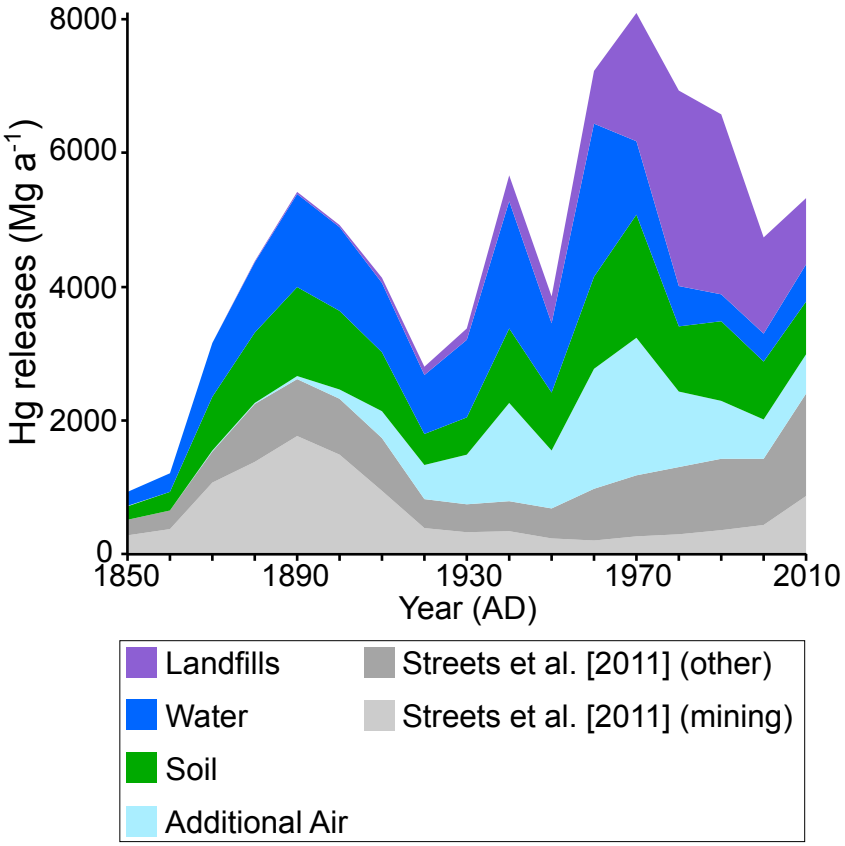

Figure 2.4: Historical global releases of Hg to the environment. The Streets et al. (2011) inventory includes atmospheric releases from combustion, smelting, mining, and chlor-alkali plants. Additional air, soil, water, and landfill releases shown are associated with commercial Hg products as quantified in this work.

sediments of freshwater and estuarine systems. The remaining 310 Gg (including 110 Gg emitted to air) cycle between biogeochemical reservoirs and represent a larger anthropogenic perturbation to the global Hg cycle than the 215 Gg of Streets et al. (2011). Commercial Hg thus represents a major, previously unquantified source of Hg to the global environment. The temporal pattern of anthropogenic Hg releases is also affected. Whereas Streets et al. (2011) indicate rising emissions since 1950, our estimate shows a decline in total releases from 1970 to 2000.

Figure 2.5 presents the historical contributions of individual commercial use categories to global environmental releases to air, water, soil, and landfills. Releases to air, water, and soil all show similar enhancements from late 19th-century mining. Differences are attributable to changes in the fate of commercial Hg over time. Emissions to air peak in 1970, mainly due to paint volatilization and incineration of batteries. Although Hg use

in batteries increased from 1970 to 1980, open-air waste burning at landfills was eliminated in developed countries like the US during this period following solid waste regulations (U.S. Environmental Protection Agency, 2003; Association, 2008). Use of explosives and weapons was a major emitter to air during 1900-1950 with a peak in WWII. Water releases also exhibit a peak during WWII, due to laboratory uses and chemicals manufacturing. The overall maximum occurs in 1960, with a steep subsequent decline following implementation of chlor-alkali liquid effluent regulations in the early 1970s in North America and Europe (Flewelling, 1971; Thorleifson, 1998). Implementation of wastewater treatment from the 1980s onward led to even greater declines in water releases (URS Research Company Hazards Assessment Directorate, 1975), but contributes a small amount to soils due to application of Hg-containing sludges (Cain et al., 2007; UNEP, 2013b). Similarly, chlor-alkali plants began capturing Hg in sludges in the 1970s, which were subsequently dumped on land or landfilled on-site (Thorleifson, 1998). The 1970 peak in soil releases is driven by Hg used in chlor-alkali plants and Hg-containing pesticides and fertilizer that were applied directly to land.

2.3.3 Implications for the Biogeochemical Hg Cycle and Atmospheric Trends.

Figure 2.6 shows simulated atmospheric Hg from 1850-present after adding our historical inventory of commercial Hg emissions and releases to the global biogeochemical Hg model described previously. Figure A.3 gives present-day reservoirs and flows. Our simulated present-day atmospheric reservoir is 5800 Mg, the mean Hg concentration in the upper ocean is 1.5 pM, and the AEF for atmospheric deposition is 4.4. The original Amos et al.4 simulation not including commercial Hg yielded a present-day atmosphere of 5300 Mg, but did not account for burial of Hg in ocean margin sediments (Amos et al., 2014). Accounting for burial without commercial Hg results in an atmosphere that is too low (2700 Mg). Conversely, including commercial Hg in the original Amos et al.4 simulation without burial of riverine Hg would yield a present-day atmospheric reservoir of 10,000 Mg, much higher than observed.

Our simulated present-day atmospheric reservoir of 5800 Mg is slightly higher than the observational range (4600-5600 Mg), but this could be accommodated by uncertainty in Hg reemission from soils (Krabbenhoft, 2013; Obrist et al., 2014). The atmospheric increase over the past decade (Figure 2.6) is driven by rising anthropogenic emissions in the Streets et al. (2011) inventory (primarily from coal burning in Asia) and

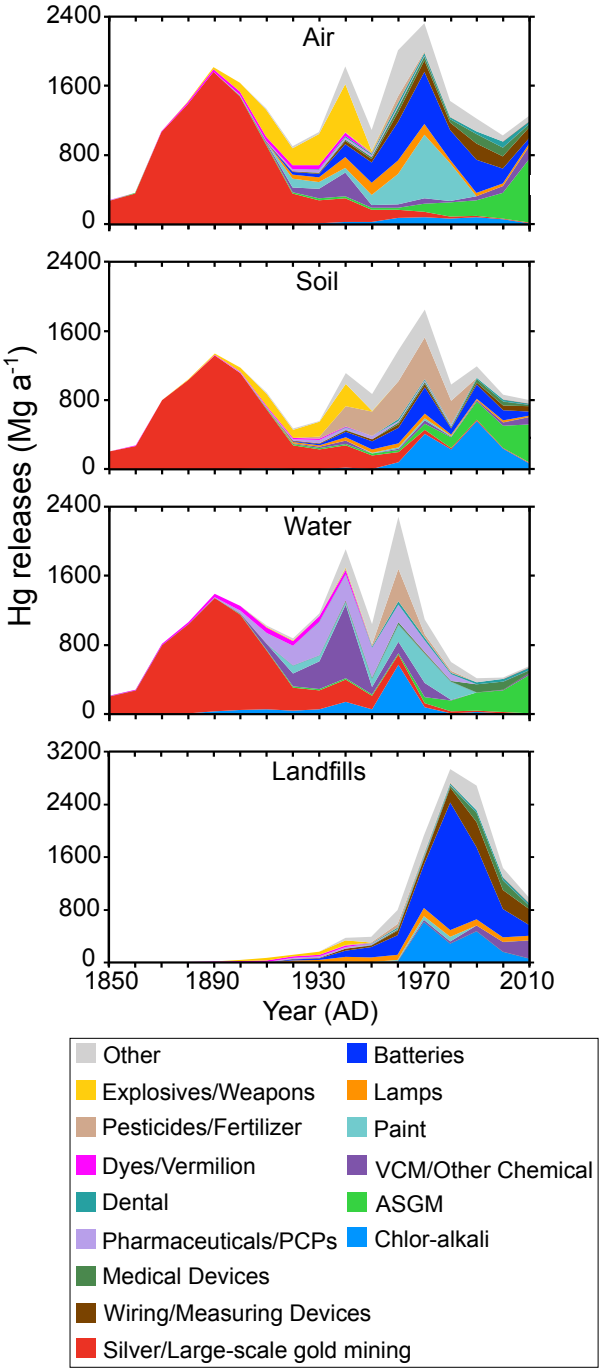

Figure 2.5: Global historical releases of commercial Hg to environmental reservoirs by use category.

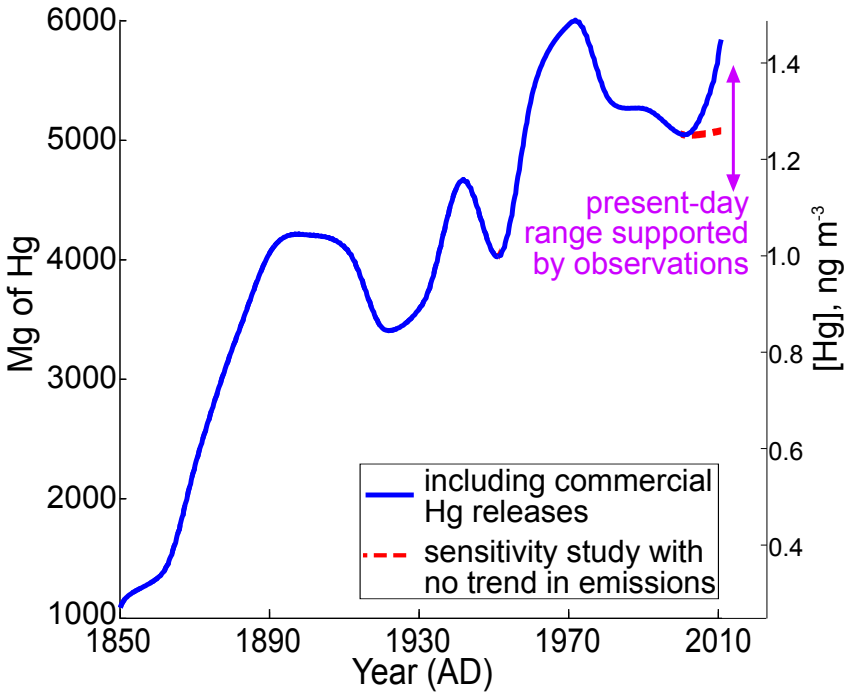

Figure 2.6: Trend in simulated atmospheric Hg from 1850 to 2010. Results for mass (left axis) and implied mean tropospheric concentration (right axis) are shown for the updated biogeochemical model including historical commercial Hg releases. The dashed line shows results from a sensitivity simulation with Streets et al. (2011) anthropogenic atmospheric emissions held constant from 2000 to 2010 (see text).

rising releases from ASGM(AMAP/UNEP, 2013) (Figures 2.3 and 2.4). However, Wilson et al. (2010) and AMAP/UNEP (2013) suggest that global total anthropogenic emissions have in fact remained constant since 2000. AMAP/UNEP estimate that coal combustion emissions specifically have remained constant since at least 2005, as increased energy production efficiency and control technologies have compensated for increases in fuel burned (AMAP/UNEP, 2013).) Moreover, the ASGM increase since 2005 may be an artifact of improved reporting (AMAP/UNEP, 2013). We conducted a sensitivity simulation holding constant anthropogenic atmospheric emissions for the 2000-2010 period, and results are shown as the dashed line in Figure 2.6. We obtain in that simulation an atmospheric reservoir of 5100 Mg, more consistent with observations, and unchanged upper ocean concentration of 1.5 pM and AEF of 4.4.

Inclusion of commercial Hg releases in the global biogeochemical model improves model consistency with archival records of atmospheric deposition. Lake sediments and ombrotrophic peat bogs generally indicate a gradual rise over the industrial era with a peak in the 1970s(Kamman & Engstrom, 2002; Engstrom et al., 2007; Fain et al., 2009; Allan et al., 2013). Figure 2.6 indicates a 1970s peak in simulated atmospheric Hg and a muted 19th century mining signal. Without the inclusion of commercial Hg, model deposition increases from 1970 to present and there is a prominent 19th century peak (Amos et al., 2013). Our inventory also helps to explain the observed 1990-present declines in atmospheric Hg over North America and Europe (Slemr et al., 2011; Soerensen et al., 2012). The model increase from 2000 to 2010 is driven by increasing global anthropogenic atmospheric emissions in the Streets et al. (2011) inventory, but holding these constant as another emissions inventory suggests (Wilson et al., 2010; AMAP/UNEP, 2013) results in a relatively flat global trend (see previous paragraph and Figure 2.6).

Our work shows that environmental releases of commercial Hg to air, water, and soil over the industrial period have represented a major and previously unquantified perturbation to Hg in the global environment. The legacy of this source in oceanic and terrestrial reservoirs has important implications for future ecosystem responses to changes in emissions. Addressing the impact of commercial Hg on regional-scale environmental Hg loadings and atmospheric trends requires better information on the geographical distribution of commercial Hg releases. Better understanding of the role of soils for long-term storage of anthropogenic Hg is also critically needed.

Acknowledgements

We acknowledge financial support for this work from the Harvard School of Engineering and Applied Sciences TomKat Fund and the Atmospheric Chemistry Program of the National Science Foundation. H.M.H. acknowledges support from NSF GRFP. We thank the editor and three anonymous reviewers for their thoughtful suggestions.

SUPPORTING INFORMATION. Additional information on data sources used to estimate distribution factors (Table A.1), distribution factors used in this study (Tables A.2-A.4), model rate coefficients (Table A.5), waste incineration emissions estimates (Figure A.1), release pathways for dental amalgam Hg (Figure A.2), present-day reservoirs and flows in the global biogeochemical model (Figure A.3), and results from sensitivity studies on the uncertainty in chlor-alkali Hg consumption. This material is available free of charge via the Internet at http://pubs.acs.org.

3

A new mechanism for atmospheric mercury redox chemistry: Implications for the global mercury budget

Abstract

Abstract. Mercury (Hg) is emitted to the atmosphere mainly as volatile elemental Hg^0. Oxidation to water-soluble Hg^{II} controls Hg deposition to ecosystems. Here we implement a new mechanism for atmospheric Hg^0/Hg^{II} redox chemistry in the GEOS-Chem global model and examine the implications for the global atmospheric Hg budget and deposition patterns. Our simulation includes a new coupling of GEOS-Chem to an ocean general circulation model (MITgcm), enabling a global 3-D representation of atmosphere-ocean Hg^0/Hg^{II} cycling. We find that atomic bromine (Br) of marine organobromine origin is the main atmospheric Hg^0 oxidant, and that second-stage HgBr oxidation is mainly by the NO_2 and HO_2 radicals. The resulting

A version of this chapter was submitted with Daniel J. Jacob, Yanxu Zhang, Theodore S. Dibble, Franz Slemr, Helen M. Amos, Johan A. Schmidt, Elizabeth S. Corbitt, Eloïse A. Marais, and Elsie M. Sunderland to Atmospheric Chemistry and Physics. The discussion paper is currently in review, doi:10.5194/acp-2016-1165.

lifetime of tropospheric Hg^0 against oxidation is 2.7 months, shorter than in previous models. Fast Hg^{II} atmospheric reduction must occur in order to match the ~6-month lifetime of Hg against deposition implied by the observed atmospheric variability of total gaseous mercury (TGM≡Hg^0+Hg^{II}(g)). We implement this reduction in GEOS-Chem as photolysis of aqueous-phase Hg^{II} -organic complexes in aerosols and clouds, resulting in a TGM lifetime of 5.2 months against deposition and matching both mean observed TGM and its variability. Model sensitivity analysis shows that the interhemispheric gradient of TGM, previously used to infer a longer Hg lifetime against deposition, is misleading because southern hemisphere Hg mainly originates from oceanic emissions rather than transport from the northern hemisphere. The model reproduces the observed seasonal TGM variation at northern mid-latitudes (maximum in February, minimum in September) driven by chemistry and oceanic evasion, but does not reproduce the lack of seasonality observed at southern hemisphere marine sites. Aircraft observations in the lowermost stratosphere show a strong TGM-ozone relationship indicative of fast Hg^0 oxidation, but we show that this relationship provides only a weak test of Hg chemistry because it is also influenced by mixing. The model reproduces observed Hg wet deposition fluxes over North America, Europe, and China, including the maximum over the US Gulf Coast driven by HgBr oxidation by NO_2 and HO_2. Low Hg wet deposition observed over rural China is attributed to fast Hg^{II} reduction in the presence of high organic aerosol concentrations. We find that 80% of global Hg^{II} deposition takes place over the oceans, reflecting the marine origin of Br and low concentrations of marine organics for Hg^{II} reduction, and most of that deposition takes place to the tropical oceans due to the availability of HO_2 and NO_2 for second-stage HgBr oxidation.

3.1 Introduction

Atmospheric mercury (Hg) cycles between two stable redox forms, elemental (Hg^0) and divalent (Hg^{II}). Most Hg emissions are as gaseous elemental Hg^0 , which is relatively inert and sparingly soluble in water. Hg^0 is oxidized in the atmosphere to Hg^{II} by loss of its two $6s^2$ electrons. Hg^{II} salts are water-soluble, partition into the aerosol, are efficiently removed from the atmosphere by wet and dry deposition, but can also be reduced back to Hg^0 . Understanding atmospheric Hg redox chemistry is critical for determining where Hg will be deposited globally. Here we propose an updated Hg^0 /Hg^{II} redox mechanism, incorporating recent kinetic

data and other observational constraints, for use in atmospheric models. We implement the mechanism in the GEOS-Chem global model (Bey et al., 2001; Holmes et al., 2010) and examine the implications for the global atmospheric Hg budget and deposition patterns.

Older models assumed gas-phase OH and ozone to be the dominant Hg^0 oxidants (Bergan & Rodhe, 2001; Dastoor & Larocque, 2004; Selin et al., 2007; Bullock et al., 2008; Travnikov & Ilyin, 2009; De Simone et al., 2014; Gencarelli et al., 2014). It is now well established that the corresponding HgOH and HgO products are too thermally unstable to enable oxidation to Hg^{II} under atmospheric conditions (Shepler & Peterson, 2003; Goodsite et al., 2004; Calvert & Lindberg, 2005; Hynes et al., 2009; Jones et al., 2016). The importance of Br atoms for Hg^0 oxidation was first recognized to explain atmospheric mercury depletion events occurring in the Arctic boundary layer in spring (Schroeder et al., 1998), where sea salt photochemistry provides a large Br source (Fan & Jacob, 1992; Steffen et al., 2008; Simpson et al., 2015). Oxidation of Hg^0 to Hg^{II} by Br is a two-stage exothermic mechanism where the second stage conversion of Hg^{I} to Hg^{II} can be carried out by a number of radical oxidants (Goodsite et al., 2004; Dibble et al., 2012). Holmes et al. (2006) first suggested Br atoms could be the main Hg^0 oxidant on a global scale, with Br originating principally from photochemical decomposition of bromoform emitted by phytoplankton (Yang et al., 2005). More recent observations of background tropospheric BrO point to ubiquitous Br radical chemistry in the troposphere (Theys et al., 2011; Wang et al., 2015). Recent aircraft observations of Hg^{II} and BrO over the Southeast US are consistent with Br atoms acting as the main Hg^0 oxidant (Gratz et al., 2015; Shah et al., 2016).

Atmospheric Hg^{II} can be deposited or alternatively reduced back to Hg^0 . Competition between these two processes determines the global patterns of Hg deposition as well as the regional fate of Hg^{II} emitted directly by combustion. Atmospheric reduction mechanisms for Hg^{II} are poorly understood but photoreduction in aquatic systems has been widely observed (Costa & Liss, 1999; Amyot et al., 2000; Mason et al., 2001). Fast in-plume reduction of Hg^{II} emitted by coal-fired power plants was reported by Edgerton et al. (2006) and Lohman et al. (2006) but more recent field observations do not suggest widespread importance (Deeds et al., 2013; Landis et al., 2014). The speciation of atmospheric Hg^{II} is unknown (Jaffe et al., 2014; Gustin et al., 2015; Jones et al., 2016). It is generally assumed from chemical equilibrium considerations that the main Hg^{II} species are $HgCl_2$ in the gas phase and Hg-chloride complexes in the aqueous phase (Hedgecock & Pirrone, 2001; Selin

et al., 2007; Holmes et al., 2009), but this has not been actually observed. Hg-chloride complexes are relatively resistant to photoreduction (Allard & Arsenie, 1991; Pehkonen & Lin, 1998). Hg^{II} also strongly binds to organic ligands, including in particular reduced sulfur complexes and carboxyl groups (Pehkonen & Lin, 1998; Haitzer et al., 2002; Ravichandran, 2004; Zheng & Hintelmann, 2009). Photoreduction of Hg^{II} bound to dissolved organic carbon (DOC) and other organic matter has been widely reported in aquatic environments (Amyot et al., 1994; Xiao et al., 1995; O'Driscoll et al., 2006; Whalin & Mason, 2006) and could also possibly take place in organic aerosols. Bash et al. (2014) found that including in-cloud aqueous photoreduction via organic acids based on the mechanism proposed by Si & Ariya (2008) improved the simulation of Hg wet deposition in a regional air quality model. Observed photochemically-driven shifts in the abundance of naturally occurring Hg isotopes in the atmosphere and precipitation support the occurrence of aqueous-phase photoreduction involving Hg^{II} -organic complexes in the atmosphere (Gratz et al., 2010; Sonke, 2011, 2015).

The GEOS-Chem model has been widely used for global simulations of atmospheric Hg and biogeochemical cycling with a focus on interpreting observations (Strode et al., 2008; Weiss-Penzias et al., 2015; Zhang et al., 2016). The Hg chemical mechanism in the current standard version of GEOS-Chem (www.geos-chem.org) is based on Holmes et al. (2010). Our updated mechanism includes more recent kinetic data and is applied with an improved GEOS-Chem simulation of halogen chemistry (Schmidt et al., 2016). As part of this work, we also introduce a new coupling of GEOS-Chem to a 3-D ocean model (Y. Zhang et al., 2015) to better interpret observed seasonal variations of atmospheric Hg in the context of both atmospheric chemistry and oceanic drivers of air-sea exchange (Soerensen et al., 2013).

3.2 Chemical mechanism

Table 3.1 lists the new chemical mechanism implemented in GEOS-Chem. Table 3.2 lists reactions proposed in the literature but subsequently estimated to be too slow to be of atmospheric relevance. Oxidation of Hg^0 to Hg^{II} in the gas phase involves a two-stage process (3.1, 3.2) with competing reactions (3.3, 3.4):

$$Hg^0 + X + M \rightarrow Hg^IX + M \tag{3.1}$$

$$Hg^IX + M \rightarrow Hg^0 + X + M \tag{3.2}$$

$$Hg^IX + Y \rightarrow Hg^0 + XY \tag{3.3}$$

$$Hg^IX + Y + M \rightarrow Hg^{II}XY + M \tag{3.4}$$

where X is the first-stage Hg^0 oxidant, Y is the second-stage Hg^I oxidant, and M is a molecule of air (Goodsite et al., 2004; Donohoue et al., 2006; Dibble et al., 2012). The Hg^I intermediate has an overall lifetime of less than a second so local steady state can be assumed. Goodsite et al. (2004) found that HgBr is sufficiently stable for Br atoms to be an effective first-stage Hg^0 oxidant, and proposed Y≡OH and Br as effective radicals to carry out the second stage of oxidation to Hg^{II} . The Cl atom can also oxidize Hg^0 to produce HgCl (Balabanov & Peterson, 2003; Donohoue et al., 2005). Dibble et al. (2012) found that a broad range of radical oxidants could oxidize HgBr and HgCl including Y≡NO_2 and HO_2, the most abundant atmospheric radicals. Other proposed first-stage gas-phase Hg^0 oxidants appear to be unimportant, including OH, O_3, I, I_2, Br_2, Cl_2, BrO, ClO, HCl, HO_2, and NO_3 (Table 3.2. Hg^0 is sparingly soluble in water but it has been suggested that fast aqueous-phase oxidation could take place in cloud droplets (Munthe & McElroy, 1992; Lin & Pehkonen, 1997, 1998; Whalin et al., 2007). We include these processes in our mechanism with O_3(aq), HOCl(aq), and OH(aq) as oxidants.

Strong complexes between Hg^{II} and organic acids may allow electrons to be transferred to Hg^{II} during photolysis (Pehkonen & Lin, 1998). Gårdfeldt & Jonsson (2003) found that direct photolysis of Hg-oxalate resulted in Hg^{II} reduction and Si & Ariya (2008) reported the same for Hg-dicarboxylates. O'Driscoll et al. (2004) reported a linear increase in the efficiency of Hg^{II} photoreduction in freshwater with increasing DOC concentrations. We assume here that Hg^{II} photreduction is dependent on the local concentration of organic aerosol (OA) and on the NO_2 photolysis frequency (j_{NO_2}) taken as proxy for for the UV actinic flux, and further assume the aerosol to be aqueous only at relative humidity greater than 35%. The scaling factor α for the reaction (Table 3.1) is adjusted in GEOS-Chem such that simulated total gaseous mercury (TGM≡Hg^0

Reaction	Rate expression[a]	Reference[b]
Gas phase		
$Hg^0 + Br + M \rightarrow HgBr + M$	$1.46 \times 10^{-32}(T/298)^{-1.86}$[$Hg^0$][Br][M]	(1)
$HgBr + M \rightarrow Hg^0 + Br$	$1.6 \times 10^{-9}(T/298)^{-1.86}\exp(-7801/T)$[HgBr][M]	(2)
$HgBr + Br \rightarrow Hg^0 + Br_2$	3.9×10^{-11}[HgBr][Br]	(3)
$HgBr + NO_2 \rightarrow Hg^0 + BrNO_2$	$3.4 \times 10^{-12}\exp(391/T)$[HgBr][$NO_2$]	(4)
$HgBr + Br \xrightarrow{M} HgBr_2$	3.0×10^{-11}[HgBr][Y]	(3) [c]
$HgBr + NO_2 \xrightarrow{M} HgBrNO_2$	k_{NO_2}([M], T) [HgBr][NO_2]	(4) [d]
$HgBr + Y \xrightarrow{M} HgBrY$	k_{HO_2}([M], T) [HgBr][Y]	(4) [d, e]
$Hg^0 + Cl + M \rightarrow HgCl + M$	$2.2 \times 10^{-32}\exp(680(1/T - 1/298))$[$Hg^0$][Cl][M]	(5)
$HgCl + Cl \rightarrow Hg^0 + Cl_2$	$1.20 \times 10^{-11}\exp(-5942/T)$[HgCl][Cl]	(6) [f]
$HgCl + Br \xrightarrow{M} HgBrCl$	3.0×10^{-11}[HgCl][Br]	(3) [c, g]
$HgCl + NO_2 \xrightarrow{M} HgClNO_2$	k_{NO_2} [M],T [HgBr][NO_2]	(4) [d, g]
$HgCl + Y \xrightarrow{M} HgClY$	k_{HO_2}([M], T) [HgBr][Y]	(4) [d, e, g]
Aqueous phase[h]		
$Hg^0_{(aq)} + O_{3(aq)} \rightarrow Hg^{II}_{(aq)}$ + products	4.7×10^7[$Hg^0_{(aq)}$][$O_{3(aq)}$]	(7)
$Hg^0_{(aq)} + HOCl_{(aq)} \rightarrow Hg^{II}_{(aq)} + OH^-_{(aq)} + Cl^-_{(aq)}$	2×10^6[$Hg^0_{(aq)}$][$HOCl_{(aq)}$]	(8), (9) [i]
$Hg^0_{(aq)} + OH_{(aq)} \rightarrow Hg^{II}_{(aq)}$ + products	2.0×10^9[$Hg^0_{(aq)}$][$OH_{(aq)}$]	(10), (11)
$Hg^{II}_{(aq)} + h\nu \rightarrow Hg^0_{(aq)}$	αj_{NO_2}[OA][$Hg^{II}_{(aq)}$]	this work [j]

Table 3.1: Redox chemical mechanism for atmospheric mercury.

[a] Rate expressions for gas-phase reactions have units of molecule cm^{-3} s^{-1} where [ ] denotes concentration in number density units of molecules cm^{-3}, [M] is the number density of air, and T is temperature in K. Rate expressions for aqueous-phase reactions have units of M s^{-1} and [$_{(aq)}$] denotes concentration in M (mol L^{-1}). Henry's law coefficients (M atm^{-1}) relating gas-phase and aqueous-phase concentrations are $1.28 \times 10^{-1}\exp(2482(1/T - 1/298))$ for Hg^0 (Sanemasa, 1975), $1.1 \times 10^{-2}\exp(2400(1/T - 1/298))$ for O_3 (Jacob, 1986), $6.6 \times 10^2\exp(5900(1/T - 1/298))$ for HOCl (Huthwelker et al., 1995), and 1.4×10^6 for Hg^{II} ($HgCl_2$; Lindqvist & Rodhe, 1985). The concentration of $OH_{(aq)}$ is estimated as given in the text. Lifetimes of Hg^I species are sufficiently short that steady-state can be assumed for atmospheric purposes.

[b] (1) Donohoue et al. (2006); (2) Dibble et al. (2012); (3) Balabanov et al. (2005); (4) Jiao & Dibble (2017); (5) Donohoue et al. (2005); (6) Wilcox (2009); (7) Munthe (1992); (8) Lin & Pehkonen (1998); (9) Wang & Pehkonen (2004); (10) Lin & Pehkonen (1997); (11) Buxton et al. (1988).

[c] This is an effective rate constant for intermediate pressures most relevant for atmospheric oxidation and uses a higher level of theory than Goodsite et al. (2004).

[d] k([M], T) $= \left(\frac{k^0(T)[M]}{1+k^0(T)[M]/k^\infty(T)}\right)0.6^p$, where $p = \left(1 + \left(\log_{10}\left(k^0(T)[M]/k^\infty(T)\right)\right)^2\right)^{-1}$. Values of $k^0(T)$ and $k^\infty(T)$ are tabulated by Jiao & Dibble (2017) for different temperatures. At $T = \{220, 260, 280, 298, 320\}$ K, $k^0_{NO_2} = \{27.4, 13.5, 9.52, 7.10, 5.09\} \times 10^{-29}$ cm^6 $molecule^{-2}$ s^{-1}; $k^\infty_{NO_2} = \{22.0, 14.2, 12.8, 11.8, 10.9\} \times 10^{-11}$ cm^3 $molecule^{-1}$ s^{-1}; $k^0_{HO_2} = \{8.40, 4.28, 3.01, 2.27, 1.64\} \times 10^{-29}$ cm^6 $molecule^{-2}$ s^{-1}; $k^\infty_{HO_2} = \{14.8, 9.10, 7.55, 6.99, 6.11\} \times 10^{-11}$ cm^3 $molecule^{-1}$ s^{-1}.

[e] We assume the same rate coefficient determined for HgBr + HO2 holds more generally for Y ≡ HO_2, OH, Cl, BrO and ClO based on similar binding energies (Dibble et al., 2012; Goodsite et al., 2004) and *ab initio* calculations from Wang et al. (2014).

[f] Abstraction alone competes with oxidation to Hg^{II} for HgCl as the rate of HgCl thermal dissociation is negligibly slow (Holmes et al., 2009).

[g] HgCl + Y rate coefficients are assumed to be the same as HgBr + Y. ClHg-Y and BrHg-Y have similar bond energies (Dibble et al., 2012).

[h] Oxidation of $Hg^0_{(aq)}$ takes place in clouds only, with concentrations of $Hg^0_{(aq)}$ and aqueous-phase oxidants determined by Henry's law equilibrium (footnote *a*). Aerosol liquid water contents under non-cloud conditions are too low for these reactions to be significant. Photoreduction of $Hg^{II}_{(aq)}$ takes place in both aqueous aerosols and clouds, with gas-aerosol partitioning of Hg^{II} as given by Amos et al. (2012) outside of clouds and Henry's law equilibrium for $HgCl_2$ in cloud (footnote *a*). The aerosol is assumed aqueous if RH > 35%.

[i] OCl^- has similar kinetics as HOCl but is negligible for typical cloud and aerosol pH given the HOCl/OCl^- pK_a = 7.53 (Harris, 2002).

[j] Parameterization for photoreduction of aqueous-phase Hg^{II}-organic complexes. Here j_{NO_2} (s^{-1}) is the local photolysis rate constant for NO_2 intended to be representative of the near-UV actinic flux, [OA] (μg m^{-3} STP) is the mass concentration of organic aerosol under standard conditions of temperature and pressure (p = 1 atm, T = 273 K), and $\alpha = 5.2 \times 10^{-2}$ m^{-3} STP μg^{-1} is a coefficient adjusted in GEOS-Chem to match observed TGM concentrations (see text).

Reaction	Reference[b]	Note
$Hg^0 + Br_2 \xrightarrow{M} HgBr_2$	Balabanov et al. (2005), Auzmendi-Murua et al. (2014)	[c]
$Hg^0 + Cl_2 \xrightarrow{M} HgCl_2$	Auzmendi-Murua et al. (2014)	[c]
$Hg^0 + I_2 \xrightarrow{M} HgI_2$	Auzmendi-Murua et al. (2014)	[c]
$Hg^0 + Br_2 \rightarrow HgBr + Br$	Auzmendi-Murua et al. (2014)	[d]
$Hg^0 + Cl_2 \rightarrow HgCl + Cl$	Auzmendi-Murua et al. (2014)	[d]
$Hg^0 + I_2 \rightarrow HgI + I$	Auzmendi-Murua et al. (2014)	[d]
$Hg^0 + OH \rightarrow HgO + H$	Hynes et al. (2009)	[d]
$Hg^0 + OH \xrightarrow{M} HgOH$	Hynes et al. (2009), Goodsite et al. (2004)	[e]
$HgOH + O_2 \rightarrow HgO + HO_2$	Shepler & Peterson (2003), Hynes et al. (2009)	[d]
$Hg^0 + HO_2 \xrightarrow{M} HgOOH$	Dibble et al. (2012)	[e]
$Hg^0 + NO_3 \xrightarrow{M} HgONO_2$	Dibble et al. (2012)	[e, f]
$Hg^0 + I \xrightarrow{M} HgI$	Goodsite et al. (2004), Greig et al. (1970), Subir et al. (2011)	[e, g]
$Hg^0 + BrO \xrightarrow{M} HgBrO$	Dibble et al. (2012, 2013), Balabanov et al. (2005), Balabanov & Peterson (2003)	[e, h]
$Hg^0 + ClO \xrightarrow{M} HgClO$	Dibble et al. (2012, 2013), Balabanov & Peterson (2003)	[e, h]
$Hg^0 + HCl \rightarrow Hg^{II} +$ products	Hall & Bloom (1993), Subir et al. (2011)	[g]
$Hg^0 + O_3 \rightarrow Hg^{II} +$ products	see note	[i]
$HgBr + I \xrightarrow{M} BrHgI$	see note	[j]
$HgBr + IO \xrightarrow{M} BrHgOI$	see note	[j]
$Hg^0_{(aq)} + HOBr_{(aq)} \rightarrow Hg^{II}_{(aq)} + OH^-_{(aq)} + Br^-_{(aq)}$	Wang & Pehkonen (2004), Hynes et al. (2009)	[k]
$Hg^0_{(aq)} + OBr^-_{(aq)} + H^+ \rightarrow Hg^{II}_{(aq)} + OH^-_{(aq)} + Br^-$	Wang & Pehkonen (2004), Hynes et al. (2009)	[k]
$Hg^0_{(aq)} + Br_{2(aq)} \rightarrow Hg^{II}_{(aq)} + 2Br^-$	Wang & Pehkonen (2004), Hynes et al. (2009)	[k]
$Hg^{II}_{(aq)} \xrightarrow{HO_2/O_2^-} Hg^{I}_{(aq)} \xrightarrow{HO_2/O_2^-} Hg^0$	Gårdfeldt & Jonsson (2003)	[d]
$HgSO_{3(aq)} \rightarrow Hg^0_{(aq)} +$ products	Van Loon et al. (2001)	[l]

Table 3.2: Reactions not included in the chemical mechanism.[a]

[a] These reactions have been inferred from kinetic studies and/or included in past models but are now thought to be too slow to be of atmospheric relevance.

[b] Reference supporting non-inclusion in the chemical mechanism.

(3) Reaction reported in laboratory studies by Ariya et al. (2002), Yan et al. (2005, 2009),Liu et al. (2007),Raofie et al. (2008), and Qu et al. (2010), but not supported by theory.

[d] Endothermic reaction.

[e] The Hg^I compounds are weakly bound and thermally dissociate too fast to allow for 2nd step of oxidation to Hg^{II}.

[f] Peleg et al. (2015) find a strong correlation between observed nighttime gaseous Hg^{II} and NO_3 radical concentrations in Jerusalem. There is theoretical evidence against NO_3 initiation of Hg^0 oxidation (Dibble et al., 2012), and NO_3 may instead serve as the second-stage oxidant of Hg^I. This would be important only in warm urban environments where nighttime NO_3 is high.

[g] Found to be negligibly slow.

[h] The formation of compounds with structural formulae BrHgO and ClHgO requires a prohibitively high activation energy. Note [e] applies to compounds with structural formulae HgBrO, HgOBr, HgClO, and HgOCl.

[i] The direct formation of $HgO_{(s)}$ from this reaction is energetically unfavorable (Calvert & Lindberg, 2005; Tossell, 2006). It has been postulated that intermediate products like HgO_3 could lead to the formation of stable $(HgO)_n$ oligomers or $HgO_{(s)}$ via decomposition to $OHgOO_{(g)}$ (Subir et al., 2011), but these must be stabilized through heterogeneous reactions on atmospheric aerosols (Calvert & Lindberg, 2005) and the associated mechanism is unlikely to be significant in the atmosphere (Hynes et al., 2009). A gas-phase reaction has been reported in chamber studies (Hall, 1995; Pal & Ariya, 2004; Sumner et al., 2005; Snider et al., 2008; Rutter & Schauer, 2007a), but this is likely to have been influenced by the walls of the chamber (as seen in Pal & Ariya (2004)) and presence of secondary organic aerosols (in Rutter & Schauer, 2007b).

[j] Atmospheric concentrations of I and IO (Volkamer et al., 2015; Dix et al., 2013; Prados-Roman et al., 2015) are too low for these reactions to be significant.

[k] Rates are too slow to be of relevance.

[l] Concentrations of $HgSO_3$ under typical atmospheric SO_2 levels are expected to be very low.

+Hg^{II} (g)) concentrations match the global mean observed at land stations.

3.3 GEOS-Chem model

3.3.1 General description

We start from the standard version v9-02 of the GEOS-Chem Hg model (www.geos-chem.org; Amos et al., 2012; Song et al., 2015) and implement a new 2010 inventory for speciated anthropogenic emissions (Zhang et al., 2016) including contributions from commercial products (Horowitz et al., 2014). We then add original updates described below for atmospheric chemistry and atmosphere-ocean coupling. The standard v9-02 model includes cycling of Hg^0 and Hg^{II} between the atmosphere, land, and the surface mixed-layer of the ocean (Selin et al., 2008; Soerensen et al., 2010). The atmospheric model transports Hg^0 and Hg^{II} as separate tracers. Gas-particle partitioning of Hg^{II} is determined by local thermodynamic equilibrium that is a function of aerosol mass concentration and temperature (Amos et al., 2012).

Holmes et al. (2010) presented the last detailed global atmospheric budget analysis of Hg in GEOS-Chem and we use it as a point of comparison for this study. Their model version included Hg^0 oxidation by Br atoms with Br concentrations specified in the troposphere and stratosphere from the p-TOMCAT and NASA Global Modeling Initiative models, respectively (Yang et al., 2005; Strahan et al., 2007). The standard v9-02 model now uses Br concentration fields from the GEOS-Chem tropospheric bromine simulation by Parrella et al. (2012), and features other model updates relative to Holmes et al. (2010) including gas-particle Hg^{II} equilibrium partitioning, a corrected washout algorithm (Amos et al., 2012), and improvements to the 2-D surface ocean model (Soerensen et al., 2010). We conduct a 3-year simulation for 2009-2011 driven by GEOS-5 assimilated meteorological data from the NASA Global Modeling and Assimilation Office (GMAO) with native horizontal resolution of 1/2°× 2/3°and 72 vertical levels extending up to the mesosphere. The GEOS-Chem simulation is conducted at 4°×5°horizontal resolution by regridding the GEOS-5 meteorological data. We use anthropogenic Hg emissions for the year 2010 from Zhang et al. (2016). The spatial distribution of soil Hg is determined following the method of Selin et al. (2008), with updated soil respiration emissions (910 Mg Hg a^{-1}) for consistency with the mechanistic terrestrial model developed by Smith-Downey et al. (2010). Emissions from snow and re-emission of deposited Hg follow Selin et al. (2008). The model is initialized with a

15-year simulation to equilibrate the stratosphere. We present model results as averages for the three simulation years (2009-2011).

3.3.2 Atmospheric chemistry

Hg^0 /Hg^{II} redox chemistry in the standard GEOS-Chem v9-02 model includes Hg^0 oxidation by Br atoms and Hg^{II} in-cloud photoreduction as described by Holmes et al. (2010), with Br concentration fields from Parrella et al. (2012). Shah et al. (2016) updated that chemistry following Dibble et al. (2012) to include 2nd-stage oxidation of HgBr by HO_2, NO_2, and BrO, as well as new kinetics for HgBr dissociation. Here we further expand and update the chemistry using the mechanism described in Table 3.1. Br and Cl radical concentrations are taken from a new GEOS-Chem simulation of tropospheric oxidant-aerosol chemistry by Schmidt et al. (2016). Unlike Parrella et al. (2012), this simulation does not include a bromine radical source from sea-salt debromination as recent evidence suggests that BrO concentrations in the marine boundary layer (MBL) are generally sub-ppt (Gómez Martín et al., 2013; Wang et al., 2015). Simulated concentrations of Br in the free troposphere are on the other hand a factor of two higher than Parrella et al. (2012), reflecting more extensive heterogeneous chemistry. Schmidt et al. (2016) show that their simulation provides a better simulation of aircraft and satellite observations of tropospheric BrO. Stratospheric concentrations of Br and Cl species are from the GEOS Chemistry Climate Model (Liang et al., 2010) and Global Modeling Initiative (Considine et al., 2008; Murray et al., 2012), respectively.

Here we use the global 3-D monthly archive of oxidant and radical concentrations from Schmidt et al. (2016). We apply diurnal scaling following Holmes et al. (2010) to the monthly mean concentrations of Br, BrO, Cl, ClO, and HOCl, a cosine function of the solar zenith angle for OH and HO_2, and NO-NO_2-O_3 photochemical equilibrium for NO_2. Fast Hg^0 oxidation in the polar spring boundary layer is simulated by specifying high BrO concentrations there when conditions for temperature, sea ice cover, sunlight, and atmospheric stability are met (Holmes et al., 2010). Monthly mean organic aerosol (OA) concentrations are archived from a separate v9-02 GEOS-Chem simulation including primary emissions from combustion and secondary production from biogenic and anthropogenic hydrocarbons (Pye et al., 2010). Aqueous-phase concentrations of Hg^0 , O_3, and HOCl are determined from the gas-phase partial pressures and Henry's law coefficients (Table

3.1). We estimate aqueous in-cloud OH concentrations following Jacob et al. (2005) as [OH(aq)] = β [OH(g)] with $\beta = 1 \times 10^{-19}$ M cm^3 molecule^{-1}.

3.3.3 Atmosphere-ocean coupling

GEOS-Chem v9-02 uses a 2-D surface-slab ocean model with no lateral transport and with fixed subsurface ocean concentration boundary conditions (Soerensen et al., 2010). Oceanic circulation and mixing between the surface mixed layer and deeper ocean strongly impacts Hg^0 concentrations in the surface ocean through the supply of reducible Hg^{II}, driving changes in oceanic evasion (Soerensen et al., 2013, 2014). Here we present a new two-way coupling of the GEOS-Chem atmospheric Hg simulation to the MITgcm 3-D oceanic general circulation model with embedded plankton ecology (Y. Zhang et al., 2015). First, the GEOS-Chem Hg model with the 2-D slab ocean is initialized over 15 years of repeated present-day emissions and meteorological data (this time is required to equilibrate the stratosphere). Starting from these initial conditions, we conduct the GEOS-Chem simulation for the desired period (here three years, 2009-2011) and archive monthly surface air Hg^0 concentrations and total Hg^{II} deposition fluxes. We then initialize the Y. Zhang et al. (2015) ocean model for 20 years with these archived surface boundary conditions to equilibrate the upper several hundred meters of the ocean. The monthly mean surface ocean Hg^0 concentrations from the final year of the simulation are then input to GEOS-Chem, replacing the 2-D slab ocean model concentrations. The 15-year GEOS-Chem simulation is repeated with this new input. This process is iterated until convergence of results is achieved. We find that two iterations are sufficient.

3.4 Global budget of atmospheric mercury

3.4.1 Budget and lifetimes

Figure refc2f1 (top panel) shows the simulated vertical and latitudinal distributions of annual zonal mean Hg^0 and Hg^{II} mixing ratios. Hg^0 decreases rapidly in the stratosphere, while Hg^{II} increases with altitude and dominates total Hg in the stratosphere. This vertical structure is driven by chemistry (Selin et al., 2007; Holmes et al., 2010) and is well established from observations (Murphy et al., 2006; Talbot et al., 2007; Lyman & Jaffe, 2012). The stratosphere in the model accounts for 12% of total Hg atmospheric mass and is in a very different

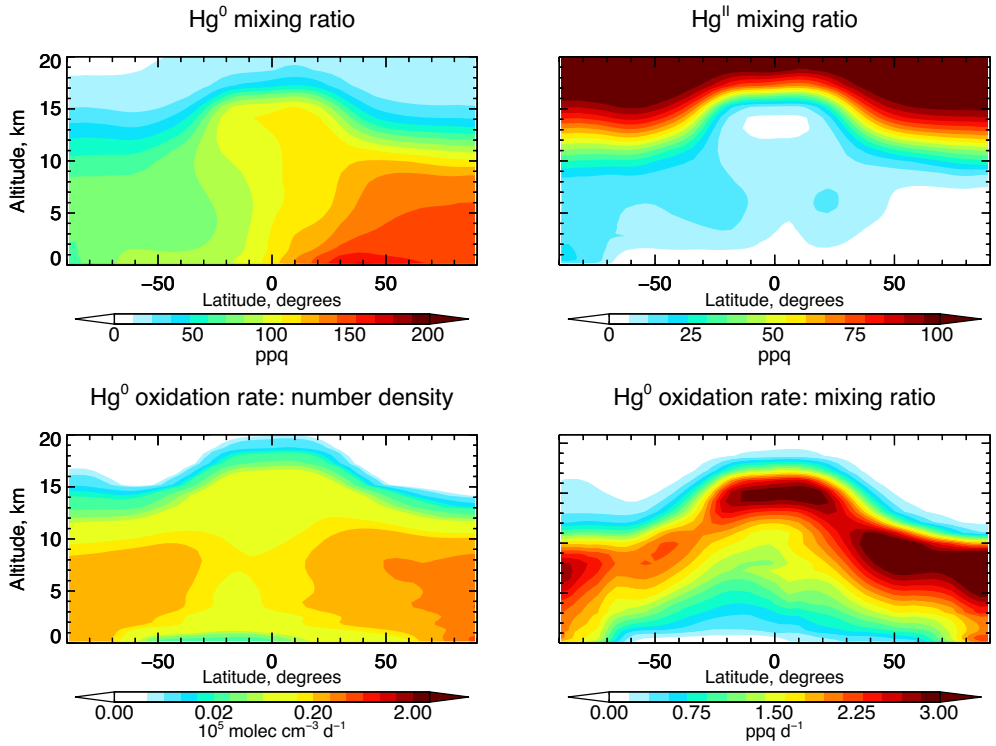

Figure 3.1: Annual (2009-2011) zonal mean mixing ratios of Hg^0 and Hg^{II} in GEOS-Chem, and Hg^0 oxidation rates in number density and mixing ratio units.

redox regime from the troposphere. Here we focus on tropospheric budgets, which are most relevant to Hg deposition. The stratosphere is discussed further in Section 3.4.4.

Figure 3.2 shows the global tropospheric Hg budget from our GEOS-Chem simulation, including rates of major Hg^0 /Hg^{II} reactions. The global tropospheric Hg reservoir is 3900 Mg, including 3500 Mg as Hg^0 and 400 Mg as Hg^{II} , smaller than the 4500 Mg reservoir in Holmes et al. (2010). In both cases, the reservoir was adjusted through the Hg^{II} photoreduction rate coefficient to match the observed annual mean TGM at long-term monitoring sites, mainly located in northern mid-latitudes (Figure 3.3). Holmes et al. (2010) used observations for 2000-2008 averaging 1.87±1.00 ng m^{-3} (n = 39 sites), whereas we use observations for 2007-2013 averaging 1.46±0.25 ng m^{-3} (n = 37). Observed atmospheric concentrations in North America and Europe

have declined on average by 1-2% a^{-1} since 1990, which has been attributed to: (1) phase-out of Hg from commercial products, (2) declines in Hg emissions from coal combustion as a co-benefit of SO2 and NOx emission controls, (3) updated artisanal and small-scale gold mining emissions (Zhang et al., 2016). This explains some of the difference between observed concentrations in the two time periods. Observations used in Holmes et al. (2010) also included very high concentrations at four East Asian sites (3-7 ng $m^{-}3$; Nguyen et al., 2007; Sakata & Asakura, 2007; Feng et al., 2008; Wan et al., 2009), whereas the more recent observations over East Asia used here (n = 6) are all less than 3 ng $m^{-}3$ (Sheu et al., 2010; Fu et al., 2012b,a; H. Zhang et al., 2015). Only one site (Mt. Changbai, China) has data available during both time periods and observed TGM concentrations decreased there by a factor of two (Fu et al., 2012a). Thus, our atmospheric loadings may be more representative of more recent (ca. 2010) conditions.

We find that the lifetime of Hg^0 against oxidation to Hg^{II} in the troposphere is 2.7 months, with Br atom-initiated pathways contributing 97% of total oxidation. This chemical lifetime is smaller than most prior model estimates, e.g., 6 months in Holmes et al. (2010), which used lower Br concentrations. The addition of NO2 and HO2 as second-stage oxidants is also important in increasing the rate of Hg^0 conversion to Hg^{II} , more than compensating for faster thermal decomposition of HgBr relative to (Holmes et al., 2010). Our results are consistent with Shah et al. (2016), who estimated an Hg^0 chemical lifetime of 1.2 to 2.8 months to reproduce aircraft measurements of Hg^{II} over the Southeast US in summer during the NOMADSS campaign (Gratz et al., 2015). The dominance of NO2 and HO2 as Hg^{I} oxidants reflects their high atmospheric abundance and is consistent with results from a box modeling study over the Pacific (Wang et al., 2014). We find Cl atoms contribute less than 1% of Hg^0 oxidation globally because the supply of Cl atoms (mean tropospheric mixing ratio of 2×10^{-4} ppt) is limited by fast conversion to the stable reservoir HCl. Aqueous-phase pathways in clouds contribute 2%. Our work suggests that the dominant Hg^{II} species produced in the gas phase are BrHgONO and BrHgOOH, though the actual speciation of Hg^{II} in the atmosphere would likely be modified through cycling in aerosols and clouds (Hedgecock & Pirrone, 2001; Lin et al., 2006).

The vertical distribution of $Hg^0 \rightarrow Hg^{II}$ oxidation rates is shown in the bottom panel of Figure 3.1 in units of number density (relevant to the mass budget) and mixing ratio (relevant to transport). Only 1% of Hg^0 oxidation occurs in the stratosphere, consistent with previous work (Holmes et al., 2010). Most Hg oxidation by

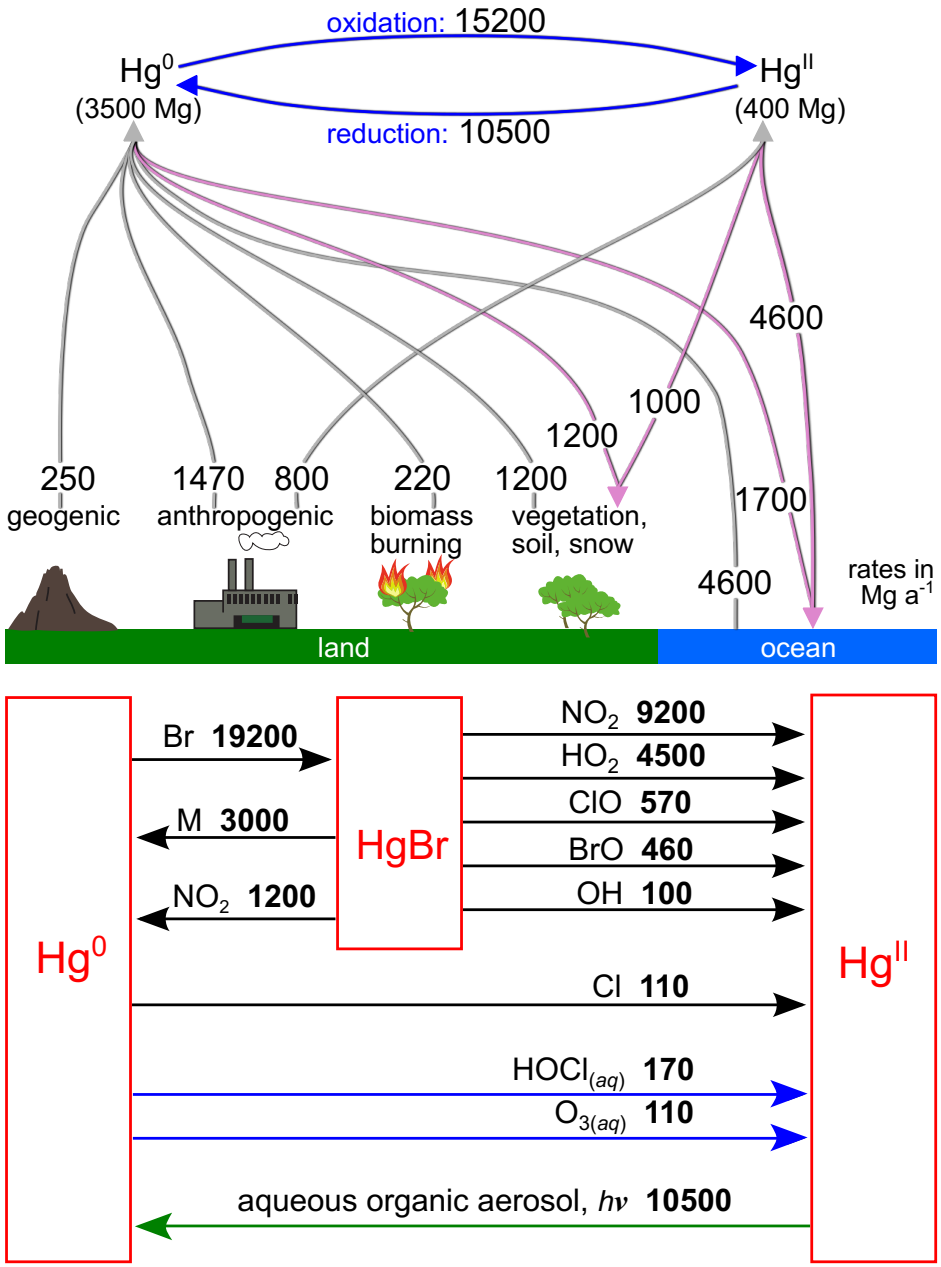

Figure 3.2: Global budget of tropospheric mercury in GEOS-Chem. Hg^{II} includes gaseous and particulate forms in local equilibrium (Amos et al., 2012). The bottom panel identifies the major chemical reactions from Table 3.1 cycling Hg^0 and Hg^{II}. Reactions with global rates lower than 100 Mg a^{-1} are not shown.

mass occurs in the extratropical free troposphere, consistent with the Br distribution (Schmidt et al., 2016), and is faster in the northern hemisphere because of higher NO2 concentrations. Hg^0 oxidation in Holmes et al. (2010) was fastest in the Southern Ocean MBL due to high Br concentrations from sea-salt aerosol debromination. This is now thought to be unlikely because the sea salt aerosol in that region remains alkaline (Murphy et al., 1998; Alexander et al., 2005; Schmidt et al., 2016). In general, the addition of 2nd-stage oxidants HO2 and NO2 shifts Hg oxidation to lower latitudes relative to Holmes et al. (2010). This has implications for Hg deposition, which we discuss in Section 3.5. Hg^0 oxidation in terms of mixing ratio features a secondary maximum in the tropical upper troposphere where the Br/BrO ratio is high (Parrella et al., 2012; Fernandez et al., 2014).

We find that the shorter chemical lifetime of Hg^0 in our simulation relative to Holmes et al. (2010) must be balanced by faster atmospheric reduction to reproduce observed TGM concentrations. This is implemented by adjusting the photoreduction coefficient α in Table 3.1. The resulting mean lifetime of Hg^{II} against reduction in the troposphere is 13 days. Shah et al. (2016) similarly found that faster Hg^0 oxidation in their NOMADSS simulation required faster Hg^{II} reduction, with a tropospheric Hg^{II} lifetime against reduction of 19 days. The lifetime of tropospheric Hg^{II} against deposition is relatively long, 26 days (see Figure 3.2), because most Hg^{II} production occurs in the free troposphere (Figure 3.1). We find here that the Hg^{II} lifetime against reduction is shorter than against deposition, emphasizing the importance of reduction in controlling the atmospheric Hg budget. By contrast, Holmes et al. (2010) found an adjusted Hg^{II} tropospheric lifetime of 50 days against reduction and 36 days against deposition, which led them to conclude that no reduction was needed if Hg^0 oxidation kinetics were decreased within their uncertainty. This is no longer possible with the much faster Hg^0 oxidation in our mechanism. We conclude that Hg^{II} reduction must take place in the atmosphere. With Hg^{II} reduction, the overall lifetime of tropospheric TGM against deposition in our simulation is 5.2 months, similar to the estimate of 6.1 months in Holmes et al. (2010). We discuss the consistency of this estimate with observations in the next section.

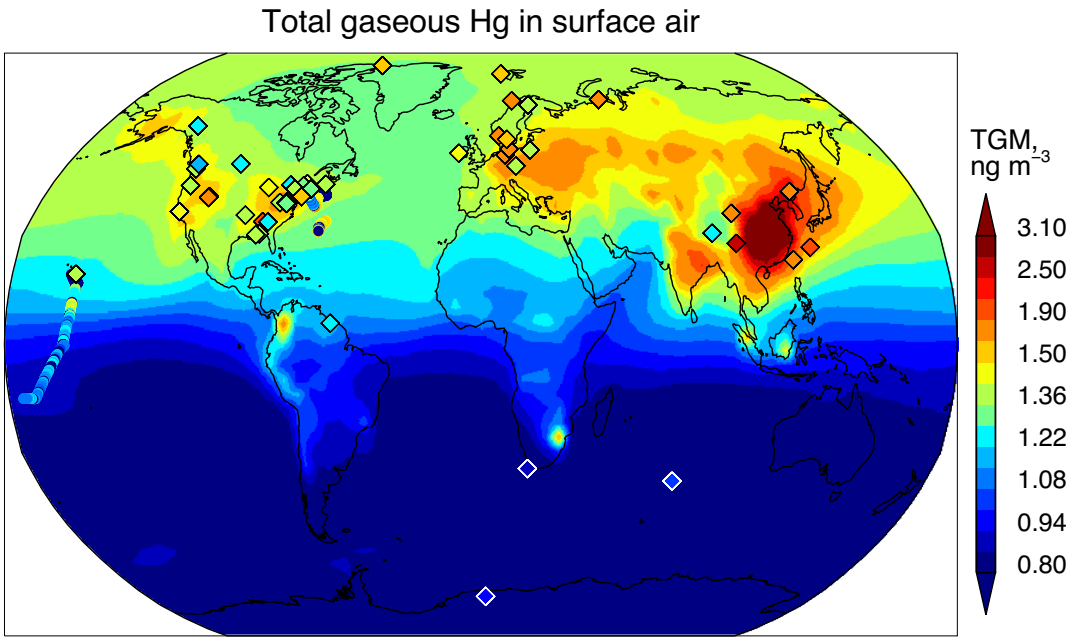

Figure 3.3: Global distribution of total gaseous mercury (TGM) concentrations in surface air. Model values (background) are annual means for 2009-2011. Observations (symbols) are for 2007-2013. Data for land sites (diamonds) are annual means for 2007-2013 as previously compiled by Song et al. (2015) and Zhang et al. (2016). Data at three Nordic stations were converted from 20°C to ng m^{-3} STP (p = 1 atm, T = 273 K), see Slemr et al. (2015). Observations from 2007-2013 ship cruises (circles) are from (Soerensen et al., 2013, 2014). Note the change in the linear color scale at 1.50 ng m^{-3}.

3.4.2 Global distribution

Figure 3.3 compares our simulation to observed 2007-2013 TGM surface concentrations. TGM includes Hg^0 and the gaseous component of Hg^{II}. Observations include annual means at 37 land sites plus ship cruises. The mean at land stations is 1.47±0.27 ng $m^{-}3$ in the observations and 1.44±0.25 ng m^{-3} in the model, with the good agreement in the mean reflecting the adjustment of the Hg^{II} photoreduction rate coefficient as explained above. The spatial correlation coefficient between model and observations is r = 0.57.

Beyond this simulation of the mean, we successfully reproduce the observed standard deviation of TGM concentrations, which places an independent constraint on the atmospheric lifetime of Hg against deposition (Junge, 1974; Hamrud, 1983). This constraint had previously been expressed in terms of the interhemispheric gradient of TGM from ship cruises, leading to TGM lifetime estimates ranging from 4.4 months to 2 years (Slemr et al., 1981; Fitzgerald et al., 1983; Lindqvist & Rodhe, 1985; Lamborg et al., 2002). However, we find the interhemispheric gradient is not a sensitive diagnostic of lifetime because atmospheric Hg in the south-

ern hemisphere is controlled more by intrahemispheric atmosphere-ocean exchange than by transport from the northern hemisphere. For example, changing the simulation of atmosphere-ocean exchange from the slab ocean to the MITgcm (Section 3.3.3) increases the TGM lifetime while also increasing the interhemispheric gradient due to changed ocean emissions. We conducted a sensitivity simulation doubling the tropospheric TGM lifetime in the model (to 10.4 months) by decreasing the rate of Hg^0 oxidation. This produced less than 20% of a decline in the interhemispheric gradient, but the relative standard deviation of TGM concentrations across land stations decreased by 40%. Thus the overall variability of TGM concentrations provides a more sensitive constraint on the TGM atmospheric lifetime, while the interhemispheric gradient can be misleading. The model's ability to reproduce the observed standard deviation across land sites supports our simulated TGM atmospheric lifetime of 5.2 months.

3.4.3 Seasonality

Figure 3.4 compares simulated and observed seasonal cycles of TGM concentrations at land stations in the northern mid-latitudes (30°to 60°N) and southern hemisphere (see Figure 3.3 for site locations). Also shown are results from a sensitivity simulation with the 2-D surface-slab ocean model (Soerensen et al., 2010). The observed seasonal cycle is successfully reproduced in the northern hemisphere. The February maximum and September minimum are driven in the model in part by Hg^0 oxidation (fastest in summer, slowest in winter) and in part by ocean evasion. Oceanic Hg^0 evasion peaks under conditions that include high wind speeds that enhance turbulent exchange and deepen the surface mixed layer, which replenishes the supply of reducible Hg^{II} from the suburface ocean. Evasion is also sensitive to the timing of seasonal productivity blooms in the spring and summer, which lead to enhanced scavenging of Hg^{II} from the mixed layer with settling particles (Mason et al., 2001; Gårdfeldt et al., 2003; Rolfus & Fitzgerald, 2004; Andersson et al., 2007; Soerensen et al., 2010; Tseng et al., 2013). Similar to Song et al. (2015), we find that the 2-D slab ocean overestimates the observed seasonality at northern mid-latitude sites (Figure 3.4). Atlantic and Pacific Ocean seawater Hg^0 measurements indicate this overestimate is a function of simplified ocean physics (Soerensen et al., 2014) and the boundary condition for subsurface ocean concentrations in the slab ocean model. We correct it here by the coupling to the MITgcm 3-D ocean simulation. In the southern hemisphere, Amsterdam Island in the Indian Ocean and Cape Point on

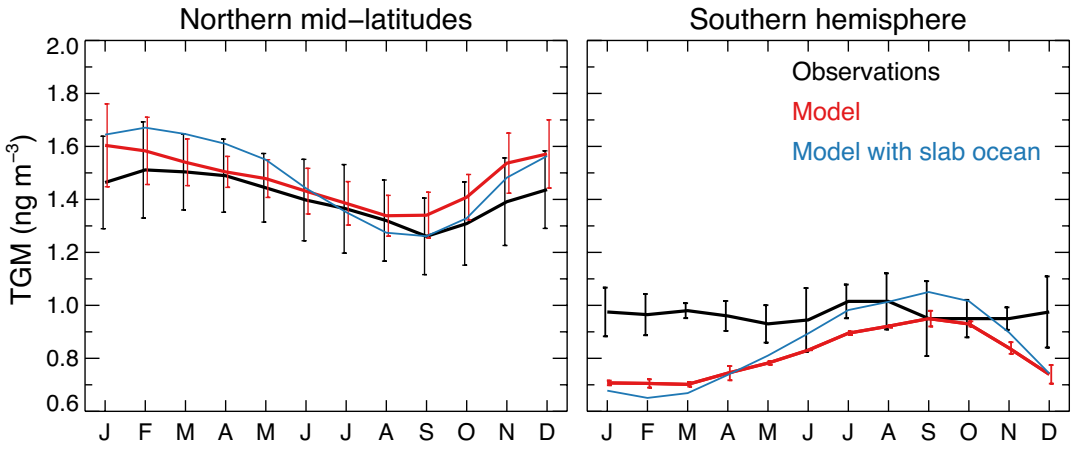

Figure 3.4: Mean seasonal variation and spatial standard deviation of total gaseous mercury (TGM) concentrations for northern mid-latitude sites (see Figure refc2f3) and southern hemisphere sites (Amsterdam Island and Cape Point). Observations are compared to results from our standard simulation (based on GEOS-Chem coupled to the MITgcm 3-D ocean model) to a sensitivity study with the 2-D surface-slab ocean model in GEOS-Chem.

the South African coast have similar monthly average concentrations and show no significant seasonal variation (Slemr et al., 2015). By contrast, the model at those sites has strong seasonality, which has been documented previously for the standard model version v9-02 (Song et al., 2015). We find a modest improvement in moving from the slab ocean simulation to the MITgcm but the seasonal bias is still large. Capturing the seasonality of atmospheric Hg in the Arctic using GEOS-Chem required parameterization of unique sea-ice, oceanic and riverine dynamics (Fisher et al., 2012, 2013; Y. Zhang et al., 2015) and a similar analysis for the Southern Ocean region has not yet been performed.

3.4.4 Vertical distribution and the stratosphere

Hg^0 concentrations in the model drop rapidly above the tropopause (Figure 3.1), consistent with observations (Talbot et al., 2007; Slemr et al., 2009). Modeled Hg^0 oxidation in the lower stratosphere is almost exclusively from Br atoms. There is no significant Hg^{II} reduction there because OA concentrations and relative humidity are very low. Extensive TGM observations in the lowermost stratosphere at northern extratropical latitudes are available from the CARIBIC program that collects measurements aboard commercial aircraft (Slemr et al., 2009, 2014, 2016). The early stratospheric data were biased low and we focus on corrected data available for April 2014-January 2015 (Slemr et al., 2016). TGM in the stratosphere is expected to be mainly Hg^0 because

Hg^{II} is incorporated into aerosol (Murphy et al., 2006; Lyman & Jaffe, 2012).

Figure 3.5 compares the stratospheric TGM concentrations measured in CARIBIC to model values sampled along the flight tracks. The CARIBIC data also include ozone (O_3) and CO concentrations (Brenninkmeijer et al., 2007). Here we use O_3 concentration as a chemical coordinate for depth into the stratosphere and exclude tropospheric data as diagnosed by $[O_3]/[CO] < 1.25$ mol mol^{-1} (Hudman et al., 2007). We correlate the logarithm of TGM concentrations, as a measure of first-order loss, to the O_3 concentrations. The observations reach higher ozone than the model, indicating that they sample air with greater stratospheric influence. The model underestimates the log(TGM)-ozone slope by a factor of 2. To test whether this underestimate is due to slow Hg^0 oxidation, we performed a sensitivity simulation doubling the stratospheric Hg^0 oxidation rate (green line in Figure 3.5). The model slope increases by only 32%. This suggests that the log(TGM)-ozone relationship in the lowermost stratosphere is set in part by mixing rather than solely by chemistry (Xiao et al., 2007). The model underestimate of the log(TGM)-ozone slope could reflect excessive dynamical mixing in the lower stratosphere, a well-known problem in stratospheric transport models (Schoeberl et al., 2003; Tan et al., 2004), or errors in the timescales of air transit across the tropopause which vary on the order of months to years (Orbe et al., 2014; Ploeger & Birner, 2016).

3.5 Implications for global Hg deposition

Figure 3.6 compares simulated and observed annual Hg wet deposition at sites in North America, Europe, and China for 2007-2013. The model captures the spatial variability across sites in North America relatively well (r=0.57). Some of this variability is driven by precipitation amount, which leads to higher modeled deposition along the Northwest coast and over the North Atlantic. The maximum along the coast of the Gulf of Mexico is due to deep convection scavenging upper tropospheric air enriched in Hg^{II} (Guentzel et al., 2001; Selin et al., 2008; Holmes et al., 2016). Previous GEOS-Chem simulations with Br-initiated oxidation of Hg^0 failed to capture this Gulf maximum because Hg^{II} production favored higher latitudes (Holmes et al., 2010; Amos et al., 2012). The inclusion of NO_2 and HO_2 as second-stage oxidants in our simulation shifts Hg^{II} production to lower latitudes and we find that this enables simulation of the Gulf of Mexico maximum. This solves what was previously considered a major objection to the Br mechanism for Hg^0 oxidation (Holmes et al., 2010).

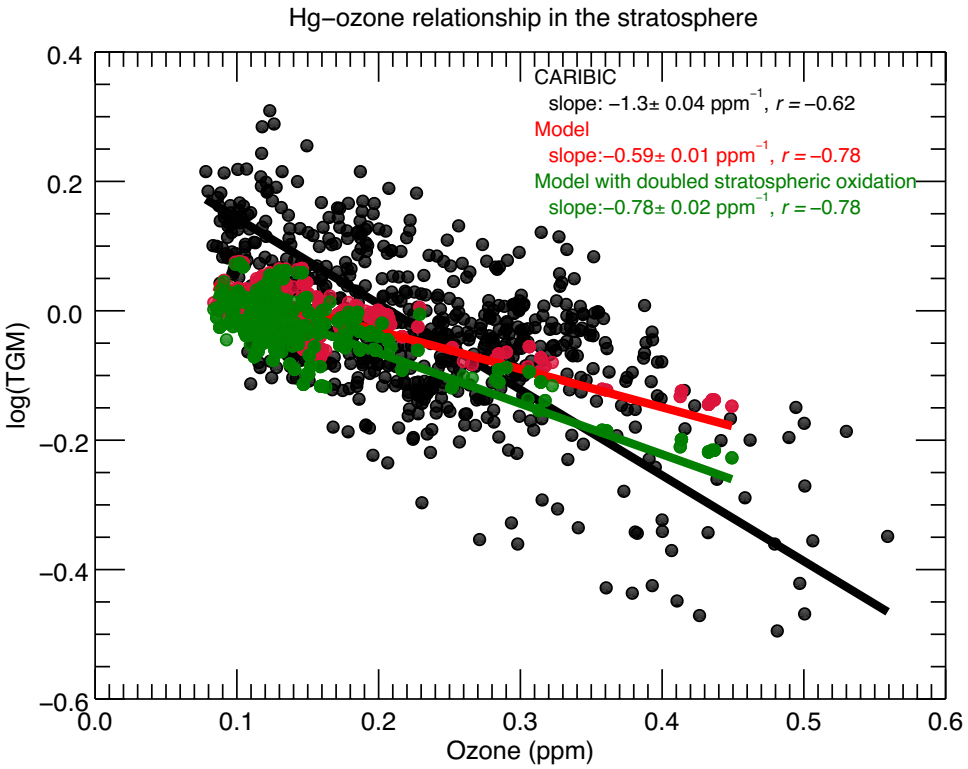

Figure 3.5: Relationship between total gaseous mercury (TGM) and ozone concentrations in the lower stratosphere. TGM is shown as the decimal logarithm of the concentration in ng m^{-3} STP. Observations are from CARIBIC commercial aircraft in the extratropical northern hemisphere for April 2014-January 2015 (Slemr et al., 2015). Tropospheric data as diagnosed by [O3]/[CO] $<$ 1.25 mol mol^{-1} are excluded. Model points are data for individual flights sampled along the CARIBIC flight tracks on the GEOS-Chem 4°$\times$ 5 °model grid. Also shown are results from a model sensitivity simulation with a doubled Hg^0 oxidation rate in the stratosphere. Reduced-major-axis (RMA) regressions for the log(TGM)-ozone relationship are shown with slopes and correlation coefficients. Errors on the slopes are estimated by the bootstrap method.

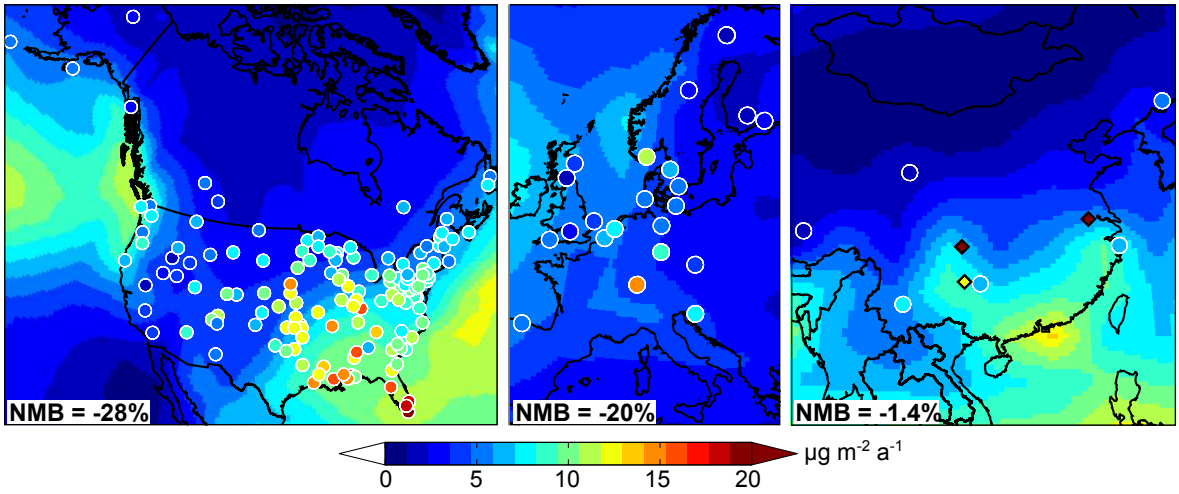

Figure 3.6: Annual Hg wet deposition fluxes over North America, Europe, and China. Model values for 2009-2011 (background contours) are compared to 2007-2013 observations from the Mercury Deposition Network (MDN, National Atmospheric Deposition Program, http://nadp.sws.uiuc.edu/mdn/) over North America (58 sites), the European Monitoring and Evaluation Program (EMEP) over Europe (20 sites), and data from (Fu et al., 2015, 2016) over China (9 sites). In the China panel, circles represent rural sites and diamonds represent urban sites as identified in Fu et al. (2015, 2016). For the MDN and EMEP networks, which collect weekly or monthly integrated samples, we only include sites with at least 75% of annual data for at least one year between 2007 and 2013; for China we only include sites with at least 9 months of data over the 2007-2013 period. MDN data are formally quality-controlled, while for EMEP data we rely on a subset of sites that have been quality-controlled (Oleg Travnikov, personal communication). Legends give the normalized mean bias (NMB) for all sites, excluding urban sites in China.

Over Europe, deposition is fairly uniform and low in the model and observations. This reflects decreased anthropogenic Hg^{II} emissions in the region from emissions controls on coal-fired power plants (Klimont et al., 2013; Muntean et al., 2014; Zhang et al., 2016). There is no area of frequent deep convection, unlike the Gulf of Mexico for the US.

Observations of Hg wet deposition over China have recently become available (Fu et al., 2015, 2016). Values at urban sites are high, likely reflecting local Hg^{II} emissions, and are correlated with high concentrations of particulate Hg^{II} (Fu et al., 2016). Values at rural sites are much lower and comparable to wet deposition observed in North America and Europe despite higher TGM concentrations in China (see Figure 3.3). We simulate these low values successfully in our model, whereas a simulation with the standard GEOS-Chem v9-02 overestimates them by a factor of 4. This reflects in part our dependence of Hg^{II} reduction on OA concentrations, which are particularly high in China (Heald et al., 2011).

Figure 3.7 shows the global distribution of wet and dry Hg^{II} deposition in the model. This deposition is the main Hg source to the open ocean (Sunderland & Mason, 2007; Soerensen et al., 2010). We find that 80% of

global Hg^{II} deposition is to the oceans, compared to 71% in Holmes et al. (2010), and that 60% of this deposition is wet. Because Br is of marine origin, its dominance as an Hg^0 oxidant favors deposition to the ocean. The dependence of Hg^{II} reduction in our mechanism on the formation of Hg-organic complexes further shifts Hg^{II} deposition away from continents where OA concentrations are highest (Heald et al., 2011). The dominance of HO_2 and NO_2 as second-stage oxidants for HgBr brings Hg^{II} deposition to lower latitudes relative to the simulation by Holmes et al. (2010), where most deposition occurred over high-latitude oceans. We now find 49% of global total Hg^{II} deposition is to oceans within the tropics (30°S - 30°N). A large Hg^{II} deposition flux to the tropical oceans is suggested by recent cruise observations of high oceanic Hg^0 concentrations across the intertropical convergence zone (ITCZ), which GEOS-Chem previously underestimated (Soerensen et al., 2014).

3.6 Conclusions

The atmospheric redox chemistry of mercury (Hg^0 /Hg^{II}) determines the global patterns of Hg deposition to surface ecosystems, where Hg is converted to the toxic and bioaccumulative methylmercury species. Here we developed and evaluated an updated mechanism for atmospheric Hg redox chemistry in the GEOS-Chem global model to gain new insights into the global Hg budget and the patterns of Hg deposition. As part of this work we also developed a new coupling between GEOS-Chem and a 3-D ocean general circulation model (MITgcm), resulting in a fully resolved simulation of Hg transport and chemistry in the atmosphere-ocean system.

The updated atmospheric Hg^0 /Hg^{II} redox mechanism includes gas-phase Br as the main Hg^0 oxidant in the troposphere and stratosphere, and second-stage oxidation of HgBr by a number of radical oxidants including NO_2 and HO_2. Br concentrations in GEOS-Chem are from the recent simulation of Schmidt et al. (2016), and are higher than previous models and more consistent with recent aircraft and satellite observations of BrO. Atmospheric reduction of Hg^{II} is hypothesized to take place by photolysis of aqueous-phase Hg^{II} -organic complexes. This is parameterized in GEOS-Chem as a function of the local concentration of organic aerosol (OA).

The global mass of atmospheric Hg simulated by GEOS-Chem is 4400 Mg, including 3900 Mg in the tro-

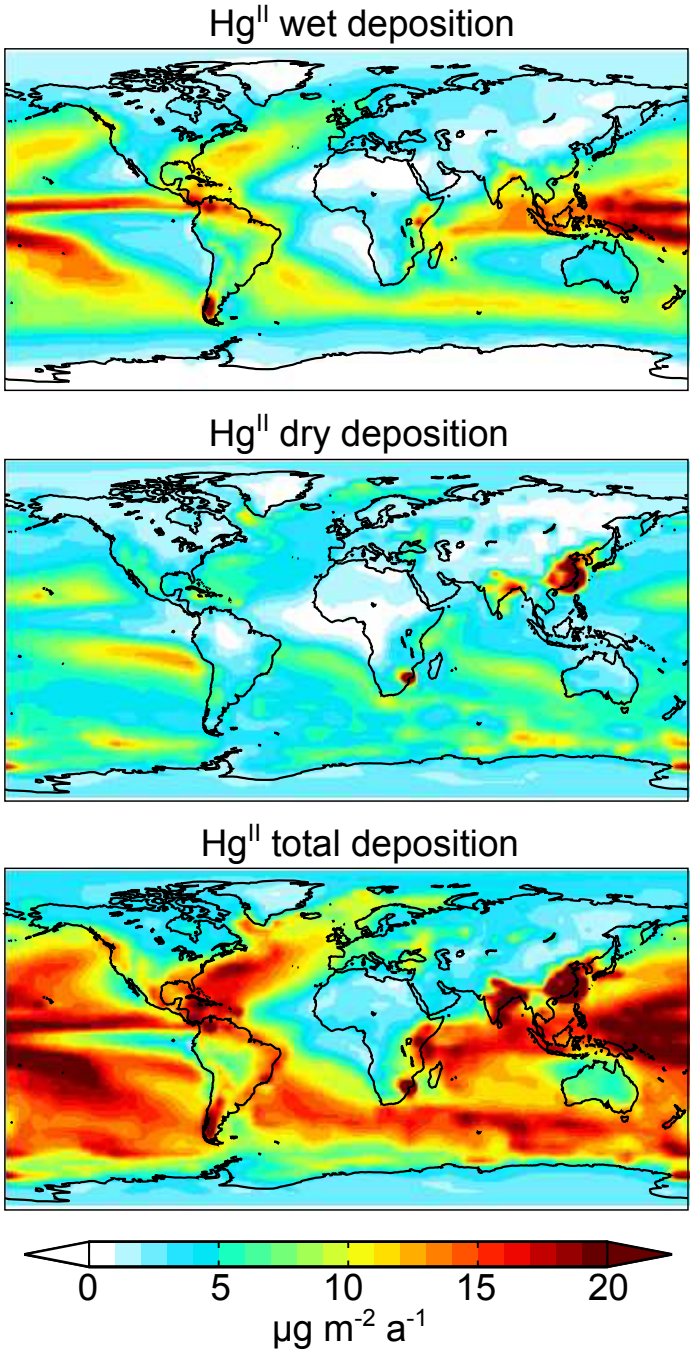

Figure 3.7: Annual 2009-2011 Hg^{II} deposition fluxes in GEOS-Chem.

posphere. The tropospheric lifetime of Hg^0 against oxidation is 2.7 months. Observations of the atmospheric variability of total gaseous mercury (TGM≡Hg^0 + Hg^{II}(g)) suggest an atmospheric lifetime against deposition of about 6 months. Thus, Hg^{II} must be reduced in the atmosphere, which is consistent with recent observations of atmospheric Hg isotope fractionation. Matching the observed mean surface TGM concentrations in GEOS-Chem implies a tropospheric Hg^{II} lifetime of 13 days against reduction and 26 days against deposition. This results in an overall tropospheric lifetime for TGM of 5.2 months against deposition and enables a successful simulation of the observed relative standard deviation of TGM concentrations across terrestrial sites. The interhemispheric difference in TGM concentrations had previously been interpreted to suggest a longer TGM lifetime against deposition, but we show this is misleading because TGM in the southern hemisphere is mostly controlled by oceanic emissions rather than transport from the northern hemisphere.

The observed seasonality of TGM concentrations in northern mid-latitudes (maximum in February, minimum in September) is reproduced by the model, where it is attributed to photochemical oxidation of Hg^0 and oceanic evasion both with similar seasonal phases. Coupling GEOS-Chem to the MITgcm 3-D ocean model improves simulation of the seasonal amplitude by lowering oceanic evasion over the North Atlantic due to elimination of the static subsurface ocean boundary condition in the GEOS-Chem slab ocean. Observations at southern hemisphere sites show little seasonality whereas the model features a spring maximum. More work is needed to understand this discrepancy.

Observations show a rapid depletion of TGM above the tropopause and we examined whether this could provide a test for Hg^0 chemistry. For that purpose we used extensive lowermost-stratospheric observations from the CARIBIC program aboard commercial aircraft, and characterized TGM first-order loss as the slope of the log(TGM)-ozone relationship. We find that the model underestimates the observed log(TGM)-ozone slope by a factor of two, but that this slope is only moderately sensitive to the rate of Hg^0 oxidation and appears to be driven in part by mixing of air parcels with different stratospheric ages. This mixing is likely too fast in GEOS-Chem, which may explain the weaker TGM-ozone slope.

Hg wet deposition fluxes in the model are consistent with observations in North America, Europe, and China, lending confidence to the simulated global atmospheric Hg budget. Inclusion of NO_2 and HO_2 as second-stage HgBr oxidants in the model shifts Hg^{II} production to lower latitudes compared to previous ver-

sions of GEOS-Chem and enables the model to capture the observed maximum in wet deposition along the Gulf Coast of the US. In rural areas of China, wet deposition is observed to be low in spite of very high TGM concentrations. This is reproduced by the model where it is due to fast Hg^{II} reduction, driven in part by very high OA concentrations.

We find that 80% of global Hg^{II} deposition takes place over the oceans, reflecting in part the marine origin of Br as well as the relatively low marine OA concentrations and hence slow Hg^{II} reduction. More Hg is deposited to the tropical oceans (49% of total Hg^{II} deposition) compared to previous versions of GEOS-Chem where debromination of sea salt aerosol drove fast Hg^0 oxidation and deposition to the Southern Ocean. This change largely reflects the dominance of photochemically driven Hg^0 oxidation in the free troposphere due to higher free tropospheric Br concentrations and the addition of the atmospherically abundant NO_2 and HO_2 radicals as second-stage oxidants for HgBr. Observations of the latitudinal gradient of Hg^{II} wet deposition over the ocean would provide a sensitive test of Hg chemistry and improve understanding of Hg inputs to different ocean regions.

Acknowledgements

This work was funded by the Atmospheric Chemistry and Chemical Oceanography Programs of the US National Science Foundation. We thank Oleg Travnikov for providing quality-controlled EMEP wet deposition measurements, and the CARIBIC team (www.caribic-atmospheric.com) for maintaining this valuable measurement program. We thank Jeroen Sonke for helpful discussions.

A

Supplementary Information for: Historical mercury releases from commercial products: global environmental implications

A.1 Waste incineration estimates

Our historical estimates are a result of the Hg used in products that would then be disposed, the distribution of waste disposal (between landfilling, open dumping on land, incineration and open burning), and emissions factors for Hg-containing waste burned based on available emissions controls, which vary in time and by level of economic development. Historical estimates from Streets et al. (2011) for 1850–1970 are scaled by population to the 1980 estimate, and from 1980 onward are calculated from activity data for total waste burned, assuming a constant Hg content of waste, and using emissions factors based on the level of control technologies.

A.2 Sensitivity studies examining uncertainty in global estimates of Hg consumption in chlor-alkali

Global Hg consumption in chlor-alkali may be even greater in the 1970s, as our estimates are based on US consumption patterns where most chlor-alkali plants used non-Hg technologies and chlor-alkali was 25% of total consumption (American Metal Mart, 1995). In Western Europe, most chlor-alkali plants used Hg cells and thus chlor-alkali likely was a larger fraction of total Hg use there (Emerson, 1974). There is only reliable quantitative information available for Sweden during this period, where chlor-alkali was 58% of total consumption in 1970 (Hylander & Meili, 2005). We performed sensitivity studies scaling the proportion Hg consumed in chlor-alkali in Sweden in 1970 alone or from 1960–1980 instead of the US fraction to estimate developed world consumption. We used two different methods to accommodate the increase in estimated developed world chlor-alkali Hg use: 1) keeping the total developed world consumption of Hg the same by decreasing consumption in other uses there; 2) decreasing total developing world consumption so developed world consumption in other uses remains the same. Though the fraction of total Hg used in chlor-alkali globally doubles (in 1970 alone or from 1960–1980), this leads to only minor changes in total releases during those decades ($<$5% decrease). There is a redistribution of Hg releases from the atmosphere to water, land, and landfills when consumption in chlor-alkali is increased, but this affects modeled atmospheric Hg mass only slightly ($\leq$10% reduction in the magnitude of the 1970s peak, a slight widening of the peak and shift in timing of 0 to 8 years earlier, and a $<$2% reduction in the present-day magnitude).

	World, 1850-1960	Developed World, 1970-2010	Devloping World, 1970-2010
Chlor-Alkali	1–4	1, 5, 26, 27	1, 5
Large-scale Gold and Silver Mining	1	5	1, 5
Artisanal and Small-Scale Gold Mining (ASGM)	1, 5	1, 5	1, 5, 35
Vinyl Chloride Monomer (VCM) and Other Chemical	2, 6, 7	2, 5 - 7, 9, 16	5, 36, 37
Paint	8–10	26, 28 - 31	5, 26, 28 - 31
Lamps	11	16, 11	5
Batteries	5	7, 8, 32, 33	5
Wiring Devices and Industrial Measuring Devices	11	11	5
Medical Devices	5, 11	11	5
Pharmaceuticals and Personal Care Products	5	5	5
Dental amalgam	5, 11	11,	5
Dyes/Vermilion	9, 12 - 16	NA	NA
Pesticides and Fertilizer	2, 5, 7	5, 7, 2	5, 7, 2
Explosives/Weapons	16 - 23	NA	NA
Solid waste	11, 24, 25	11, 24, 25, 34	5, 38
Wastewater	5	5, 11	5

Table A.1: Sources used to generate distribution factors.

1. Streets, D. G.; Devane, M. K.; Lu, Z.; Bond, T. C.; Sunderland, E. M.; Jacob, D. J. All-Time Releases of Mercury to the Atmosphere from Human Activities. Environmental Science & Technology 2011, 45, (24), 10485-10491.

2. Materials balance and technology assessment of mercury and its compounds on national and regional bases; EPA 560/3-75-007; U.S. Environmental Protection Agency Office of Toxic Substances: Washington, D.C., October, 1975.

3. Trip, L.; Thorleifson, M. The Canadian Mercury Cell Chlor-Alkali industry: Mercury Emissions and Status of Facilities 1935 - 1996; Environment Canada, Transboundary Air Issues Branch: Quebec, Canada, April, 1998.

4. Flewelling, F. J. In Loss of mercury to the environment from chlor-alkali plants, Special symposium on mercury in man's environment, Ottawa, Canada, February 15-16, 1971; Watkin, J. E., Ed.; National Research Council of Canada: Ottawa, Canada, 1971.

5. Toolkit for Identification and Quantification of Mercury Sources, Reference Report and Guidline for Inventory Level 2, Version 1.2, April 2013; UNEP Chemicals Branch: Geneva, Switzerland, 2013.

6. Watson, W. D. Economic considerations in controlling mercury pollution. In The biogeochemistry of mercury in the environment, Nriagu, J. O., Ed.; Elsevier/North-Holland Biomedical Press: Amsterdam, the Netherlands, 1979; pp 41-68

7. Loder, T.; Coniglio, B.; Garrett, D. A Survey - Sources of Mercury Pollution and Potential Human Exposure, U.S.; Mercury Task Force, Office of Toxic Substances: 1975.

8. Nriagu, J. O. Production and uses of mercury. In The biogeochemistry of mercury in the environment; Nriagu, J. O. Ed.; Elsevier/North-Holland Biomedial Press: Amsterdam, the Netherlands, 1979; pp 23-40.

9. D'Itri, P. A.; D'Itri, F. M. Mercury Contamination: A Human Tragedy; John Wiley & Sons: New York, 1977.

10. Montague, K.; Montague, P. Mercury; Sierra Club: San Francisco, CA, 1971.

11. Cain, A.; Disch, S.; Twaroski, C.; Reindl, J.; Case, C. R. Substance flow analysis of mercury intentionally used in products in the United States. Journal of Industrial Ecology 2007, 11, (3), 61-75.

12. Japan's Current Status of Supply and Demand of Mercury, and Activities implemented to Reduce Risks using the Most Advanced Technologies [Online]; Japan Government submission to UNEP; www.chem.unep.ch/mercury/Call_for_information/Japan-submission.pdf

    (accessed June 6, 2012).

13. Vermilion. Wikipedia [Online]; http://en.wikipedia.org/wiki/Vermilion (accessed October 24, 2012).

14. Noah Seelam/AFP/Getty Images. INDIA-RELIGION-HINDU-SINDHOOR. www.gettyimages.com/detail/news-photo/indian-women-put-vermilion-on-each-other-and-offer-sweets-news-photo/154661149

    (accessed March 4, 2013).

15. Sindoor. Wikipedia [Online]; http://en.wikipedia.org/wiki/Sindoor (accessed March 4, 2013).

16. Berthelot; Vieille. Etude des propri□t□s explosives du fulminate de mercure. Comptes rendus de l'Acadámie des Sciences 1880, 90, 946 - 952.

17. Garner, W. E.; Hailes, H. R. Thermal decomposition and detonation of mercury fulminate. P R Soc Lond a-Conta 1933, 139, (839), 576-595.

18. Davis, T. L. Pyrotechnic snakes. Journal of Chemical Edcuation 1940, 17, (6), 268-270.

19. Brown, M. E.; Swallowe, G. M. The Thermal-Decomposition of the Silver(I) and Mercury(Ii) Salts of 5-Nitrotetrazole and of Mercury(Ii) Fulminate. Thermochim Acta 1981, 49, (2-3), 333-349.

20. Characterization of Products Containing Mercury in Muncipal Solid Waste in the United States, 1970 to 2000; U.S. Environmental Protection Agency, Office of Solid Waste, Municipal and Industrial Solid Waste Division: Washington, DC, 1992.

21. Wallace, J. S., Discharge residue from mercury fulminate-primed ammunition. Sci Justice 1998, 38, (1), 7-14.

22. PowerLabs Fulminate Explosives Synthesis. http://www.powerlabs.org/chemlabs/fulminate.htm (accessed March 4, 2013).

23. Calvert, J. B. Mercury. http://mysite.du.edu/~jcalvert/phys/mercury.htm (accessed February 1, 2012).

24. Modern Landfills: A Far Cry from the Past; National Solid Wastes Management Association: Washington, DC, 2008.

25. Municipal Solid Waste in the United States: 2001 Facts and Figures; EPA530-R-03-011; U.S. Environmental Protection Agency, Office of Solid Waste and Emergency Response: Washington, DC, 2003.

26. Jasinski, S. M. The materials flow of mercury in the United States; Bureau of Mines Information Circular IC 9412; U.S. Department of the Interior: Washington, DC, 1994.

27. MPCA 2000 / Kohlasch 2000 mercury grade caustic soda report p 2;

28. Taylor, C. G.; Tickle, W.; Dwyer, A., Radiometric Studies of Mercury Loss from Fungicidal Paints, II - Comparison of Three Phenyl Mercury Compounds. Journal of Applied Chemistry 1969, 19, (1), 8-13.

29. Taylor, C. G.; Hunter, G. H., Radiometric Studies of Mercury Loss from Fungicidal Paints, III - Loss from Three Paints with Various Mercury Contents. J Appl Chem Biotechn 1972, 22, (6), 711-718.

30. Husar, J. D.; Husar, R. B. Trends of Anthropogenic Mercury Mass Flows and Emissions in Florida; Florida DEP PO# S3700 303975; Tetra Tech, Inc subcontract agreement 11718-02; Latern Corporation: Clayton, MO, 2002.

31. Substance Flow Analysis of Mercury in Products; Barr Engineering: Minneapolis, MN, August 15, 2001.

32. Floyd, P.; Zarogiannis, P.; Crane, M.; Tarkowski, S.; Bencko, V. Risks to health and the environment related to the use of mercury products; Risk & Policy Analysts for the European Commission, DG Enterprise: Norfolk, UK, 2002.

33. Kindbom, K.; Munthe, J. Product-related emissions of Mercury to Air in the European Union; IVL Swedish Environmental Research Institute Ltd. : G□teborg, Sweden, 2007.

34. EPA 1971: "Initiating a National Effort to Improve Solid Waste Management" ; SW-14; "A comprehensive chronicle of activities and accomplishments in solid waste management within the U.S. Department of Health, Education, and Welfare under authority of the Solid Waste Disposal Act of 1965;

35. Technical Background Report for the Global Mercury Assessment 2013; Arctic Monitoring and Assessment Programme (AMAP), Oslo, Norway/UNEP Chemicals Branch, Geneva, Switzerland: 2013.

36. NRDC submission to UNEP in response to March 2006 request for information on mercury supply, demand, and trade; National Resources Defense Council (NRDC): Washington, DC, May, 2006.

37. Lassen, C.; Andersen, B. H.; Maag, J.; Maxson, P. Options for reducing mercury use in products and applications, and the fate of mercury already circulating in society; ENV.G.2/ETU/2007/0021; COWI and Concorde East/West for the European Commission Directorate-General Environment: 2008.

38. Cheng, H. F.; Hu, Y. A., Mercury in Municipal Solid Waste in China and Its Control: A Review. Environmental Science & Technology 2012, 46, (2), 593-605.

	Air	Water	Soil	Recycled	Solid Waste	Wastewater	Other Disposal
Chlor-Alkali Plants	0.12	0.62	0.08	0.11	0.075		
Silver and Large-scale Gold Mining	0.40*	0.3	0.3	0			
Artisanal and Small-Scale Gold Mining (ASGM)	0.4	0.3	0.3				
Vinyl Chloride Monomer (VCM) and Other Chemical	0.11	0.2	0.01	0.48		0.2	
Paint	0.5	0.31			0.04	0.15	
Lamps	0.1				0.9		
Batteries					1		
Wiring Devices and Industrial Measuring Devices	0.02			0.09	0.87	0.01	
Medical Devices	0.1				0.47	0.18	0.27
Pharmaceuticals and Personal Care Products			0.05		0.05	0.9	
Dental amalgam†	0.02		0.02		0.23	0.15	
Dyes/Vermilion‡	0.06				0.313	0.313	
Pesticides and Fertilizer			0.85		0.075	0.075	
Explosives/Weapons	0.5		0.245		0.245	0.01	

Table A.2: Selected distribution factors: Global Tier 1 distribution factors, 1850 - 1950
*Emissions factor to air varies decadally to be consistent with Streets et al. (2011); the decrease in air emissions with time is compensated by a corresponding increase in recycling of Hg. †Factors do not add up to 1; the remainder of Hg used in dental amalgam resides in teeth and will be eventually released through cremation pathways or stored permanently through burial. ‡Factors do not add up to 1; the remaining fraction is permanently stored in artifacts.

	World, 1960	Developing & Developed World, 1970-2010	World, 1960	Developing World, 1970-2010	Developed World, 2000	World, 1960	Developing World, 1970-2010
Air	0.52	0.52	0.05	0.12	0.04	0.12	0.03
Water	0.28	0.26	0.62	0.02	0.01	0.2	
Soil			0.08	0.42	0.16	0.06	
Recycled			0.18	0.33	0.4	0.42	0.48
Solid Waste	0.08	0.1	0.075	0.11	0.003		0.47
Wastewater	0.06	0.02				0.2	0.03
Other Disposal					0.4		

Table A.3: Selected distribution factors: Time-varying Tier 1 distribution factors for selected uses and decades.
*Factors do not add up to 1; the remainder of Hg used in paint is stored in painted surfaces and paint cans.

		World, 1850-1960	Developing World, 1970-2010	Developed World, 1970	Developed World, 2010
Solid Waste Treatment Tier 2	incineration	0.36		0.27	0.18
	landfill	0.32	0.57	0.37	0.79
	direct air*	0.16	0.26	0.18	
	direct soil*	0.16	0.18	0.18	
Fraction Released to Air from Incineration Tier 3	Solid waste	0.9	†	0.9	0.05
	medical/ hazardous waste	0.64	†	0.64	0.02
	iron & steel recycling	NA	NA	0.94	0.94
	cremation	0.75	0.75	0.75	0.75
Wastewater Treatment Tier 2	water	0.9	0.9	0.9	0.07
	sludge	0.1	0.1	0.1	0.93
Sewage sludge distribution Tier 3	general solid waste	1	1		
	landfill			0.5	0.13
	air				0.11
	soil			0.5	0.77

Table A.4: Selected distribution factors: Tier 2 and Tier 3 distribution factors for solid waste, other disposal, and wastewater treatment.

*Direct releases to air and soil from waste treatment represent open dumping and burning of waste.

†Fraction through these pathways is not explicitly represented for the developing world but taken into account through direct air emissions.

	Rate Coefficient (a^{-1})
Atmosphere	
Hg(II) deposition to ocean	0.72
Hg(0) deposition to ocean	0.34
Hg(II) deposition to land	0.3
Hg(0) deposition to land	0.3
Surface ocean	
Hg(0) evasion	1.6
Particle settling to subsurface ocean	1.1
Water transfer to subsurface ocean	1.8
Subsurface ocean	
Particle settling to deep ocean	0.0036
Water transfer to surface ocean	0.053
Water transfer to deep ocean	0.0026
Deep ocean	
Burial to deep sediments	9.50E-04
Water transfer to subsurface ocean	7.90E-04
Fast terrestrial	
Evasion due to respiration of organic carbon	0.048
Photochemical re-emission of deposited Hg	0.088
Biomass burning	0.03
Transfer to slow pool	0.034
Transfer to armored pool	9.40E-04
River runoff: total reaching estuary, including burial in benthic sediments of coastal marine systems	0.54
River runoff: transfer to surface ocean alone	0.16
Slow soil	
Evasion due to respiration of organic carbon	0.0072
Biomass burning	2.20E-04
Transfer to fast pool	0.0059
Transfer to armored pool	1.40E-05
River runoff: total reaching estuary, including burial in benthic sediments of coastal marine systems	0.003
River runoff: transfer to surface ocean alone	0.0012
Armored soil	
Evasion due to respiration of organic carbon	1.30E-04
Biomass burning	2.10E-05
Transfer to fast pool	7.70E-05
River runoff: total reaching estuary, including burial in benthic sediments of coastal marine systems	1.10E-04
River runoff: transfer to surface ocean alone	3.80E-04
Landfills	
Emission to atmosphere	4.70E-05

Table A.5: Rate coefficients used in global biogeochemical box model in this work
Rate coefficients are from Holmes et al. (2010) for the atmosphere and biomass burning, Soerensen et al. (2010) and Sunderland & Mason (2007) for the ocean, Smith-Downey et al. (2010) for the soil pools, Amos et al. (2014) for river runoff. See Methods (Section 2.2) for source of landfills rate coefficient.

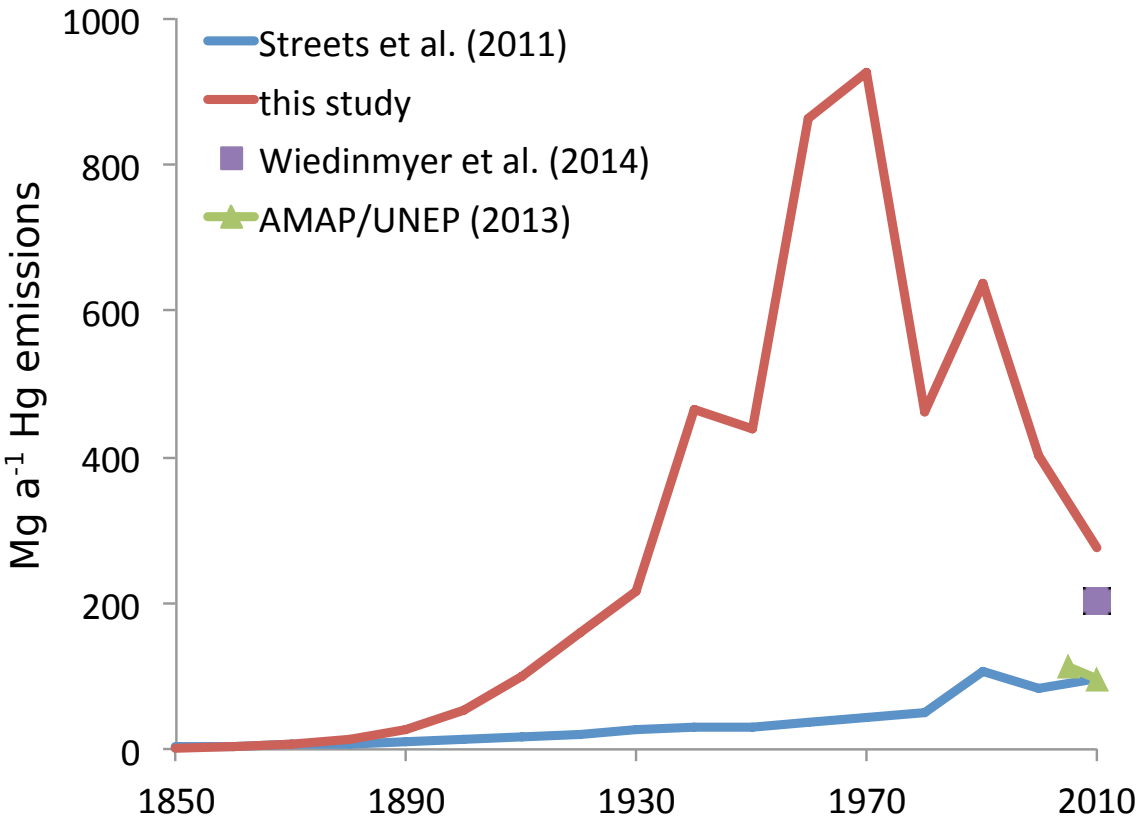

Figure A.1: Comparison of waste incineration emissions estimates. In the present-day, Wiedinmyer et al. (2014) estimate illegal trash burning emissions only, which would likely be in addition to waste incineration estimates from Streets et al. (2011) and AMAP/UNEP (2013) Our estimate attempts to include all forms of waste incineration including open burning, though this was not an explicit focus of the present study. See discussion in section A.1

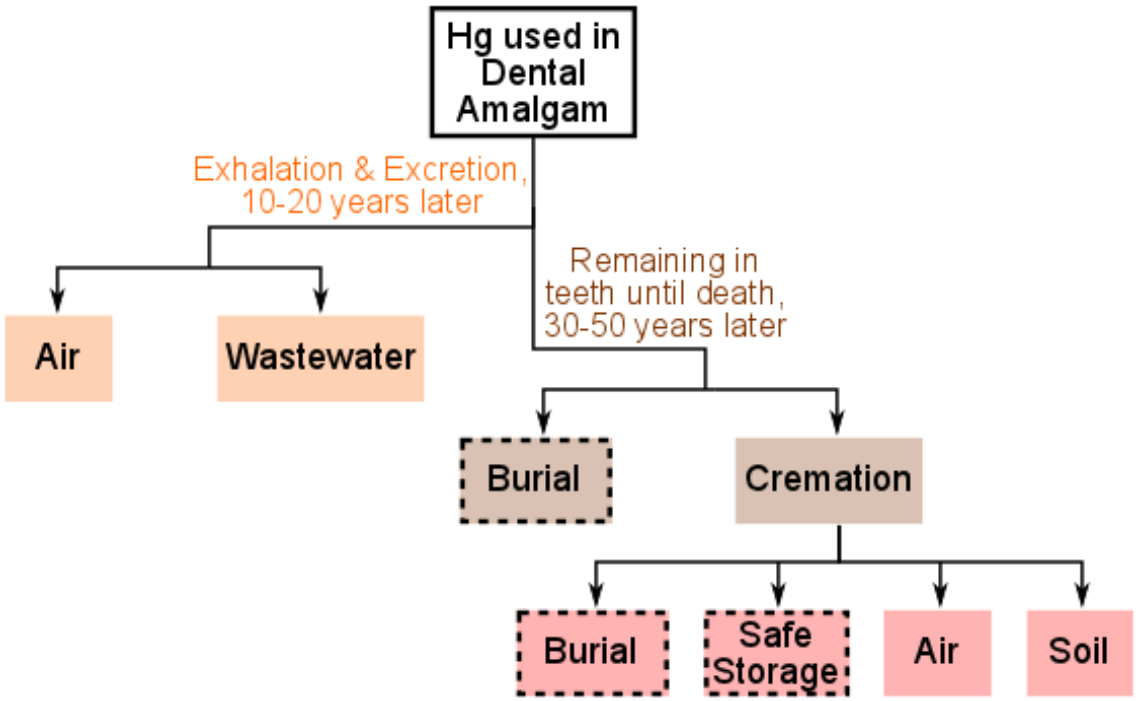

Figure A.2: Additional release pathways for Dental amalgam. Pathways shown are in addition to those indicated in Figure 2.2 of the manuscript and are delayed in time from the initial consumption of Hg. Dashed lines mark pathways that result in permanent sequestration of Hg.

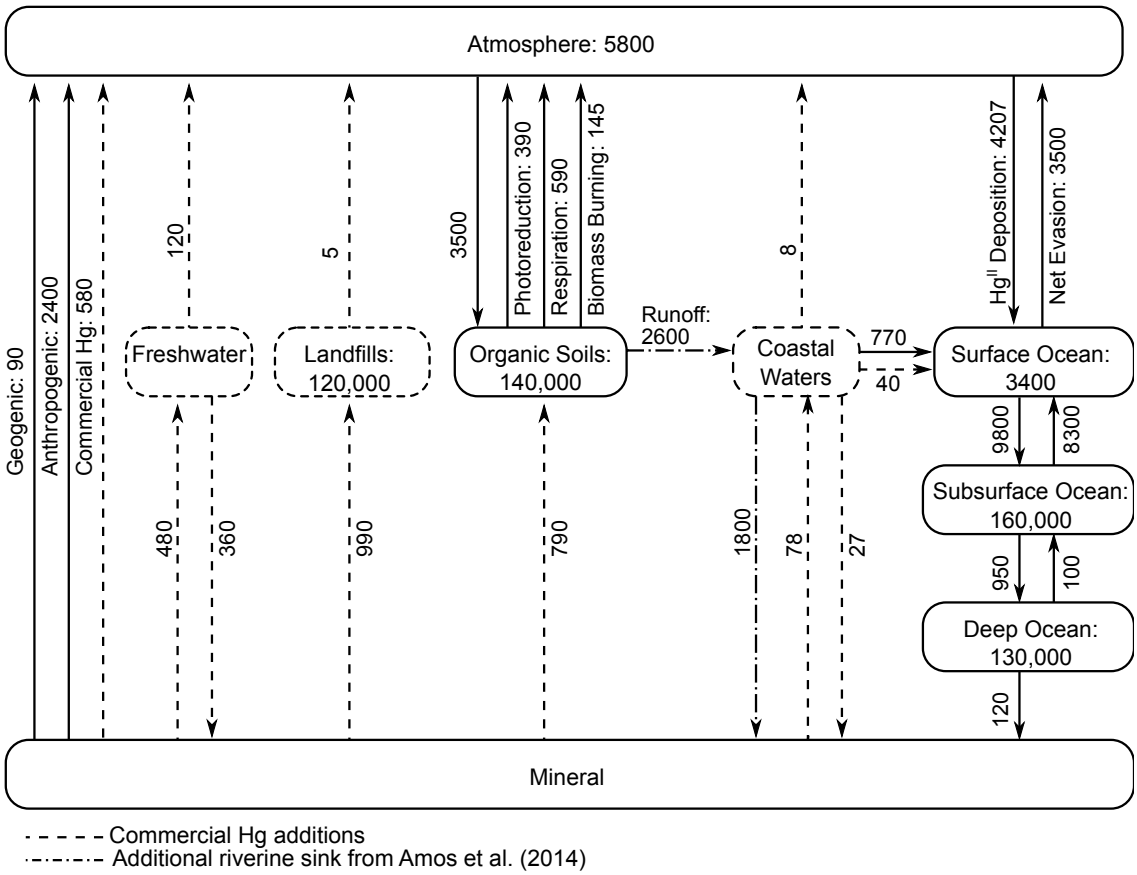

Figure A.3: Global present-day mass flows in the biogeochemical box model. Reservoir inventories are in Mg, and rates of exchange between reservoirs are in Mg a^{-1}. Additions to Amos et al. (2013) for our commercial Hg work are shown in dashed lines and the new riverine Hg sink through burial in coastal sediments from Amos et al. (2014) is indicated in dot-dash lines.

References

ACAP (2005). *Assessment of Mercury Releases from the Russian Federation*. Report, Arctic Council Action Plan to Eliminate Pollution of the Arctic (ACAP), Russian Federal Service for Environmental, Technological and Atomic Supervision & Danish Environmental Protection Agency.

Alexander, B., Park, R. J., Jacob, D. J., Li, Q. B., Yantosca, R. M., Savarino, J., Lee, C. C. W., & Thiemens, M. H. (2005). Sulfate formation in sea-salt aerosols: Constraints from oxygen isotopes. *Journal of Geophysical Research-Atmospheres*, 110(D10).

Allan, M., Le Roux, G., Sonke, J. E., Piotrowska, N., Streel, M., & Fagel, N. (2013). Reconstructing historical atmospheric mercury deposition in western europe using: Misten peat bog cores, belgium. *Science of the Total Environment*, 442, 290–301.

Allard, B. & Arsenie, I. (1991). Abiotic reduction of mercury by humic substances in aquatic system - an important process for the mercury cycle. *Water Air and Soil Pollution*, 56, 457–464.

AMAP/UNEP (2008). *Technical Background Report to the Global Atmospheric Mercury Assessment*. Report, Arctic Monitoring and Assessment Programme/UNEP Chemicals Branch.

AMAP/UNEP (2013). *Technical Background Report for the Global Mercury Assessment 2013*. Report, Arctic Monitoring and Assessment Programme, Oslo, Norway/UNEP Chemicals Branch, Geneva, Switzerland.

American Metal Mart (1960 - 1995). *Metal statistics*. New York: American Metal Mart.

Amos, H. M., Jacob, D. J., Holmes, C. D., Fisher, J. A., Wang, Q., Yantosca, R. M., Corbitt, E. S., Galarneau, E., Rutter, A. P., Gustin, M. S., Steffen, A., Schauer, J. J., Graydon, J. A., St Louis, V. L., Talbot, R. W., Edgerton, E. S., Zhang, Y., & Sunderland, E. M. (2012). Gas-particle partitioning of atmospheric hg(ii) and its effect on global mercury deposition. *Atmospheric Chemistry and Physics*, 12(1), 591–603.

Amos, H. M., Jacob, D. J., Kocman, D., Horowitz, H. M., Zhang, Y., Dutkiewicz, S., Horvat, M., Corbitt, E. S., Krabbenhoft, D. P., & Sunderland, E. M. (2014). Global biogeochemical implications of mercury discharges from rivers and sediment burial. *Environmental Science & Technology*, DOI: 10.1021/es502134t.

Amos, H. M., Jacob, D. J., Streets, D. G., & Sunderland, E. M. (2013). Legacy impacts of all-time anthropogenic emissions on the global mercury cycle. *Global Biogeochemical Cycles*, 27(2), 410–421.

Amos, H. M., Sonke, J. E., Obrist, D., Robins, N., Hagan, N., Horowitz, H. M., Mason, R. P., Witt, M., Hedgecock, I. M., Corbitt, E. S., et al. (2015). Observational and modeling constraints on global anthropogenic enrichment of mercury. *Environmental science & technology*, 49(7), 4036–4047.

Amos, H. M., Sunderland, E., Corbitt, E. S., Hedgecock, I., Kocman, D., Krabbenhoft, D., Lamborg, C. H., Obrist, D., Pirrone, N., Sonke, J. E., Witt, M. L. I., & Horowitz, H. M. (in prep.). Defining natural and anthropogenic mercury impacts.

Amyot, M., Lean, D. R. S., Poissant, L., & Doyon, M. R. (2000). Distribution and transformation of elemental mercury in the st. lawrence river and lake ontario. *Canadian Journal of Fisheries and Aquatic Sciences*, 57, 155–163.

Amyot, M., Mierle, G., Lean, D., & McQueen, D. (1994). Sunlight-induced formation of dissolved gaseous mercury in lake waters. *Environmental Science & Technology*, 28(13), 2366–2371.

Andersson, M. E., Gårdfeldt, K., Wängberg, I., Sprovieri, F., Pirrone, N., & Lindqvist, O. (2007). Seasonal and daily variation of mercury evasion at coastal and off shore sites from the mediterranean sea. *Marine Chemistry*, 104(3-4), 214–226.

Andren, M. O. & Nriagu, J. O. (1979). *The global cycle of mercury*. John Wiley & Sons.

Arenholt-Bindslev, D. (1998). Environmental aspects of dental filling materials. *European Journal of Oral Sciences*, 106(2), 713–720.

Ariya, P. A., Khalizov, A., & Gidas, A. (2002). Reactions of gaseous mercury with atomic and molecular halogens: Kinetics, product studies, and atmospheric implications. *Journal of Physical Chemistry A*, 106(32), 7310–7320.

Association, N. S. W. M. (2008). *Modern Landfills: A Far Cry from the Past*. Report, National Solid Wastes Management Association.

Auzmendi-Murua, I., Castillo, A., & Bozzelli, J. (2014). Mercury oxidation via chlorine, bromine, and iodine under atmospheric conditions: Thermochemistry and kinetics. *Journal of Physical Chemistry A*, 118(16), 2959–2975.

Balabanov, N. & Peterson, K. (2003). Mercury and reactive halogens: The thermochemistry of hg+Cl-2, Br-2, BrCl, ClO, and BrO. *Journal of Physical Chemistry A*, 107(38), 7465–7470.

Balabanov, N., Shepler, B., & Peterson, K. (2005). Accurate global potential energy surface and reaction dynamics for the ground state of hgbr2. *Journal of Physical Chemistry A*, 109(39), 8765–8773.

Bash, J., Carlton, A., Hutzell, W., & Bullock, O. (2014). Regional air quality model application of the aqueous-phase photo reduction of atmospheric oxidized mercury by dicarboxylic acids. *Atmosphere*, 5(1), 1–15.

Bergan, T. & Rodhe, H. (2001). Oxidation of elemental mercury in the atmosphere; constraints imposed by global scale modelling. *Journal of Atmospheric Chemistry*, 40(2), 191–212.

Bey, I., Jacob, D. J., Yantosca, R. M., Logan, J. A., Field, B. D., Fiore, A. M., Li, Q. B., Liu, H. G. Y., Mickley, L. J., & Schultz, M. G. (2001). Global modeling of tropospheric chemistry with assimilated meteorology: Model description and evaluation. *Journal of Geophysical Research-Atmospheres*, 106(D19), 23073–23095.

Brenninkmeijer, C. A. M., Crutzen, P., Boumard, F., Dauer, T., Dix, B., Ebinghaus, R., Filippi, D., Fischer, H., Franke, H., Friess, U., Heintzenberg, J., Helleis, F., Hermann, M., Kock, H. H., Koeppel, C., Lelieveld, J., Leuenberger, M., Martinsson, B. G., Miemczyk, S., Moret, H. P., Nguyen, H. N., Nyfeler, P., Oram, D.,

O'Sullivan, D., Penkett, S., Platt, U., Pupek, M., Ramonet, M., Randa, B., Reichelt, M., Rhee, T. S., Rohwer, J., Rosenfeld, K., Scharffe, D., Schlager, H., Schumann, U., Slemr, F., Sprung, D., Stock, P., Thaler, R., Valentino, F., van Velthoven, P., Waibel, A., Wandel, A., Waschitschek, K., Wiedensohler, A., Xueref-Remy, I., Zahn, A., Zech, U., & Ziereis, H. (2007). Civil aircraft for the regular investigation of the atmosphere based on an instrumented container: The new caribic system. *Atmospheric Chemistry and Physics*, 7(18), 4953–4976.

Brooks, W. E. & Matos, G. R. (2005). *Mercury recycling in the United States in 2000*. Book section, United States Geological Survey.

Bullock, O. R., Atkinson, D., Braverman, T., Civerolo, K., Dastoor, A., Davignon, D., Ku, J. Y., Lohman, K., Myers, T. C., Park, R. J., Seigneur, C., Selin, N. E., Sistla, G., & Vijayaraghavan, K. (2008). The north american mercury model intercomparison study (nammis): Study description and model-to-model comparisons. *Journal of Geophysical Research-Atmospheres*, 113(D17).

Buxton, G., Greenstock, C., Helman, W., & Ross, A. (1988). Critical review of rate constants for reactions of hydrated electrons, hydrogen atoms and hydroxyl radicals (·oh/·o-) in aqueous solution. *Journal of Physical and Chemical Reference Data*, 17(2), 513–886.

Cain, A., Disch, S., Twaroski, C., Reindl, J., & Case, C. R. (2007). Substance flow analysis of mercury intentionally used in products in the united states. *Journal of Industrial Ecology*, 11(3), 61–75.

Calvert, J. G. & Lindberg, S. E. (2005). Mechanisms of mercury removal by o-3 and oh in the atmosphere. *Atmospheric Environment*, 39(18), 3355–3367.

Chakraborty, L. B., Qureshi, A., Vadenbo, C., & Hellweg, S. (2013). Anthropogenic mercury flows in india and impacts of emission controls. *Environmental Science & Technology*, 47(15), 8105–8113.

Considine, D. B., Logan, J. A., & Olsen, M. A. (2008). Evaluation of near-tropopause ozone distributions in the global modeling initiative combined stratosphere/troposphere model with ozonesonde data. *Atmospheric Chemistry and Physics*, 8(9), 2365–2385.

Corbitt, E. S., Jacob, D. J., Holmes, C. D., Streets, D. G., & Sunderland, E. M. (2011). Global source–receptor relationships for mercury deposition under present-day and 2050 emissions scenarios. *Environmental science & technology*, 45(24), 10477–10484.

Costa, M. & Liss, P. S. (1999). Photoreduction of mercury in sea water and its possible implications for hg(0) air-sea fluxes. *Marine Chemistry*, 68(1-2), 87–95.

Dastoor, A. P. & Larocque, Y. (2004). Global circulation of atmospheric mercury: a modelling study. *Atmospheric Environment*, 38(1), 147–161.

De Simone, F., Gencarelli, C. N., Hedgecock, I. M., & Pirrone, N. (2014). Global atmospheric cycle of mercury: a model study on the impact of oxidation mechanisms. *Environmental Science and Pollution Research*, 21(6), 4110–4123.

Deeds, D., Banic, C., Lu, J., & Daggupaty, S. (2013). Mercury speciation in a coal-fired power plant plume: An aircraft-based study of emissions from the 3640 mw nanticoke generating station, ontario, canada. *Journal of Geophysical Research-Atmospheres*, 118(10), 4919–4935.

Dibble, T. S., Zelie, M. J., & Mao, H. (2012). Thermodynamics of reactions of clhg and brhg radicals with atmospherically abundant free radicals. *Atmospheric Chemistry and Physics*, 12(21), 10271–10279.

Dibble, T. S., Zelie, M. J., & Mao, H. (2013). Corrigendum to "thermodynamics of reactions of clhg and brhg radicals with atmospherically abundant free radicals" published in atmos. chem. phys. 12, 10271–10279, 2012. *Atmospheric Chemistry and Physics*, 13, 9211–9212.

D'Itri, P. A. & D'Itri, F. M. (1977). *Mercury Contamination: A Human Tragedy*. New York: John Wiley & Sons.

Dix, B., Baidara, S., Bresch, J., Hall, S., Schmidt, K., Wang, S., & Volkamer, R. (2013). Detection of iodine monoxide in the tropical free troposphere. *Proceedings of the National Academy of Sciences of the United States of America*, 110(6), 2035–2040.

Donohoue, D., Bauer, D., Cossairt, B., & Hynes, A. (2006). Temperature and pressure dependent rate coefficients for the reaction of hg with br and the reaction of br with br: A pulsed laser photolysis-pulsed laser induced fluorescence study. *Journal of Physical Chemistry A*, 110(21), 6623–6632.

Donohoue, D. L., Bauer, D., & Hynes, A. J. (2005). Temperature and pressure dependent rate coefficients for the reaction of hg with cl and the reaction of cl with cl: A pulsed laser photolysis-pulsed laser induced fluorescence study. *Journal of Physical Chemistry A*, 109(34), 7732–7741.

Edgerton, E. S., Hartsell, B. E., & Jansen, J. J. (2006). Mercury speciation in coal-fired power plant plumes observed at three surface sites in the southeastern us. *Environmental Science & Technology*, 40(15), 4563–4570.

Emerson, D. (1974). The industrial uses of mercury. In *I congreso internacional del mercurio* (pp. 29 – 37). Madrid, Spain: Fabrica Nacional de Moneda y Timbre.

Engineering, B. (2001). *Substance Flow Analysis of Mercury in Products*. Report, Barr Engineering.

Engstrom, D. R., Balogh, S. J., & Swain, E. B. (2007). History of mercury inputs to minnesota lakes: Influences of watershed disturbance and localized atmospheric deposition. *Limnology and Oceanography*, 52(6), 2467–2483.

Fain, X., Ferrari, C. P., Dommergue, A., Albert, M. R., Battle, M., Severinghaus, J., Arnaud, L., Barnola, J. M., Cairns, W., Barbante, C., & Boutron, C. (2009). Polar firn air reveals large-scale impact of anthropogenic mercury emissions during the 1970s. *Proceedings of the National Academy of Sciences of the United States of America*, 106(38), 16114–16119.

Fan, S.-M. & Jacob, D. J. (1992). Surface ozone depletion in arctic spring sustained by bromine reactions on aerosols. *Nature*, 359, 522–524.

Feng, X., Wang, S., Qiu, G., He, T., Li, G., Li, Z., & Shang, L. (2008). Total gaseous mercury exchange between water and air during cloudy weather conditions over hongfeng reservoir, guizhou, china. *Journal of Geophysical Research: Atmospheres*, 113(D15).

Fernandez, R. P., Salawitch, R. J., Kinnison, D. E., Lamarque, J. F., & Saiz-Lopez, A. (2014). Bromine partitioning in the tropical tropopause layer: implications for stratospheric injection. *Atmospheric Chemistry and Physics*, 14(24), 13391–13410.

Fisher, J. A., Jacob, D. J., Soerensen, A. L., Amos, H. M., Corbitt, E. S., Streets, D. G., Wang, Q. Q., Yantosca, R. M., & Sunderland, E. M. (2013). Factors driving mercury variability in the arctic atmosphere and ocean over the past 30 years. *Global Biogeochemical Cycles*, 27(4), 1226–1235.

Fisher, J. A., Jacob, D. J., Soerensen, A. L., Amos, H. M., Steffen, A., & Sunderland, E. M. (2012). Riverine source of arctic ocean mercury inferred from atmospheric observations. *Nature Geoscience*, 5, 499–504.

Fitzgerald, W., Gill, G. A., & Hewitt, A. D. (1983). *Air-sea exchange of mercury*. Plenum Publishing Company.

Fitzgerald, W. F., Engstrom, D. R., Mason, R. P., & Nater, E. A. (1998). The case for atmospheric mercury contamination in remote areas. *Environmental Science & Technology*, 32(1), 1–7.

Flewelling, F. (1971). Loss of mercury to the environment from chlor-alkali plants. In J. Watkin (Ed.), *Special symposium on mercury in man's environment*: National Research Council of Canada.

Floyd, P., Zarogiannis, P., Crane, M., Tarkowski, S., & Bencko, V. (2002). *Risks to health and the environment related to the use of mercury products*. Report, Risk & Policy Analysts for the European Commission, DG Enterprise.

Fu, X. W., Feng, X., Liang, P., Deliger, Zhang, H., Ji, J., & Liu, P. (2012a). Temporal trend and sources of speciated atmospheric mercury at waliguan gaw station, northwestern china. *Atmospheric Chemistry and Physics*, 12(4), 1951–1964.

Fu, X. W., Feng, X., Shang, L. H., Wang, S. F., & Zhang, H. (2012b). Two years of measurements of atmospheric total gaseous mercury (tgm) at a remote site in mt. changbai area, northeastern china. *Atmospheric Chemistry and Physics*, 12(9), 4215–4226.

Fu, X. W., Yang, X., Lang, X. F., Zhou, J., Zhang, H., Yu, B., Yan, H. Y., Lin, C. J., & Feng, X. B. (2016). Atmospheric wet and litterfall mercury deposition at urban and rural sites in china. *Atmospheric Chemistry and Physics*, 16(18), 11547–11562.

Fu, X. W., Zhang, H., Yu, B., Wang, X., Lin, C. J., & Feng, X. B. (2015). Observations of atmospheric mercury in china: a critical review. *Atmospheric Chemistry and Physics*, 15(16), 9455–9476.

Gårdfeldt, K. & Jonsson, M. (2003). Is bimolecular reduction of hg(ii) complexes possible in aqueous systems of environmental importance. *Journal of Physical Chemistry A*, 107(22), 4478–4482.

Gårdfeldt, K., Sommar, J., Ferrara, R., Ceccarini, C., Lanzillotta, E., Munthe, J., Wängberg, I., Lindqvist, O., Pirrone, N., Sprovieri, F., Pesenti, E., & Strömberg, D. (2003). Evasion of mercury from coastal and open waters of the atlantic ocean and the mediterranean sea. *Atmospheric Environment*, 37, 78–84.

Gencarelli, C. N., De Simone, F., Hedgecock, I. M., Sprovieri, F., & Pirrone, N. (2014). Development and application of a regional-scale atmospheric mercury model based on wrf/chem: a mediterranean area investigation. *Environmental Science and Pollution Research*, 21(6), 4095–4109.

Gill, G. A., Bloom, N. S., Cappellino, S., Driscoll, C. T., Dobbs, C., McShea, L., Mason, R., & Rudd, J. W. M. (1999). Sediment-water fluxes of mercury in lavaca bay, texas. *Environmental Science & Technology*, 33(5), 663–669.

Gómez Martín, J. C., Mahajan, A. S., Hay, T. D., Prados-Roman, C., Ordonez, C., MacDonald, S. M., Plane, J. M. C., Sorribas, M., Gil, M., Mora, J. F. P., Reyes, M. V. A., Oram, D. E., Leedham, E., & Saiz-Lopez, A. (2013). Iodine chemistry in the eastern pacific marine boundary layer. *Journal of Geophysical Research-Atmospheres*, 118(2), 887–904.

Goodsite, M., Plane, J., & Skov, H. (2004). A theoretical study of the oxidation of hg-0 to hgbr2 in the troposphere. *Environmental Science & Technology*, 38(6), 1772–1776.

Gratz, L., Keeler, G., Blum, J., & Sherman, L. (2010). Isotopic composition and fractionation of mercury in great lakes precipitation and ambient air. *Environmental Science & Technology*, 44(20), 7764–7770.

Gratz, L. E., Ambrose, J. L., Jaffe, D. A., Shah, V., Jaegle, L., Stutz, J., Festa, J., Spolaor, M., Tsai, C., Selin, N. E., Song, S., Zhou, X., Weinheimer, A. J., Knapp, D. J., Montzka, D. D., Flocke, F. M., Campos, T. L., Apel, E., Hornbrook, R., Blake, N. J., Hall, S., Tyndall, G. S., Reeves, M., Stechman, D., & Stell, M. (2015). Oxidation of mercury by bromine in the subtropical pacific free troposphere. *Geophysical Research Letters*, 42(23).

Greig, G., Gunning, H. E., & Strausz, O. P. (1970). Reactions of metal atoms .3. combination of mercury and iodine atoms and spectrum of hgi. *Journal of Chemical Physics*, 52(9), 4569–&.

Guentzel, J. L., Landing, W. M., Gill, G. A., & Pollman, C. D. (2001). Processes influencing rainfall deposition of mercury in florida. *Environmental Science & Technology*, 35(5), 863–873.

Gustin, M. S., Amos, H. M., Huang, J., Miller, M. B., & Heidecorn, K. (2015). Measuring and modeling mercury in the atmosphere: a critical review. *Atmospheric Chemistry and Physics*, 15(10), 5697–5713.

Hagreen, L. A. & Lourie, B. A. (2004). Canadian mercury inventories: the missing pieces. *Environmental Research*, 95(3), 272–281.

Haitzer, M., Aiken, G. R., & Ryan, J. N. (2002). Binding of mercury(ii) to dissolved organic matter: The role of the mercury-to-dom concentration ratio. *Environmental Science & Technology*, 36(16), 3564–3570.

Hall, B. (1995). The gas phase oxidation of elemental mercury by ozone. *Water, Air, and Soil Pollution*, 80, 301–315.

Hall, B. & Bloom, N. (1993). Report to epri, electric power research institute. *Rapport technique, EPRI, Palo Alto*.

Hamrud, M. (1983). Residence time and spatial variability for gases in the atmosphere. *Tellus Series B-Chemical and Physical Meteorology*, 35(5), 295–303.

Harris, D. C. (2002). *Quantitative Chemical Analysis*. New York: W. H. Freeman and Co.

Heald, C. L., Coe, H., Jimenez, J. L., Weber, R. J., Bahreini, R., Middlebrook, A. M., Russell, L. M., Jolleys, M., Fu, T. M., Allan, J. D., Bower, K. N., Capes, G., Crosier, J., Morgan, W. T., Robinson, N. H., Williams, P. I., Cubison, M. J., DeCarlo, P. F., & Dunlea, E. J. (2011). Exploring the vertical profile of atmospheric organic aerosol: comparing 17 aircraft field campaigns with a global model. *Atmospheric Chemistry and Physics*, 11(24), 12673–12696.

Hedgecock, I. & Pirrone, N. (2001). Mercury and photochemistry in the marine boundary layer-modelling studies suggest the in situ production of reactive gas phase mercury. *Atmospheric Environment*, 35(17), 3055–3062.

Holmes, C. D., Jacob, D. J., Corbitt, E. S., Mao, J., Yang, X., Talbot, R., & Slemr, F. (2010). Global atmospheric model for mercury including oxidation by bromine atoms. *Atmospheric Chemistry and Physics*, 10(24), 12037–12057.

Holmes, C. D., Jacob, D. J., Mason, R. P., & Jaffe, D. A. (2009). Sources and deposition of reactive gaseous mercury in the marine atmosphere. *Atmospheric Environment*, 43(14), 2278–2285.

Holmes, C. D., Jacob, D. J., & Yang, X. (2006). Global lifetime of elemental mercury against oxidation by atomic bromine in the free troposphere. *Geophysical Research Letters*, 33(20), 5.

Holmes, C. D., Krishnamurthy, N. P., Caffrey, J. M., Landing, W. M., Edgerton, E. S., Knapp, K. R., & Nair, U. S. (2016). Thunderstorms increase mercury wet deposition. *Environmental Science & Technology*, 50(17), 9343–9350.

Horowitz, H. M., Jacob, D. J., Amos, H. M., Streets, D. G., & Sunderland, E. M. (2014). Historical mercury releases from commercial products: Global environmental implications. *Environmental Science & Technology*, 48(17), 10242–10250.

Hudman, R. C., Jacob, D. J., Turquety, S., Leibensperger, E. M., Murray, L. T., Wu, S., Gilliland, A. B., Avery, M., Bertram, T. H., Brune, W., Cohen, R. C., Dibb, J. E., Flocke, F. M., Fried, A., Holloway, J., Neuman, J. A., Orville, R., Perring, A., Ren, X., Sachse, G. W., Singh, H. B., Swanson, A., & Wooldridge, P. J. (2007). Surface and lightning sources of nitrogen oxides over the united states: Magnitudes, chemical evolution, and outflow. *Journal of Geophysical Research-Atmospheres*, 112(D12).

Huthwelker, T., Peter, T., Luo, B. P., Clegg, S. L., Carslaw, K. S., & Brimblecombe, P. (1995). Solubility of hocl in water and aqueous h2so4 to stratospheric temperatures. *Journal of Atmospheric Chemistry*, 21(1), 81–95.

Hylander, L. D. & Meili, M. (2003). 500 years of mercury production: global annual inventory by region until 2000 and associated emissions. *Science of the Total Environment*, 304(1-3), 13–27.

Hylander, L. D. & Meili, M. (2005). The rise and fall of mercury: Converting a resource to refuse after 500 years of mining and pollution. *Critical Reviews in Environmental Science and Technology*, 35(1), 1–36.

Hynes, A. J., Donohoue, D. L., Goodsite, M. E., & Hedgecock, I. M. (2009). *Our Current Understanding of Major Chemical and Physical Processes Affecting Mercury Dynamics in the Atmosphere and At the Air-Water/Terrestrial Interfaces*, book section 14, (pp. 427–457). Springer Science+Business Media, LLC.

Jacob, D., Field, B., Li, Q., Blake, D., de Gouw, J., Warneke, C., Hansel, A., Wisthaler, A., Singh, H., & Guenther, A. (2005). Global budget of methanol: Constraints from atmospheric observations. *Journal of Geophysical Research-Atmospheres*, 110(D8).

Jacob, D. J. (1986). Chemistry of oh in remote clouds and its role in the production of formic-acid and peroxymonosulfate. *Journal of Geophysical Research-Atmospheres*, 91(D9), 9807–9826.

Jaffe, D. A., Lyman, S., Amos, H. M., Gustin, M. S., Huang, J. Y., Selin, N. E., Levin, L., ter Schure, A., Mason, R. P., Talbot, R., Rutter, A., Finley, B., Jaegle, L., Shah, V., McClure, C., Arnbrose, J., Gratz, L., Lindberg, S., Weiss-Penzias, P., Sheu, G. R., Feddersen, D., Horvat, M., Dastoor, A., Hynes, A. J., Mao, H. T., Sonke, J. E., Slemr, F., Fisher, J. A., Ebinghaus, R., Zhang, Y. X., & Edwards, G. (2014). Progress on understanding atmospheric mercury hampered by uncertain measurements. *Environmental Science & Technology*, 48(13), 7204–7206.

Jasinski, S. M. (1995). The materials flow of mercury in the united states. *Resources Conservation and Recycling*, 15(3-4), 145–179.

Jiao, Y. & Dibble, T. S. (2017). First kinetic study of the atmospherically important reactions brhg*+ no 2 and brhg*+ hoo. *Physical Chemistry Chemical Physics*.

Jones, C. P., Lyman, S. N., Jaffe, D. A., Allen, T., & O'Neil, T. L. (2016). Detection and quantification of gas-phase oxidized mercury compounds by gc/ms. *Atmospheric Measurement Techniques*, 9(5), 2195–2205.

Junge, C. E. (1974). Residence time and variability of tropospheric trace gases. *Tellus*, 26(4), 477–488.

Kamman, N. C. & Engstrom, D. R. (2002). Historical and present fluxes of mercury to vermont and new hampshire lakes inferred from pb-210 dated sediment cores. *Atmospheric Environment*, 36(10), 1599–1609.

Karagas, M. R., Choi, A. L., Oken, E., Horvat, M., Schoeny, R., Kamai, E., Cowell, W., Grandjean, P., & Korrick, S. (2012). Evidence on the human health effects of low-level methylmercury exposure. *Environmental Health Perspectives*, 120(6), 799–806.

Kim, S., Karl, T., Guenther, A., Tyndall, G., Orlando, J., Harley, P., Rasmussen, R., & Apel, E. (2010). Emissions and ambient distributions of biogenic volatile organic compounds (bvoc) in a ponderosa pine ecosystem: interpretation of ptr-ms mass spectra. *Atmospheric Chemistry and Physics*, 10(4), 1759–1771.

Kindbom, K. & Munthe, J. (2007). *Product-related emissions of Mercury to Air in the European Union*. Report, IVL Swedish Environmental Research Institute Ltd.

Klimont, Z., Smith, S. J., & Cofala, J. (2013). The last decade of global anthropogenic sulfur dioxide: 2000-2011 emissions. *Environmental Research Letters*, 8(1).

Knightes, C. D., Sunderland, E. M., Barber, M. C., Johnston, J. M., & Ambrose, R. B. (2009). Application of ecosystem-scale fate and bioaccumulation models to predict fish mercury response times to changes in atmospheric deposition. *Environmental Toxicology and Chemistry*, 28(4), 881–893.

Kocman, D., Horvat, M., & et al. (in prep.). A global inventory of present-day mercury releases to aquatic environments.

Kocman, D., Horvat, M., Pirrone, N., & Cinnirella, S. (2013). Contribution of contaminated sites to the global mercury budget. *Environmental Research*, 125, 160–170.

Krabbenhoft, D. (2013). Understanding the propagation of atmospheric mercury through terrestrial landscapes: After twenty five years of research does the story make sense? In *11th International Conference on Mercury as a Global Pollutant, Edinburgh, Scotland*, volume Krabbenhoft, D.: „ 2013.

Lamborg, C., Fitzgerald, W., O'Donnell, J., & Torgersen, T. (2002). A non-steady state box model of global-scale mercury biogeochemistry with interhemispheric atmospheric gradients. *Abstracts of Papers of the American Chemical Society*, 223, U520–U520.

Landis, M., Ryan, J., ter Schure, A., & Laudal, D. (2014). Behavior of mercury emissions from a commercial coal-fired power plant: The relationship between stack speciation and near-field plume measurements. *Environmental Science & Technology*, 48(22), 13540–13548.

Li, Z. G., Feng, X., Li, P., Liang, L., Tang, S. L., Wang, S. F., Fu, X. W., Qiu, G. L., & Shang, L. H. (2010). Emissions of air-borne mercury from five municipal solid waste landfills in guiyang and wuhan, china. *Atmospheric Chemistry and Physics*, 10(7), 3353–3364.

Liang, Q., Stolarski, R., Kawa, S., Nielsen, J., Douglass, A., Rodriguez, J., Blake, D., Atlas, E., & Ott, L. (2010). Finding the missing stratospheric br-y: a global modeling study of chbr3 and ch2br2. *Atmospheric Chemistry and Physics*, 10(5), 2269–2286.

Lin, C. & Pehkonen, S. (1997). Aqueous photoreduction of divalent mercury with organic acids: Implications of mercury chemistry in the atmosphere. *Abstracts of Papers of the American Chemical Society*, 213, 41–ENVR.

Lin, C. & Pehkonen, S. (1998). Oxidation of elemental mercury by aqueous chlorine (hocl/ocl-): Implications for tropospheric mercury chemistry. *Journal of Geophysical Research-Atmospheres*, 103(D21), 28093–28102.

Lin, C. J., Pongprueksa, P., Lindberg, S. E., Pehkonen, S. O., Byun, D., & Jang, C. (2006). Scientific uncertainties in atmospheric mercury models i: Model science evaluation. *Atmospheric Environment*, 40(16), 2911–2928.

Lindberg, S. E., Southworth, G. R., Bogle, M. A., Blasing, T. J., Owens, J., Roy, K., Zhang, H., Kuiken, T., Price, J., Reinhart, D., & Sfeir, H. (2005). Airborne emissions of mercury from municipal solid waste. i: New measurements from six operating landfills in florida. *Journal of the Air & Waste Management Association*, 55(7), 859–869.

Lindqvist, O. & Rodhe, H. (1985). Atmospheric mercury - a review. *Tellus Series B-Chemical and Physical Meteorology*, 37(3), 136–159.

Liu, S. H., Yan, N. Q., Liu, Z. R., Qu, Z., Wang, P., Chang, S. G., & Miller, C. (2007). Using bromine gas to enhance mercury removal from flue gas of coal-fired power plants. *Environmental Science & Technology*, 41(4), 1405–1412.

Lohman, K., Seigneur, C., Edgerton, E., & Jansen, J. (2006). Modeling mercury in power plant plumes. *Environmental Science & Technology*, 40(12), 3848–3854.

Lyman, S. & Jaffe, D. (2012). Formation and fate of oxidized mercury in the upper troposphere and lower stratosphere. *Nature Geoscience*, 5(2), 114–117.

Mahaffey, K. R., Sunderland, E. M., Chan, H. M., Choi, A. L., Grandjean, P., Marien, K., Oken, E., Sakamoto, M., Schoeny, R., Weihe, P., Yan, C. H., & Yasutake, A. (2011). Balancing the benefits of n-3 polyunsaturated fatty acids and the risks of methylmercury exposure from fish consumption. *Nutrition Reviews*, 69(9), 493–508.

Mason, R. P., Fitzgerald, W. F., & Morel, F. M. M. (1994). The biogeochemical cycling of elemental mercury - anthropogenic influences. *Geochimica Et Cosmochimica Acta*, 58(15), 3191–3198.

Mason, R. P., Lawson, N. M., Lawrence, A. L., Leaner, J. J., Lee, J. G., & Sheu, G. R. (1999). Mercury in the chesapeake bay. *Marine Chemistry*, 65(1-2), 77–96.

Mason, R. P., Lawson, N. M., & Sheu, G. R. (2001). Mercury in the atlantic ocean: factors controlling air-sea exchange of mercury and its distribution in the upper waters. *Deep-Sea Research Part Ii-Topical Studies in Oceanography*, 48(13), 2829–2853.

Maxson, P. (2004). *Mercury flows in Europe and the world: the impact of decommissioned chlor-alkali plants*. Report, Concorde East/West Sprl for the European Commission Environment Directorate-General.

Muntean, M., Janssens-Maenhout, G., Song, S. J., Selin, N. E., Olivier, J. G. J., Guizzardi, D., Maas, R., & Dentener, F. (2014). Trend analysis from 1970 to 2008 and model evaluation of edgarv4 global gridded anthropogenic mercury emissions. *Science of the Total Environment*, 494, 337–350.

Munthe, J. (1992). The aqueous oxidation of elemental mercury by ozone. *Atmospheric Environment Part a-General Topics*, 26(8), 1461–1468.

Munthe, J. & McElroy, W. J. (1992). Some aqueous reactions of potential importance in the atmospheric chemistry of mercury. *Atmospheric Environment Part a-General Topics*, 26(4), 553–557.

Murphy, D. M., Anderson, J. R., Quinn, P. K., McInnes, L. M., Brechtel, F. J., Kreidenweis, S. M., Middlebrook, A. M., Posfai, M., Thomson, D. S., & Buseck, P. R. (1998). Influence of sea-salt on aerosol radiative properties in the southern ocean marine boundary layer. *Nature*, 392(6671), 62–65.

Murphy, D. M., Hudson, P. K., Thomson, D. S., Sheridan, P. J., & Wilson, J. C. (2006). Observations of mercury-containing aerosols. *Environmental Science & Technology*, 40(10), 3163–3167.

Murray, L. T., Jacob, D. J., Logan, J. A., Hudman, R. C., & Koshak, W. J. (2012). Optimized regional and interannual variability of lightning in a global chemical transport model constrained by lis/otd satellite data. *Journal of Geophysical Research-Atmospheres*, 117.

Nguyen, H. T., Kim, K.-H., Kim, M.-Y., Hong, S., Youn, Y.-H., Shon, Z.-H., & Lee, J. S. (2007). Monitoring of atmospheric mercury at a global atmospheric watch (gaw) site on an-myun island, korea. *Water, air, and soil pollution*, 185(1-4), 149–164.

NRDC. (2006). *NRDC submission to UNEP in response to March 2006 request for information on mercury supply, demand, and trade*. Report, National Resources Defense Council.

Nriagu, J. O. (1979). *Production and uses of mercury*, book section 2, (pp. 23–40). Topics in environmental health. Elsevier/North-Holland Biomedial Press: Amsterdam, the Netherlands.

Obrist, D., Pokharel, A., & Moore, C. (2014). Vertical profile measurements of soil air suggest immobilization of gaseous elemental mercury in mineral soil. *Environmental Science & Technology*, 48(4), 2242–2252.

O'Driscoll, N., Siciliano, S., Lean, D., & Amyot, M. (2006). Gross photoreduction kinetics of mercury in temperate freshwater lakes and rivers: Application to a general model of dgm dynamics. *Environmental Science & Technology*, 40(3), 837–843.

O'Driscoll, N. J., Lean, D. R. S., Loseto, L. L., Carignan, R., & Siciliano, S. D. (2004). Effect of dissolved organic carbon on the photoproduction of dissolved gaseous mercury in lakes: Potential impacts of forestry. *Environmental Science & Technology*, 38(9), 2664–2672.

Orbe, C., Holzer, M., Polvani, L. M., Waugh, D. W., Li, F., Oman, L. D., & Newman, P. A. (2014). Seasonal ventilation of the stratosphere: Robust diagnostics from one-way flux distributions. *Journal of Geophysical Research-Atmospheres*, 119(1), 293–306.

Pacyna, E. G., Pacyna, J. M., Sundseth, K., Munthe, J., Kindbom, K., Wilson, S., Steenhuisen, F., & Maxson, P. (2010). Global emission of mercury to the atmosphere from anthropogenic sources in 2005 and projections to 2020. *Atmospheric Environment*, 44(20), 2487–2499.

Pal, B. & Ariya, P. A. (2004). Gas-phase ho center dot-initiated reactions of elemental mercury: Kinetics, product studies, and atmospheric implications. *Environmental Science & Technology*, 38(21), 5555–5566.

Parrella, J. P., Jacob, D. J., Liang, Q., Zhang, Y., Mickley, L. J., Miller, B., Evans, M. J., Yang, X., Pyle, J. A., Theys, N., & Van Roozendael, M. (2012). Tropospheric bromine chemistry: implications for present and pre-industrial ozone and mercury. *Atmospheric Chemistry and Physics*, 12(15), 6723–6740.

Pehkonen, S. O. & Lin, C. J. (1998). Aqueous photochemistry of mercury with organic acids. *Journal of the Air & Waste Management Association*, 48(2), 144–150.

Peleg, M., Tas, E., Obrist, D., Matveev, V., Moore, C., Gabay, M., & Luria, M. (2015). Observational evidence for involvement of nitrate radicals in nighttime oxidation of mercury. *Environmental Science & Technology*, 49(24), 14008–14018.

Pirrone, N., Cinnirella, S., Feng, X., Finkelman, R. B., Friedli, H. R., Leaner, J., Mason, R., Mukherjee, A. B., Stracher, G. B., Streets, D. G., & Telmer, K. (2010). Global mercury emissions to the atmosphere from anthropogenic and natural sources. *Atmospheric Chemistry and Physics*, 10(13), 5951–5964.

Ploeger, F. & Birner, T. (2016). Seasonal and inter-annual variability of lower stratospheric age of air spectra. *Atmospheric Chemistry and Physics*, 16(15), 10195–10213.

Prados-Roman, C., Cuevas, C. A., Hay, T., Fernandez, R. P., Mahajan, A. S., Royer, S. J., Gali, M., Simo, R., Dachs, J., Grossmann, K., Kinnison, D. E., Lamarque, J. F., & Saiz-Lopez, A. (2015). Iodine oxide in the global marine boundary layer. *Atmospheric Chemistry and Physics*, 15(2), 583–593.

Pye, H., Chan, A., Barkley, M., & Seinfeld, J. (2010). Global modeling of organic aerosol: the importance of reactive nitrogen (nox and no3). *Atmospheric Chemistry and Physics*, 10(22), 11261–11276.

Qu, Z., Yan, N. Q., Liu, P., Jia, J. P., & Yang, S. J. (2010). The role of iodine monochloride for the oxidation of elemental mercury. *Journal of Hazardous Materials*, 183(1-3), 132–137.

Raofie, F., Snider, G., & Ariya, P. A. (2008). Reaction of gaseous mercury with molecular iodine, atomic iodine, and iodine oxide radicals - kinetics, product studies, and atmospheric implications. *Canadian Journal of Chemistry-Revue Canadienne De Chimie*, 86(8), 811–820.

Ravichandran, M. (2004). Interactions between mercury and dissolved organic matter - a review. *Chemosphere*, 55(3), 319–331.

Rissanen, K. & Miettinen, J. K. (1972). *Use of mercury compounds in agriculture and its implications*. Book section, International Atomic Energy Agency, Vienna, Austria.

Rolfus, K. R. & Fitzgerald, W. F. (2004). Mechanisms and temporal variability of dissolved gaseous mercury production in coastal seawater. *Marine Chemistry*, 90, 126–136.

Rudd, J. W. M., Turner, M. A., Furutani, A., Swick, A. L., & Townsend, B. E. (1983). The english wabigoon river system .1. a synthesis of recent research with a view towards mercury amelioration. *Canadian Journal of Fisheries and Aquatic Sciences*, 40(12), 2206–2217.

Rutter, A. & Schauer, J. (2007a). The effect of temperature on the gas-particle partitioning of reactive mercury in atmospheric aerosols. *Atmospheric Environment*, 41(38), 8647–8657.

Rutter, A. & Schauer, J. (2007b). The impact of aerosol composition on the particle to gas partitioning of reactive mercury. *Environmental Science & Technology*, 41(11), 3934–3939.

Sakata, M. & Asakura, K. (2007). Estimating contribution of precipitation scavenging of atmospheric particulate mercury to mercury wet deposition in japan. *Atmospheric Environment*, 41(8), 1669–1680.

Sanemasa, I. (1975). Solubility of elemental mercury-vapor in water. *Bulletin of the Chemical Society of Japan*, 48(6), 1795–1798.

Schmidt, J. A., Jacob, D. J., Horowitz, H. M., Hu, L., Sherwen, T., Evans, M. J., Liang, Q., Suleiman, R. M., Oram, D. E., Le Breton, M., Percival, C. J., Wang, S., & Volkamer, R. (2016). Modeling the observed tropospheric bro background: Importance of multiphase chemistry and implications for ozone, oh, and mercury. *Journal of Geophysical Research-Atmospheres*, 121.

Schoeberl, M. R., Douglass, A. R., Zhu, Z. X., & Pawson, S. (2003). A comparison of the lower stratospheric age spectra derived from a general circulation model and two data assimilation systems. *Journal of Geophysical Research-Atmospheres*, 108(D3).

Schroeder, W. H., Anlauf, K. G., Barrie, L. A., Lu, J. Y., Steffen, A., Schneeberger, D. R., & Berg, T. (1998). Arctic springtime depletion of mercury. *Nature*, 394(6691), 331–332.

Selin, N. E., Jacob, D. J., Park, R. J., Yantosca, R. M., Strode, S., Jaegle, L., & Jaffe, D. (2007). Chemical cycling and deposition of atmospheric mercury: Global constraints from observations. *Journal of Geophysical Research-Atmospheres*, 112(D2).

Selin, N. E., Jacob, D. J., Yantosca, R. M., Strode, S., Jaegle, L., & Sunderland, E. M. (2008). Global 3-d land-ocean-atmosphere model for mercury: Present-day versus preindustrial cycles and anthropogenic enrichment factors for deposition. *Global Biogeochemical Cycles*, 22(2).

Serrano, O., Martinez-Cortizas, A., Mateo, M. A., Biester, H., & Bindler, R. (2013). Millennial scale impact on the marine biogeochemical cycle of mercury from early mining on the iberian peninsula. *Global Biogeochemical Cycles*, 27(1), 21–30.

Shah, V., Jaegle, L., Gratz, L. E., Ambrose, J. L., Jaffe, D. A., Selin, N. E., Song, S., Campos, T. L., Flocke, F. M., Reeves, M., Stechman, D., Stell, M., Festa, J., Stutz, J., Weinheimer, A. J., Knapp, D. J., Montzka, D. D., Tyndall, G. S., Apel, E. C., Hornbrook, R. S., Hills, A. J., Riemer, D. D., Blake, N. J., Cantrell, C. A., & Mauldin, R. L. (2016). Origin of oxidized mercury in the summertime free troposphere over the southeastern us. *Atmospheric Chemistry and Physics*, 16(3), 1511–1530.

Shepler, B. C. & Peterson, K. A. (2003). Mercury monoxide: A systematic investigation of its ground electronic state. *Journal of Physical Chemistry A*, 107(11), 1783–1787.

Sheu, G. R., Lin, N. H., Wang, J. L., Lee, C. T., Yang, C. F. O., & Wang, S. H. (2010). Temporal distribution and potential sources of atmospheric mercury measured at a high-elevation background station in taiwan. *Atmospheric Environment*, 44(20), 2393–2400.

Si, L. & Ariya, P. A. (2008). Reduction of oxidized mercury species by dicarboxylic acids (c(2)-c(4)): Kinetic and product studies. *Environmental Science & Technology*, 42(14), 5150–5155.

Simpson, W. R., Brown, S. S., Saiz-Lopez, A., Thornton, J. A., & von Glasow, R. (2015). Tropospheric halogen chemistry: Sources, cycling, and impacts. *Chemical Reviews*, 115(10), 4035–4062.

Slemr, F., Angot, H., Dommergue, A., Magand, O., Barret, M., Weigelt, A., Ebinghaus, R., Brunke, E. G., Pfaffhuber, K. A., Edwards, G., Howard, D., Powell, J., Keywood, M., & Wang, F. (2015). Comparison of mercury concentrations measured at several sites in the southern hemisphere. *Atmospheric Chemistry and Physics*, 15(6), 3125–3133.

Slemr, F., Brunke, E. G., Ebinghaus, R., & Kuss, J. (2011). Worldwide trend of atmospheric mercury since 1995. *Atmospheric Chemistry and Physics*, 11(10), 4779–4787.

Slemr, F., Ebinghaus, R., Brenninkmeijer, C., Hermann, M., Kock, H., Martinsson, B., Schuck, T., Sprung, D., van Velthoven, P., Zahn, A., & Ziereis, H. (2009). Gaseous mercury distribution in the upper troposphere and lower stratosphere observed onboard the caribic passenger aircraft. *Atmospheric Chemistry and Physics*, 9(6), 1957–1969.

Slemr, F., Schuster, G., & Seiler, W. (1985). Distribution, speciation, and budget of atmospheric mercury. *Journal of Atmospheric Chemistry*, 3(4), 407–434.

Slemr, F., Seiler, W., & Schuster, G. (1981). Latitudinal distribution of mercury over the atlantic-ocean. *Journal of Geophysical Research-Oceans and Atmospheres*, 86(NC2), 1159–1166.

Slemr, F., Weigelt, A., Ebinghaus, R., Brenninkmeijer, C., Baker, A., Schuck, T., Rauthe-Schoch, A., Riede, H., Leedham, E., Hermann, M., van Velthoven, P., Oram, D., O'Sullivan, D., Dyroff, C., Zahn, A., & Ziereis, H. (2014). Mercury plumes in the global upper troposphere observed during flights with the caribic observatory from may 2005 until june 2013. *Atmosphere*, 5(2), 342–369.

Slemr, F., Weigelt, A., Ebinghaus, R., Kock, H. H., Bodewadt, J., Brenninkmeijer, C. A. M., Rauthe-Schoch, A., Weber, S., Hermann, M., Becker, J., Zahn, A., & Martinsson, B. (2016). Atmospheric mercury measurements onboard the caribic passenger aircraft. *Atmospheric Measurement Techniques*, 9(5), 2291–2302.

Smith-Downey, N. V., Sunderland, E. M., & Jacob, D. J. (2010). Anthropogenic impacts on global storage and emissions of mercury from terrestrial soils: Insights from a new global model. *Journal of Geophysical Research-Biogeosciences*, 115.

Snider, G., Raofie, F., & Ariya, P. (2008). Effects of relative humidity and co(g) on the o(3)-initiated oxidation reaction of hg(0)(g): kinetic & product studies. *Physical Chemistry Chemical Physics*, 10(36), 5616–5623.

Soerensen, A. L., Jacob, D. J., Streets, D. G., Witt, M. L. I., Ebinghaus, R., Mason, R. P., Andersson, M., & Sunderland, E. M. (2012). Multi-decadal decline of mercury in the north atlantic atmosphere explained by changing subsurface seawater concentrations. *Geophysical Research Letters*, 39.

Soerensen, A. L., Mason, R. P., Balcom, P. H., Jacob, D. J., Zhang, Y. X., Kuss, J., & Sunderland, E. M. (2014). Elemental mercury concentrations and fluxes in the tropical atmosphere and ocean. *Environmental Science & Technology*, 48(19), 11312–11319.

Soerensen, A. L., Mason, R. P., Balcom, P. H., & Sunderland, E. M. (2013). Drivers of surface ocean mercury concentrations and air-sea exchange in the west atlantic ocean. *Environmental Science & Technology*, 47(14), 7757–7765.

Soerensen, A. L., Sunderland, E. M., Holmes, C. D., Jacob, D. J., Yantosca, R. M., Skov, H., Christensen, J. H., Strode, S. A., & Mason, R. P. (2010). An improved global model for air-sea exchange of mercury: High concentrations over the north atlantic. *Environmental Science & Technology*, 44(22), 8574–8580.

Song, S., Selin, N., Soerensen, A., Angot, H., Artz, R., Brooks, S., Brunke, E., Conley, G., Dommergue, A., Ebinghaus, R., Holsen, T., Jaffe, D., Kang, S., Kelley, P., Luke, W., Magand, O., Marumoto, K., Pfaffhuber, K., Ren, X., Sheu, G., Slemr, F., Warneke, T., Weigelt, A., Weiss-Penzias, P., Wip, D., & Zhang, Q. (2015). Top-down constraints on atmospheric mercury emissions and implications for global biogeochemical cycling. *Atmospheric Chemistry and Physics*, 15(12), 7103–7125.

Sonke, J. E. (2011). A global model of mass independent mercury stable isotope fractionation. *Geochimica Et Cosmochimica Acta*, 75(16), 4577–4590.

Sonke, J. E. (2014). GET-Observatoire Midi-Pyrené es, CNRS, Université de Toulouse III, Toulouse, France. Personal Communications.

Sonke, J. E. (2015). A stable isotope view of the atmospheric hg cycle. In *Goldschmidt, Prague*.

Steffen, A., Douglas, T., Amyot, M., Ariya, P., Aspmo, K., Berg, T., Bottenheim, J., Brooks, S., Cobbett, F., Dastoor, A., Dommergue, A., Ebinghaus, R., Ferrari, C., Gardfeldt, K., Goodsite, M. E., Lean, D., Poulain, A. J., Scherz, C., Skov, H., Sommar, J., & Temme, C. (2008). A synthesis of atmospheric mercury depletion event chemistry in the atmosphere and snow. *Atmospheric Chemistry and Physics*, 8(6), 1445–1482.

Strahan, S. E., Duncan, B. N., & Hoor, P. (2007). Observationally derived transport diagnostics for the lowermost stratosphere and their application to the gmi chemistry and transport model. *Atmospheric Chemistry and Physics*, 7(9), 2435–2445.

Streets, D. G., Devane, M. K., Lu, Z., Bond, T. C., Sunderland, E. M., & Jacob, D. J. (2011). All-time releases of mercury to the atmosphere from human activities. *Environmental Science & Technology*, 45(24), 10485–10491.

Strode, S. A., Jaegle, L., Jaffe, D. A., Swartzendruber, P. C., Selin, N. E., Holmes, C., & Yantosca, R. M. (2008). Trans-pacific transport of mercury. *Journal of Geophysical Research-Atmospheres*, 113(D15).

Subir, M., Ariya, P. A., & Dastoor, A. P. (2011). A review of uncertainties in atmospheric modeling of mercury chemistry i. uncertainties in existing kinetic parameters - fundamental limitations and the importance of heterogeneous chemistry. *Atmospheric Environment*, 45(32), 5664–5676.

Sumner, A. L., Spicer, C. W., Statola, J., Mangaraj, R., Cowen, K. A., & Landis, M. S. (2005). *Environmental chamber studies of mercury reactions in the atmosphere*. USA: Springer.

Sunderland, E. M., Dalziel, J., Heyes, A., Branfireun, B. A., Krabbenhoft, D. P., & Gobas, F. A. P. C. (2010). Response of a macrotidal estuary to changes in anthropogenic mercury loading between 1850 and 2000. *Environmental Science & Technology*, 44(5), 1698–1704.

Sunderland, E. M., Krabbenhoft, D. P., Moreau, J. W., Strode, S. A., & Landing, W. M. (2009). Mercury sources, distribution, and bioavailability in the north pacific ocean: Insights from data and models. *Global Biogeochemical Cycles*, 23(2).

Sunderland, E. M. & Mason, R. P. (2007). Human impacts on open ocean mercury concentrations. *Global Biogeochemical Cycles*, 21(4).

Sundseth, K., Pacyna, J., Pacyna, E., & Panasiuk, D. (2011). Substance flow analysis of mercury affecting water quality in the european union. *Water, Air, & Soil Pollution*, (pp. 1–14).

Talbot, R., Mao, H., Scheuer, E., Dibb, J., & Avery, M. (2007). Total depletion of hg° in the upper troposphere-lower stratosphere. *Geophysical Research Letters*, 34(23).

Tan, W. W., Geller, M. A., Pawson, S., & da Silva, A. (2004). A case study of excessive subtropical transport in the stratosphere of a data assimilation system. *Journal of Geophysical Research-Atmospheres*, 109(D11).

Taylor, C. G. (1965). The loss of mercury from fungicidal paints. *Journal of Applied Chemistry*, (pp. 232–236).

Telmer, K. M. & Veiga, M. M. (2009). World emissions of mercury from artisanal and small scale gold mining. *Mercury Fate and Transport in the Global Atmosphere*, (pp. 131–172).

Theys, N., Van Roozendael, M., Hendrick, F., Yang, X., De Smedt, I., Richter, A., Begoin, M., Errera, Q., Johnston, P. V., Kreher, K., & De Maziere, M. (2011). Global observations of tropospheric bro columns using gome-2 satellite data. *Atmospheric Chemistry and Physics*, 11(4), 1791–1811.

Thorleifson, M. (1998). *The Canadian Mercury Cell Chlor-Alkali industry: Mercury Emissions and Status of Facilities 1935 - 1996*. Report, Environment Canada, Transboundary Air Issues Branch.

Tossell, J. A. (2006). Calculation of the energetics for the oligomerization of gas phase hgo and hgs and for the solvolysis of crystalline hgo and hgs. *Journal of Physical Chemistry A*, 110(7), 2571–2578.

Travnikov, O. & Ilyin, I. (2009). The emep/msc-e mercury modeling system. *Mercury Fate and Transport in the Global Atmosphere*, (pp. 571–587).

Tseng, C. M., Lamborg, C. H., & Hsu, S. C. (2013). A unique seasonal pattern in dissolved elemental mercury in the south china sea, a tropical and monsoon-dominated marginal sea. *Geophysical Research Letters*, 40, 167–172.

UNEP (2008). *Report on the major mercury-containing products and processes, their substitutes and experience in switching to mercury-free products and processes.* Report UNEP(DTIE)/Hg/OEWG.2/7/Add.1, UNEP.

UNEP (2013a). *Minamata Convention on Mercury: Text and Annexes*. Report, United Nations Environment Programme.

UNEP (2013b). *Toolkit for Identification and Quantification of Mercury Sources, Reference Report and Guidline for Inventory Level 2, Version 1.2, April 2013*. Report, UNEP Chemicals Branch.

United Nations Department of Economic and Social Affairs Population Division (2011). *World Population Prospects: The 2010 Revision, Volume I: Comprehensive Tables*. Report ST/ESA/SER.A/313, United Nations.

United Nations Statistics Division (2012). Gdp and its breakdown at constant 2005 prices in us dollars - all countries and regions/subregions (totals) for all years. *National Accounts Main Aggregates Database*.

URS Research Company Hazards Assessment Directorate (1975). *Materials balance and technology assessment of mercury and its compounds on national and regional bases*. Report EPA 560/3-75-007, Environmental Protection Agency Office of Toxic Substances.

U.S. Bureau of Mines (1941 - 1968). *Minerals Yearbook*. Washington, D.C., USA: US Department of the Interior, Government Printing Office.

U.S. Environmental Protection Agency (1992). *Characterization of Products Containing Mercury in Muncipal Solid Waste in the United States, 1970 to 2000*. Report, Office of Solid Waste, Municipal and Industrial Solid Waste Division.

U.S. Environmental Protection Agency (1997). *Mercury Study Report to Congress Volume II: An Inventory of Anthropogenic Mercury Emissions in the United States*. Report, Office of Air Quality Planning & Standards and Office of Research and Development, U.S. Environmental Protection Agency.

U.S. Environmental Protection Agency (2003). *Municipal Solid Waste in the United States: 2001 Facts and Figures*. Report EPA530-R-03-011, Office of Solid Waste and Emergency Response.

USGS/Bureau of Mines (1882 - 1929). *Mineral Resources of the United States*. Washington, D.C.: US Department of the Interior, Government Printing Office.

Van Loon, L. L., Mader, E. A., & Scott, S. L. (2001). Sulfite stabilization and reduction of the aqueous mercuric ion: Kinetic determination of sequential formation constants. *Journal of Physical Chemistry A*, 105(13), 3190–3195.

Volkamer, R., Baidar, S., Campos, T. L., Coburn, S., DiGangi, J. P., Dix, B., Eloranta, E. W., Koenig, T. K., Morley, B., Ortega, I., Pierce, B. R., Reeves, M., Sinreich, R., Wang, S., Zondlo, M. A., & Romashkin, P. A. (2015). Aircraft measurements of bro, io, glyoxal, no2, h2o, o-2-o-2 and aerosol extinction profiles in the tropics: comparison with aircraft-/ship-based in situ and lidar measurements. *Atmospheric Measurement Techniques*, 8(5), 2121–2148.

Wan, Q., Feng, X., Lu, J., Zheng, W., Song, X., Han, S., & Xu, H. (2009). Atmospheric mercury in changbai mountain area, northeastern china i. the seasonal distribution pattern of total gaseous mercury and its potential sources. *Environmental research*, 109(3), 201–206.

Wang, F., Saiz-Lopez, A., Mahajan, A., Martin, J., Armstrong, D., Lemes, M., Hay, T., & Prados-Roman, C. (2014). Enhanced production of oxidised mercury over the tropical pacific ocean: a key missing oxidation pathway. *Atmospheric Chemistry and Physics*, 14(3), 1323–1335.

Wang, S. Y., Schmidt, J. A., Baidar, S., Coburn, S., Dix, B., Koenig, T. K., Apel, E., Bowdalo, D., Campos, T. L., Eloranta, E., Evans, M. J., DiGangi, J. P., Zondlo, M. A., Gao, R. S., Haggerty, J. A., Hall, S. R., Hornbrook, R. S., Jacob, D., Morley, B., Pierce, B., Reeves, M., Romashkin, P., ter Schure, A., & Volkamer, R. (2015). Active and widespread halogen chemistry in the tropical and subtropical free troposphere. *Proceedings of the National Academy of Sciences of the United States of America*, 112(30), 9281–9286.

Wang, Z. & Pehkonen, S. (2004). Oxidation of elemental mercury by aqueous bromine: atmospheric implications. *Atmospheric Environment*, 38(22), 3675–3688.

Weiss-Penzias, P., Amos, H. M., Selin, N. E., Gustin, M. S., Jaffe, D. A., Obrist, D., Sheu, G. R., & Giang, A. (2015). Use of a global model to understand speciated atmospheric mercury observations at five high-elevation sites. *Atmospheric Chemistry and Physics*, 15(3), 1161–1173.

Whalin, L., Kim, E. H., & Mason, R. (2007). Factors influencing the oxidation, reduction, methylation and demethylation of mercury species in coastal waters. *Marine Chemistry*, 107(3), 278–294.

Whalin, L. & Mason, R. (2006). A new method for the investigation of mercury redox chemistry in natural waters utilizing deflatable teflon (r) bags and additions of isotopically labeled mercury. *Analytica Chimica Acta*, 558(1-2), 211–221.

Wiedinmyer, C., Yokelson, R. J., & Gullett, B. K. (2014). Global emissions of trace gases, particulate matter, and hazardous air pollutants from open burning of domestic waste. *Environmental Science & Technology*, DOI: 10.1021/es502250z.

Wilcox, J. (2009). A kinetic investigation of high-temperature mercury oxidation by chlorine. *Journal of Physical Chemistry A*, 113(24), 6633–6639.

Wilson, S., Munthe, J., Sundseth, K., Kindbom, K., Maxson, P., Pacyna, J. M., & Steenhuisen, F. (2010). *Updating Historical Global Inventories of Anthropogenic Mercury Emissions to Air*. Report, Arctic Monitoring and Assessment Program (AMAP).

Xiao, Y., Jacob, D. J., & Turquety, S. (2007). Atmospheric acetylene and its relationship with co as an indicator of air mass age. *Journal of Geophysical Research*, 112, D12305.

Xiao, Z. F., Stromberg, D., & Lindqvist, O. (1995). Influence of humic substances on photolysis of divalent mercury in aqueous-solution. *Water Air and Soil Pollution*, 80(1-4), 789–798.

Yan, N. Q., Liu, S. H., Chang, S. G., & Miller, C. (2005). Method for the study of gaseous oxidants for the oxidation of mercury gas. *Industrial & Engineering Chemistry Research*, 44(15), 5567–5574.

Yan, N. Q., Qu, Z., Chi, Y., Qiao, S. H., Dod, R. L., Chang, S. G., & Miller, C. (2009). Enhanced elemental mercury removal from coal-fired flue gas by sulfur-chlorine compounds. *Environmental Science & Technology*, 43(14), 5410–5415.

Yang, X., Cox, R., Warwick, N., Pyle, J., Carver, G., O'Connor, F., & Savage, N. (2005). Tropospheric bromine chemistry and its impacts on ozone: A model study. *Journal of Geophysical Research-Atmospheres*, 110(D23).

Zhang, Y. X., Jacob, D. J., Horowitz, H. M., Chen, L., Amos, H. M., Krabbenhoft, D. P., Slemr, F., St Louis, V. L., & Sunderland, E. M. (2016). Observed decrease in atmospheric mercury explained by global decline in anthropogenic emissions. *Proceedings of the National Academy of Sciences of the United States of America*, 113(3), 526–531.

Zhang, H., Fu, X. W., Lin, C. J., Wang, X., & Feng, X. B. (2015). Observation and analysis of speciated atmospheric mercury in shangri-la, tibetan plateau, china. *Atmospheric Chemistry and Physics*, 15(2), 653–665.

Zhang, Y. X., Jacob, D., Dutkiewicz, S., Amos, H., Long, M., & Sunderland, E. (2015). Biogeochemical drivers of the fate of riverine mercury discharged to the global and arctic oceans. *Global Biogeochemical Cycles*, 29(6), 854–864.

Zheng, W. & Hintelmann, H. (2009). Mercury isotope fractionation during photoreduction in natural water is controlled by its hg/doc ratio. *Geochimica Et Cosmochimica Acta*, 73(22), 6704–6715.

Zhu, W., Li, Z. G., Chai, X. L., Hao, Y. X., Lin, C. J., Sommar, J., & Feng, X. B. (2013). Emission characteristics and air-surface exchange of gaseous mercury at the largest active landfill in asia. *Atmospheric Environment*, 79, 188–197.